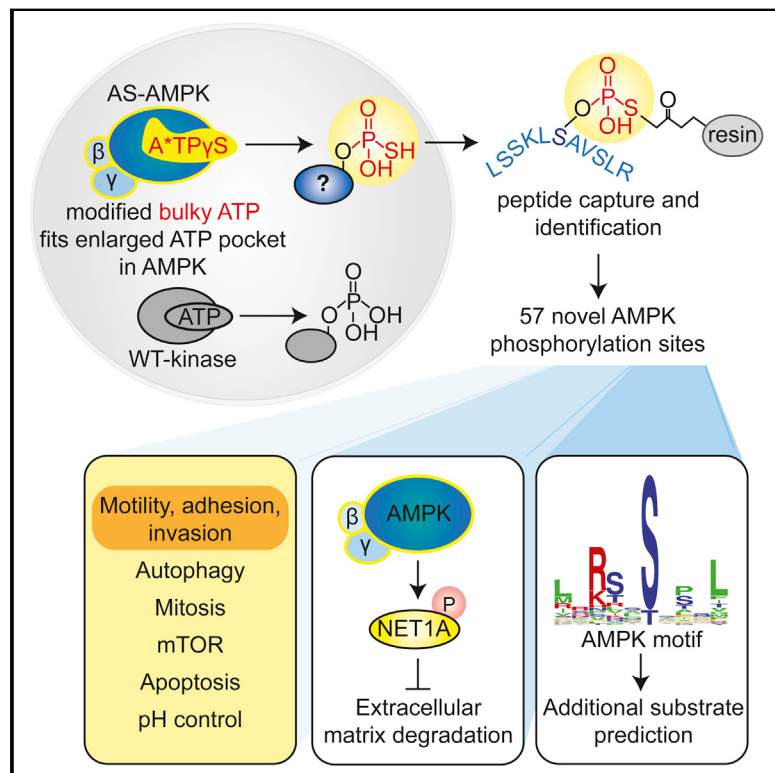


# Cell Metabolism

## Identification of AMPK Phosphorylation Sites Reveals a Network of Proteins Involved in Cell Invasion and Facilitates Large-Scale Substrate Prediction

### Graphical Abstract



### Authors

Bethany E. Schaffer, Rebecca S. Levin, Nicholas T. Hertz, ..., Reuben J. Shaw, Kevan M. Shokat, Anne Brunet

### Correspondence

abrunet1@stanford.edu

### In Brief

Schaffer et al. use a proteomic screen to identify novel AMPK substrates and phosphorylation sites in cancer cells. Several substrates have roles in cell motility and invasion, which could be important for metastasis. Identification of AMPK phosphorylation sites also facilitates construction of a computational platform for *in silico* substrate prediction.

### Highlights

- A screen identifies AMPK substrates and phosphorylation sites in human cancer cells
- Many novel AMPK substrates have roles in cell motility, adhesion, and invasion
- AMPK phosphorylation of one new substrate, NET1A, inhibits cell invasion
- A computational pipeline using the AMPK motif can predict additional substrates

# Identification of AMPK Phosphorylation Sites Reveals a Network of Proteins Involved in Cell Invasion and Facilitates Large-Scale Substrate Prediction

Bethany E. Schaffer,<sup>1,2</sup> Rebecca S. Levin,<sup>3</sup> Nicholas T. Hertz,<sup>3</sup> Travis J. Maures,<sup>2</sup> Michael L. Schoof,<sup>2</sup> Pablo E. Hollstein,<sup>4</sup> Bérénice A. Benayoun,<sup>2</sup> Max R. Banko,<sup>2</sup> Reuben J. Shaw,<sup>4</sup> Kevan M. Shokat,<sup>3</sup> and Anne Brunet<sup>1,2,5,\*</sup>

<sup>1</sup>Cancer Biology Program, Stanford University, Stanford, CA 94305, USA

<sup>2</sup>Department of Genetics, Stanford University, Stanford, CA 94305, USA

<sup>3</sup>Department of Cellular and Molecular Pharmacology, Howard Hughes Medical Institute, University of California, San Francisco, CA 94158, USA

<sup>4</sup>Molecular and Cell Biology Laboratory, Salk Institute for Biological Studies, La Jolla, CA 92037, USA

<sup>5</sup>Glenn Laboratories for the Biology of Aging, Stanford, CA 94305, USA

\*Correspondence: abrunet1@stanford.edu

<http://dx.doi.org/10.1016/j.cmet.2015.09.009>

## SUMMARY

AMP-activated protein kinase (AMPK) is a central energy gauge that regulates metabolism and has been increasingly involved in non-metabolic processes and diseases. However, AMPK's direct substrates in non-metabolic contexts are largely unknown. To better understand the AMPK network, we use a chemical genetics screen coupled to a peptide capture approach in whole cells, resulting in identification of direct AMPK phosphorylation sites. Interestingly, the high-confidence AMPK substrates contain many proteins involved in cell motility, adhesion, and invasion. AMPK phosphorylation of the RHOA guanine nucleotide exchange factor NET1A inhibits extracellular matrix degradation, an early step in cell invasion. The identification of direct AMPK phosphorylation sites also facilitates large-scale prediction of AMPK substrates. We provide an AMPK motif matrix and a pipeline to predict additional AMPK substrates from quantitative phosphoproteomics datasets. As AMPK is emerging as a critical node in aging and pathological processes, our study identifies potential targets for therapeutic strategies.

## INTRODUCTION

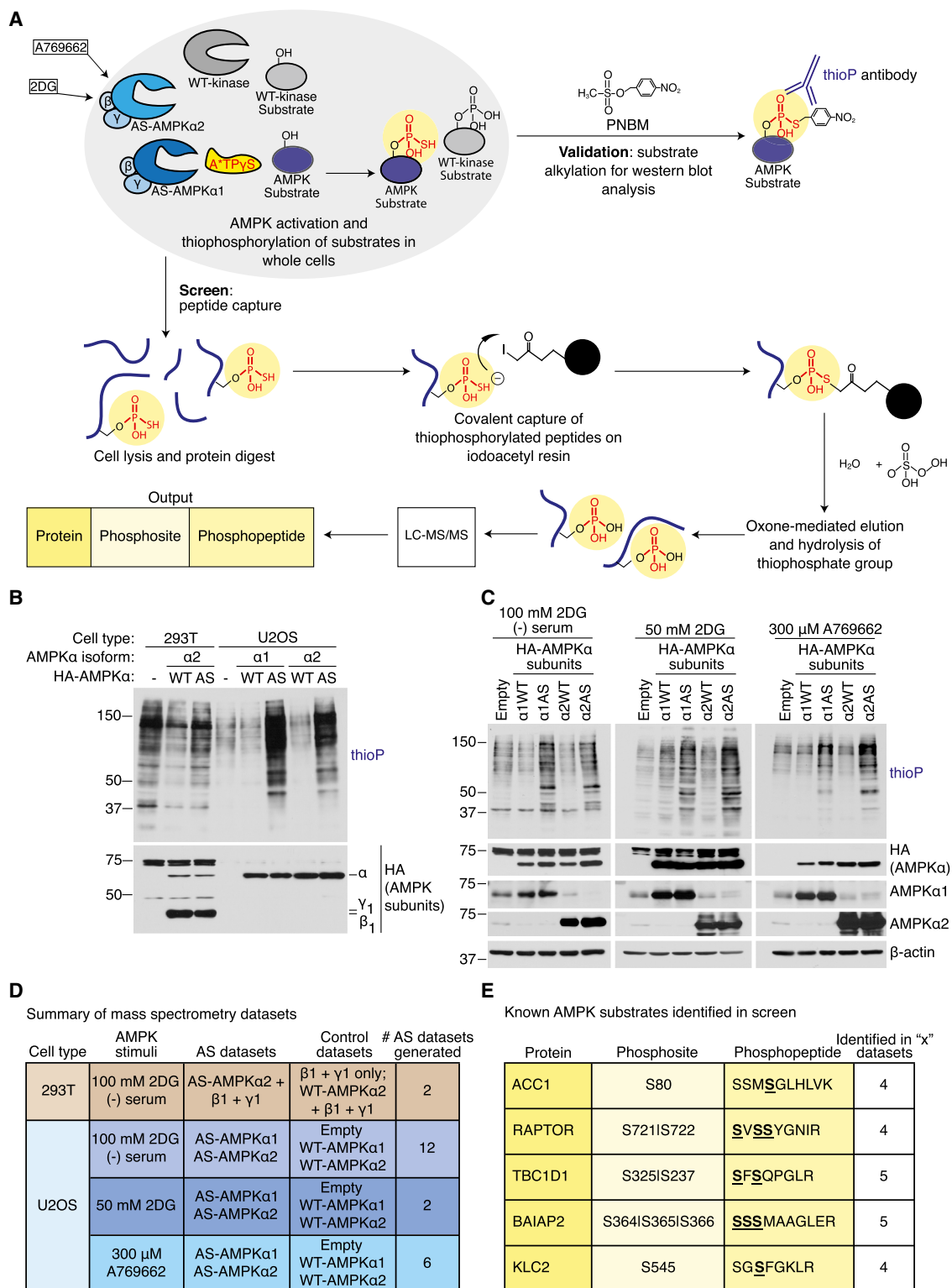
The ability to adjust to nutrient stress is critical for cellular and organismal functions. Central to this process is AMP-activated protein kinase (AMPK), an energy-sensing protein kinase that regulates metabolic processes (Hardie and Carling, 1997). At the cellular level, AMPK responds to low energy levels by promoting glucose uptake (Kurth-Kraczek et al., 1999), increasing catabolism (Egan et al., 2011; Wang et al., 2001), and inhibiting anabolic processes (Gwinn et al., 2008; Sim and Hardie, 1988) through a repertoire of substrates. Systemically, AMPK integrates hormonal signals to trigger food intake and prevent energy expenditure (Andersson et al., 2004; Hardie and Ashford,

2014). The critical role of AMPK in metabolic regulation has made it an attractive pharmacological target for treatment of metabolic diseases like diabetes (Winder and Hardie, 1999). Indeed, several AMPK activating compounds have recently been identified (Hawley et al., 2012; Zadra et al., 2014; Zhou et al., 2001). As AMPK has been implicated in extending lifespan in several organisms, including potentially humans (Apfeld et al., 2004; Burkewitz et al., 2014; Greer et al., 2007; Mair et al., 2011), it is also an attractive target to delay aspects of aging.

AMPK activity has also been linked with processes that are not directly viewed as metabolic, including mitosis (Banko et al., 2011; Bettencourt-Dias et al., 2004; Vazquez-Martin et al., 2009), development (Lee et al., 2007), and cell polarity (Zhang et al., 2006; Zheng and Cantley, 2007). While many of the substrates that mediate AMPK's effect on metabolism have been well studied (Chen et al., 2008; Gwinn et al., 2008; Sim and Hardie, 1988), those connecting AMPK to non-metabolic roles are largely unknown. Additionally, aberrant AMPK activity has been associated with diseases like cancer (Kato et al., 2002; Liang and Mills, 2013; Xiang et al., 2004), and the functionally relevant substrates in disease often remain obscure. The emergence of unexpected roles of AMPK and the increasing effort to pharmacologically target this kinase make it critical to fully understand the AMPK substrate network in the context of specific diseases and cellular states.

Central to a kinase-substrate interaction is the exact phosphorylated residue. Previous efforts to characterize the AMPK network in whole cells have focused on protein substrate, but not phosphorylation site, identification (Banko et al., 2011). Additionally, while in vitro phosphorylation motif libraries have helped predict AMPK substrates (Egan et al., 2011; Gwinn et al., 2008), large-scale identification of AMPK phosphorylation sites has never been done. Interestingly, a new approach was developed to identify direct phosphorylation sites of a protein kinase in vitro (Blethrow et al., 2008; Hengeveld et al., 2012). However, this method had not been used in whole cells.

To understand the AMPK substrate network at the resolution of the phosphorylated site, we combined a chemical genetic screen (Banko et al., 2011) and peptide capture approach (Blethrow et al., 2008), allowing us to identify direct AMPK $\alpha$ 1 and  $\alpha$ 2 phosphorylation sites. We provide a comprehensive resource

**Figure 1. Screening Strategy to Identify AMPK $\alpha$ 1 and  $\alpha$ 2 Substrates and Phosphorylation Sites in Cells**

(A) Schematic of the peptide-capture technique used to identify analog-specific (AS) AMPK $\alpha$ 1 and  $\alpha$ 2 substrates and phosphorylation sites in whole cells. AS-AMPK uses A $\gamma$ T $\gamma$ S, a bulky ATP analog, to thiophosphorylate substrates. Upper panel: thiophosphorylated substrates are alkylated by p-nitrobenzyl mesylate (PNBM) and recognized by an antibody to the thiophosphate moiety (thioP). Lower panel: thiophosphorylated peptides are captured on a resin, eluted, and identified using liquid chromatography-tandem mass spectrometry (LC-MS/MS). 2DG, 2-deoxy-D-glucose.

(legend continued on next page)

of over 50 AMPK substrates and phosphorylation sites in a human cancer cell line. This screen revealed that AMPK controls different aspects of cellular motility and invasion. We also provide an AMPK motif matrix and pipeline to further predict additional components of the AMPK network, which should have critical implications in pharmacological targeting of AMPK in disease or aging.

## RESULTS

### A Comprehensive Physiological Screen for AMPK $\alpha$ 1 and $\alpha$ 2 Substrates in a Human Cancer Cell Line

To characterize the AMPK network, we conducted a screen to identify direct AMPK substrates and phosphorylation sites. We used an analog-specific (AS) method of kinase-substrate identification (Banko et al., 2011; Shah et al., 1997), which utilizes a mutant of AMPK that accepts N<sup>6</sup>-(phenethyl) ATP $\gamma$ S, a bulky form of ATP introduced into cells with gentle digitonin permeabilization, to tag direct substrates with a thiophosphate moiety (Figure 1A). We coupled this approach to a peptide capture system, allowing identification of the exact phosphorylation site by tandem mass spectrometry (Blethow et al., 2008; Hertz et al., 2010) (Figure 1A).

AMPK is a heterotrimeric protein kinase composed of a catalytic  $\alpha$  subunit ( $\alpha$ 1 or  $\alpha$ 2) as well as regulatory  $\beta$  and  $\gamma$  subunits. We had previously screened for AMPK $\alpha$ 2 substrates by overexpressing an analog-specific (AS) version of AMPK $\alpha$ 2 together with  $\beta$  and  $\gamma$  subunits in 293T cells (Banko et al., 2011). To extend our screen to AMPK $\alpha$ 1 and better approximate physiological kinase activity, we generated stable U2OS cell lines that inducibly express AS or wild-type (WT) AMPK $\alpha$ 1 or  $\alpha$ 2 upon doxycycline addition (Figures S1A and S1B). While AMPK $\alpha$ 1 or  $\alpha$ 2 subunits were overexpressed in these U2OS cell lines, this did not lead to substantial dysregulation of endogenous AMPK substrates (Figure S1D), probably because the endogenous  $\beta$  and  $\gamma$  subunits keep the activity of the exogenous  $\alpha$  subunit in check. Thus, this system provides screening conditions that better approximate physiological AMPK activity.

Both AS-AMPK $\alpha$ 1 and  $\alpha$ 2 were able to use N<sup>6</sup>-(phenethyl) ATP $\gamma$ S to thiophosphorylate endogenous substrates in U2OS cells upon activation by serum starvation and 2-deoxy-D-glucose (2DG) (Figure 1B). They did so with less background thiophosphorylation than in 293T cells overexpressing all AMPK subunits (Figure 1B) (Banko et al., 2011). AS-AMPK $\alpha$ 1 and  $\alpha$ 2 also thiophosphorylated endogenous substrates when activated by 2DG alone or by the specific AMPK activator A769662 (Cool et al., 2006) (Figure 1C). They also thiophosphorylated the known AMPK substrate

PPP1R12C in U2OS cells with less background than in 293T cells (Figure S1C) (Banko et al., 2011).

To use the analog-specific approach to identify not only AMPK substrates, but also the exact AMPK phosphorylation sites, we coupled it to a peptide capture method developed for concurrent AS-substrate and phosphosite identification (Blethow et al., 2008; Hertz et al., 2010) (Figure 1A). Since this peptide capture method had not yet been used in whole cells, we first determined its efficacy in 293T cells overexpressing AS-AMPK $\alpha$ 2,  $\beta$ 1, and  $\gamma$ 1 subunits or their respective controls (Figure 1D, top row). We successfully identified phosphopeptides unique to AS-AMPK $\alpha$ 2 (Figure S1G). We then performed ten biological experiments in U2OS cells expressing AS-AMPK $\alpha$ 1 and AS-AMPK $\alpha$ 2 or their respective controls (Figure 1D, bottom rows; Figure S1G), using several methods of AMPK activation (Figure 1D). Importantly, the known phosphorylation sites on five established AMPK substrates (ACC1 [S80], Davies et al., 1990; RAPTOR [S722], Gwinn et al., 2008; TBC1D1 [S237], Chen et al., 2008; BAIAP2 [S366], Banko et al., 2011; and KLC2 [S545], Amato et al., 2011; Johnson et al., 2011) were identified in multiple independent datasets (Figure 1E). Thus, this whole-cell peptide capture approach can be used to identify AMPK phosphorylation sites. However, the presence of background phosphopeptides (Figures S1F and S1G) and lack of saturation across replicates (Figures S1F and S1G) indicate that this method is not yet sensitive enough to compare AMPK activity between different conditions.

### Identification of Over 50 Potential AMPK Substrates and Their Phosphorylation Sites, Including 21 Previously Unknown High-Confidence Substrates

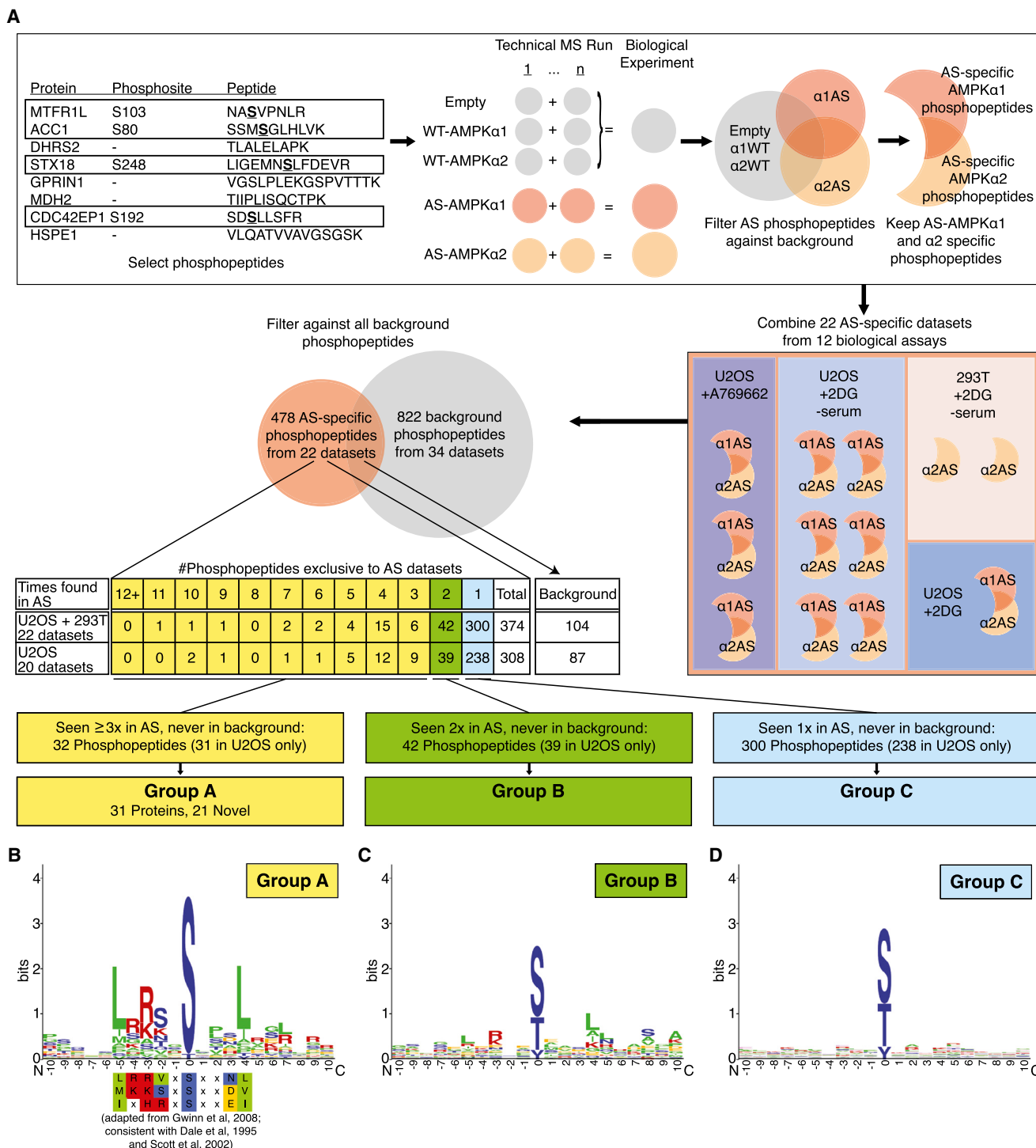
To identify high-confidence AMPK substrates and phosphorylation sites, we developed a stringent pipeline to analyze the tandem mass spectrometry data (Figure 2A). Phosphopeptides that were found in experimental datasets, but never in control datasets (see *Supplemental Experimental Procedures*), were further considered. All AS-AMPK-specific phosphopeptides are presented in *List S2*. The motifs surrounding phosphorylation sites on phosphopeptides seen in 3 or more of the 22 experimental datasets (Group A) strongly adhered to the known AMPK motif (Dale et al., 1995; Gwinn et al., 2008; Scott et al., 2002) (Figures 2B and S2B), while those seen less frequently adhered less well to the AMPK motif (Figures 2C, 2D, and S2C). In addition, many known AMPK substrates were identified in Group A (Figure 4A). Thus, there is high confidence that the 21 previously unknown substrates identified in Group A are AMPK targets. We will first focus on the high-confidence Group A substrates, but we will return to all identified phosphopeptides in Figure 6.

(B) HA-tagged AS-AMPK $\alpha$ 1 and  $\alpha$ 2 thiophosphorylate endogenous substrates in U2OS cells without overexpression of the  $\beta$  and  $\gamma$  subunits. Cells were serum-starved for 2 hr and stimulated for 5 min with 100 mM 2DG, then incubated with A<sup>\*</sup>TP $\gamma$ S. Whole-cell lysates were analyzed for the presence of thiophosphorylation (thioP) and exogenous AMPK subunits (HA tag).

(C) HA-tagged AS-AMPK $\alpha$ 1 and  $\alpha$ 2 thiophosphorylate endogenous substrates under different AMPK-activating conditions. Whole-cell lysates were analyzed for the presence of thiophosphorylation (thioP) and AMPK $\alpha$  (HA tag, AMPK $\alpha$ 1, AMPK $\alpha$ 2). First panel: 2 hr of serum starvation with 5 min of 100 mM 2DG; second panel: 15 min of 50 mM 2DG; third panel: 30 min of 300  $\mu$ M A769662. Representative of 6, 1, and 3 independent experiments for 2DG (–) serum, 2DG, and A769662, respectively. Empty, empty vector;  $\alpha$ 1WT, WT-AMPK $\alpha$ 1;  $\alpha$ 1AS, AS-AMPK $\alpha$ 1;  $\alpha$ 2WT, WT-AMPK $\alpha$ 2;  $\alpha$ 2AS, AS-AMPK $\alpha$ 2.

(D) Summary of mass spectrometry datasets. AMPK-activating conditions as in Figure 1C. See Figure S1G and *List S1* for more information. Empty, empty vector.

(E) Known AMPK substrates identified in multiple AS-AMPK datasets. Underlined and bold residues, phosphorylated sites on the identified phosphopeptide (more than one is shown if the phosphopeptide had multiple or ambiguous phosphorylation site identification). “Phosphosite” column, identified phosphorylation site corresponding to the known AMPK site. “[ ]”, ambiguous site identification. S722, known AMPK site on RAPTOR; S237, known site on TBC1D1; S366, known site on BAIAP2.

**Figure 2. Identification of High-Confidence AS-AMPK Substrates with a Tailored Pipeline**

(A) Schematic of the pipeline used to identify AS-AMPK substrates in LC-MS/MS datasets. See [Supplemental Experimental Procedures](#). Phosphopeptides only found in AS-AMPK datasets were classified as Group A, B, or C based on the number of biological samples in which they were identified.  $\alpha$ 1WT,  $\alpha$ 2WT,  $\alpha$ 1AS,  $\alpha$ 2AS: WT or AS-AMPK $\alpha$ 1 or  $\alpha$ 2.

(B-D) Logo motif of the most common phosphorylation sites on each phosphopeptide from Group A (B), Group B (C), and Group C (D). The established in vitro AMPK phosphorylation motif displayed below Group A is modified with permission from [\(Gwinn et al., 2008\)](#) and was generated in that study using a positional scanning peptide library. Green, hydrophobic residues; red, basic; yellow, acidic; blue, neutral polar. See [Figure S2A](#) and [Supplemental Experimental Procedures](#) for selection of the most common phosphorylation sites.

## Validation of AMPK Substrates and Phosphorylation Sites

We next validated several AMPK substrates from Group A. AS-AMPK $\alpha$ 1 and  $\alpha$ 2 strongly thiophosphorylated all of the substrates we tested: SNX17 (Figure 3A), NET1A (a short isoform of NET1) (Figure 3B), CDC42EP1 (Figure 3C), SH3PXD2A (Figure 3D), SNAP29 (Figure S3A), MTFR1L (Figure S3B), and RBM14 (Figure S3C). In most cases, AS-AMPK $\alpha$ 1 and  $\alpha$ 2 thiophosphorylated these proteins equally well, although SNAP29 was a better substrate of AS-AMPK $\alpha$ 2 (Figures S3A and S3D), while MTFR1L was a better substrate of AS-AMPK $\alpha$ 1 (Figures S3B and S3E). Thus, several proteins from Group A were validated as good substrates for both AMPK isoforms, though there may be some isoform-preferred substrates.

To confirm the identified AMPK phosphorylation sites on three validated substrates, SNX17, NET1A, and CDC42EP1, we mutated the identified site on these proteins (Figure 3E). These mutations reduced (SNX17 S437A; Figure 3F) or completely removed (NET1A S46A, CDC42EP1 S192A; Figures 3G and 3H) thiophosphorylation by AS-AMPK. Mutation of the identified site on another validated substrate, SH3PXD2A, did not decrease thiophosphorylation (Figure S3F), though this may be due to the presence of many potential AMPK phosphorylation sites on this protein (Figures S3F and S3G). Thus, the identified sites are likely bona fide AMPK phosphorylation sites.

To validate phosphorylation sites independently of the analog-specific approach, we focused on SNX17 pS437 and NET1A pS46. For SNX17, we generated a phosphospecific antibody against pS437. We verified that this antibody recognized the WT, but not the S437A phosphorylation mutant, form of SNX17 (Figure S3H). Activation of endogenous AMPK by the specific AMPK activator A769662 increased the phosphorylation of endogenous SNX17 at S437 in U2OS cells (Figure 3I). Furthermore, shRNA knockdown of both AMPK $\alpha$ 1 and  $\alpha$ 2 diminished the phosphorylation of endogenous SNX17 at S437 in response to A769662 (Figure 3I). Long-term activation of AMPK with either A769662 or nutrient deprivation correlated with decreased total levels of SNX17 (Figures 3J and S3I), raising the possibility that phosphorylation at this site leads to degradation of SNX17. Together, these results indicate that SNX17 pS437 is an endogenous AMPK target. For NET1A, we generated a phosphospecific antibody against pS46, but it was not potent enough to recognize NET1A pS46 in cells (data not shown). We thus used an antibody that recognizes the general AMPK phosphorylation motif (Ducommun et al., 2015; Gwinn et al., 2008; Zhang et al., 2002). Activation of endogenous AMPK by the specific AMPK activator A769662 increased the phosphorylation of the exogenously expressed WT, but not the S46A phosphorylation mutant, form of NET1A in U2OS cells (Figure 3K). In addition, knockdown of both AMPK $\alpha$ 1 and  $\alpha$ 2 diminished phosphorylation of NET1A in response to A769662 (Figure 3K). These results indicate that endogenous AMPK is important for exogenous NET1A phosphorylation at S46, although other kinases could be contributing to NET1A basal phosphorylation. Collectively, these results confirm that the phosphorylation sites in Group A are likely bona fide endogenous AMPK targets.

## Many High-Confidence AMPK Substrates Have Known Roles in Cell Motility, Adhesion, and Invasion

We mined the literature and used GO terms to determine the functions of the AMPK substrates in Group A (Figure 4A, List S3). As expected, some of the substrates further link AMPK with metabolic signaling pathways (Figures 4A and 4B). For example, WDFY3, a phosphatidylinositol 3-phosphate binding protein, promotes recycling of protein aggregates by autophagy (Simonsen et al., 2004). Interestingly, 14 AMPK substrates are involved in cellular motility, adhesion, or invasion as defined by literature mining and GO terms (Figure 4A, orange rows, and Figures 4B, S4A, and S4B). For example, NET1A is a RHOA guanine nucleotide exchange factor (GEF) that can promote cell migration and invasion (Carr et al., 2013), and ERBB2IP is an adaptor protein that can inhibit cell migration (Liu et al., 2013). While unbiased GO analysis did not reveal any significant enrichment, probably due to the small size of the list, 11 of the 31 substrates were identified in a compiled list of GO terms encompassing aspects of cell motility, adhesion, and invasion (Figures S4A and S4B). Consistently, studies have recently implicated AMPK in cell motility, adhesion, and invasion, in part via the known substrates ACC1 and CLIP-170 (Nakano et al., 2010; Scott et al., 2012; Zhang et al., 2006). Thus, our screen provides additional substrates and phosphorylation sites that could help in functionally analyzing the role of AMPK in cell motility, adhesion, and invasion, processes that are key for wound healing and metastasis.

## AMPK Phosphorylation of NET1A Inhibits Extracellular Matrix Degradation

Cell invasion was recently found to be regulated by ACC1, a well-known AMPK substrate (Scott et al., 2012), but the exact roles of AMPK in cell invasion and the other potential substrates involved are largely unknown. We first tested whether manipulating AMPK activity indeed impacted a cell's ability to degrade the extracellular matrix (ECM), an early step in cell invasion, by using a gelatin-degradation assay (Bowden et al., 2001). U2OS cells stably expressing an shRNA against both AMPK $\alpha$ 1 and  $\alpha$ 2 (Figure S5A and Banko et al., 2011) displayed a slight, but significant, increase in gelatin degradation (Figure 5A). Because U2OS cells are not a highly invasive cell line (Yuan et al., 2009) (Figure 5A, see basal levels), we also used RPMI-7951 cells, a metastatic melanoma cell line that extends invadopodia—protrusions that degrade the ECM (Seals et al., 2005). RPMI-7951 cells stably expressing an shRNA against AMPK $\alpha$ 1 and  $\alpha$ 2 (Figure S5B) also displayed a significant increase in ECM degradation (Figure 5B). Conversely, activation of AMPK by A769662 in RPMI-7951 cells inhibited ECM degradation (Figure 5C). Together, these results suggest that AMPK impedes this early step of cell invasion.

As NET1A can promote cell invasion (Carr et al., 2013), we next asked if the AMPK phosphorylation site on NET1A (S46, Figures 3G and 3K) mediates ECM degradation. To this end, we generated RPMI-7951 and U2OS cell lines that express either WT or phosphomutant (S46A) NET1A in a doxycycline inducible manner (Figures S5C–S5F). We verified that doxycycline induces similar levels of WT and S46A NET1A in these cell lines at the doses used in these assays (Figures S5C–S5F). Overexpression of NET1A S46A resulted in a strong increase in gelatin degradation in RPMI-7951 cells compared to both WT NET1A and empty

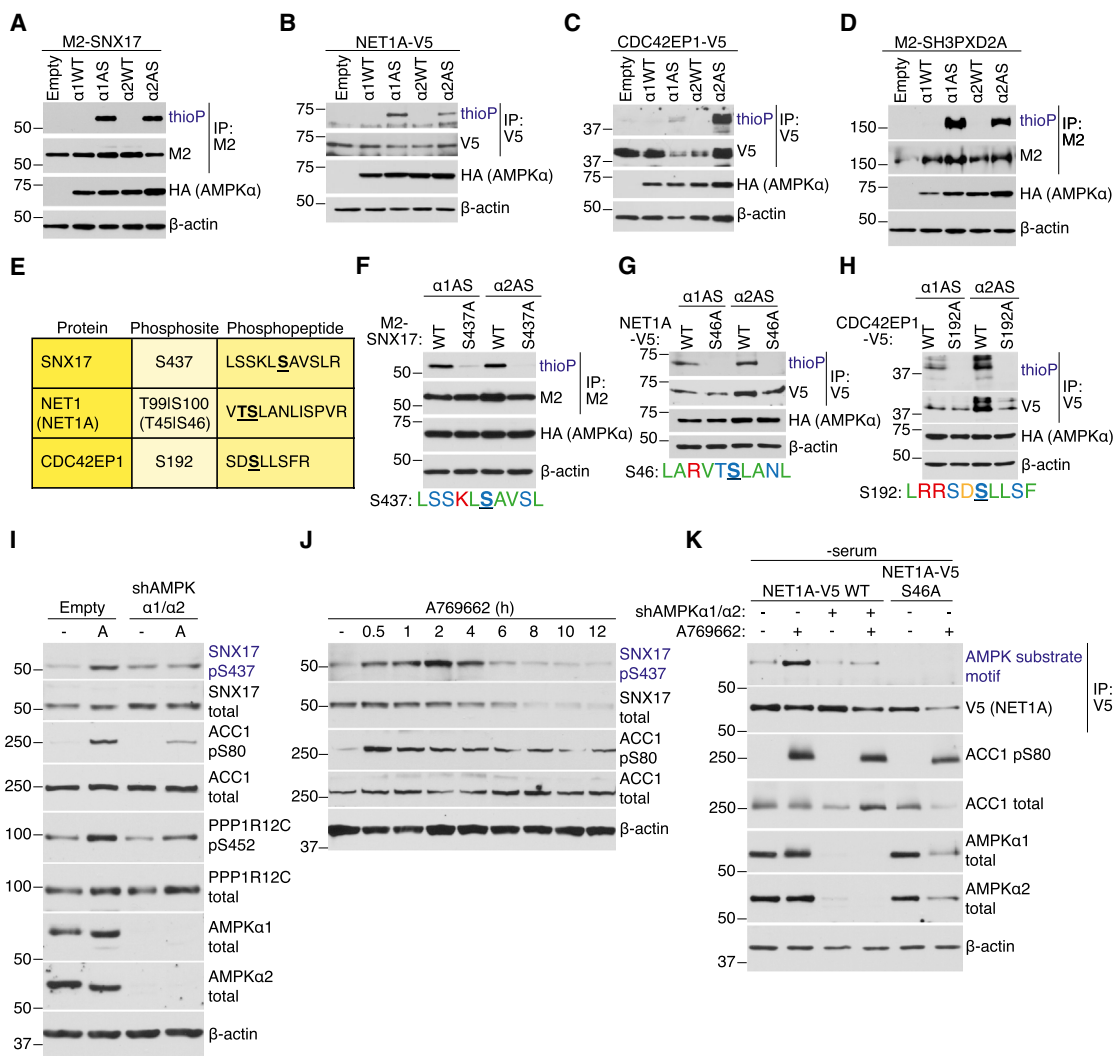


**Figure 3. AS-AMPK Directly Phosphorylates Several High-Confidence Substrates, Including SNX17 and NET1A**

(A–D) AS-AMPK thiophosphorylates SNX17 (A), NET1A (B), CDC42EP1 (C), and SH3PXD2A (D). Tagged proteins were overexpressed in empty vector or AMPK $\alpha$ -expressing (HA-tagged WT or AS-AMPK $\alpha$ 1 or  $\alpha$ 2) U2OS cell lines, immunoprecipitated, and analyzed by western blot for the presence of thiophosphorylation. AMPK was activated in all conditions with 15 min of 50 mM 2DG. Representative of 3, 1, 1, and 2 independent experiments, respectively. (E) Mass spectrometry-predicted AMPK phosphorylation sites and corresponding phosphopeptides for SNX17, NET1A, and CDC42EP1. Labeled as in Figure 1E. S100 on NET1 (S46 on the short isoform NET1A) was used as the NET1/NET1A site as its surrounding motif resembled the AMPK motif better than that of T99. (F–H) AS-AMPK thiophosphorylates SNX17 (F), NET1A (G), and CDC42EP1 (H) at the identified residues. Tagged WT and predicted phosphorylation site mutants of the indicated substrates were overexpressed in U2OS AS-AMPK $\alpha$ 2 and  $\alpha$ 1 cell lines, immunoprecipitated, and analyzed as in Figures 3A–3D. The phosphorylation motif for the predicted residue is shown. The phosphorylated residue is underlined and bold. Color coding is as in Figure 2B. Each panel is representative of two independent experiments.

(I) AMPK phosphorylates S437 on SNX17 endogenously. AMPK was activated in U2OS cells stably expressing an shRNA against AMPK $\alpha$ 1 and  $\alpha$ 2 or empty vector control. Phosphorylation of the known substrates ACC1 S80 and PPP1R12C S452 are shown as controls for AMPK activation. Note that there is still some degree of AMPK substrate phosphorylation in cells with stable knockdown of AMPK $\alpha$ 1 and  $\alpha$ 2, probably due to residual AMPK expression in these cells. “—,” no drug (DMSO vehicle control); A, A769662, 300  $\mu$ M for 30 minutes. Representative of two independent experiments.

(J) Specific activation of AMPK decreases SNX17 protein levels. AMPK was activated in U2OS cells with 300  $\mu$ M of A769662 for the indicated amount of time. Representative of two independent experiments.

(K) Overexpressed NET1A is phosphorylated at S46 in response to endogenous AMPK activation. NET1A-V5 WT or S46A was expressed in a doxycycline-inducible manner in U2OS cell lines. NET1A-V5 WT was also expressed in U2OS cell lines with shRNA knockdown of both AMPK $\alpha$ 1 and  $\alpha$ 2. Cells were serum-starved overnight, which was important to decrease basal NET1A phosphorylation, and NET1A-V5 expression was induced by 2 hr of doxycycline exposure (see [Supplemental Experimental Procedures](#)). AMPK was activated with 300  $\mu$ M A769662 for 30 min. Following NET1A-V5 immunoprecipitation, samples were immunoblotted with an AMPK substrate motif antibody. Representative of three independent experiments.

vector control (Figure 5D). This trend was also observed in U2OS cells (Figure S5G). These observations suggest that phosphorylation of S46 on NET1A inhibits ECM degradation. Activation of AMPK by A769662 reduced gelatin degradation in the presence of WT, but not S46A, NET1A in RPMI-7951 cells (Figure 5E). AMPK phosphorylation of NET1A did not seem to affect NET1A localization or the ability to activate RHOA (data not shown). Collectively, these results suggest that AMPK inhibits ECM degradation in part by phosphorylating NET1A at S46, although how phosphorylation affects NET1A function is still unclear. Given that other AMPK substrates are involved in cell motility, adhesion, and invasion, AMPK likely modulates a network of proteins to affect these processes, perhaps dependent on cellular or environmental contexts.

### Using the AMPK Phosphorylation Motif to Computationally Rank and Identify Low-Frequency Substrates

Given the successful validation of Group A substrates from our screen, we surmised that some of the phosphopeptides identified only once (Group C) or twice (Group B) could also be AMPK substrates instead of background. Group A substrates resemble the *in vitro* AMPK motif (Dale et al., 1995; Gwinn et al., 2008; Scott et al., 2002) (Figure 2B). They also closely match a curated motif that we built from 50 published AMPK substrates that were validated in cells (Figures 6A, top left panel, *Supplemental Experimental Procedures*). This similarity suggests that the AMPK phosphorylation motif could be used to identify additional likely AMPK substrates identified at low frequency in the screen.

To rank the phosphorylation sites from our screen based on their similarity to the AMPK motif, we built a “position-weight matrix” (PWM) algorithm using the 50 published AMPK substrates (Figures 6A and S6A, *List S4, Supplemental Experimental Procedures*). PWM algorithms are frequently used to score the likelihood of a motif being targeted by a specific kinase (e.g., Scansite; Obenauer et al., 2003). Constructing our own PWM algorithm allowed us to base it on well-validated AMPK phosphorylation sites. We then used our algorithm to score and rank each phosphorylation site from the screen (Figures 6A and 6B, *List S5*). The motifs of highly ranked sites matched the validated AMPK motif, whereas the lower ranked ones did not (Figure 6B). Consistently, Group A sites (in yellow) ranked higher than Group B sites (in green), which themselves ranked higher than Group C sites (in blue) (Figures 6B and S6B). We noted that there was also a cluster of lower ranked Group A sites (Figures 6B and S6B); those sites mostly resembled the AMPK motif (Figure S6C) but contained one amino acid that was not present in the validated AMPK motif, resulting in a scoring penalty. Therefore, our PWM algorithm selectively and stringently identifies phosphorylation motifs that closely resemble the AMPK motif, although it can also miss some substrates.

To predict which Group B and C phosphorylation sites could be real AMPK substrates, we applied a stringent cutoff score (1.037, see Figure S6D) to the ranked list (Figure 6B). Fifty phosphorylation sites scored above this cutoff, including most sites from Group A as well as 31 sites from Groups B and C (Figure S6E). These 31 additional sites, while found infrequently in our screen, likely represent real AMPK substrates. Indeed, two

known substrates, CDC27 and TP53BP2 (Banko et al., 2011), are present in this group. Similar to Group A substrates, the 31 highly scoring Group B and C proteins are involved in a variety of cellular processes, including aspects of cell motility, adhesion, and invasion (Figures 6C and S6E, second tab of *List S5*), further suggesting that these processes likely represent an important aspect of the AMPK network in U2OS cancer cells. However, because the phosphorylation motif of other AMPK family members is highly similar to that of AMPK (Goodwin et al., 2014), some of these sites may also be targeted by other kinases, and indeed S227 of RAB11FIP2 is a known target of the AMPK-related kinase MARK2 (Ducharme et al., 2006). Thus, this AMPK motif matrix algorithm helped maximize our screen, revealing a total of 57 previously unknown AMPK phosphorylation sites. These sites serve as a resource for future studies seeking to functionally understand the AMPK-substrate network.

### In Silico Analysis of AMPK Network Dynamics and Prediction of AMPK Phosphorylation Sites

We next sought to extend our analysis of the AMPK network to other contexts (e.g., cell type, stimuli) and use our algorithm to facilitate large-scale substrate prediction. We first examined the dynamics of AMPK phosphorylation sites in publicly available quantitative phosphoproteomic datasets (Figure 7A, top panel). We selected large-scale datasets generated under conditions where AMPK is likely active. One dataset was generated from human luminal breast cancer xenografts, where ischemia—a condition that can lead to AMPK activation (Kudo et al., 1995; Russell et al., 2004)—was mimicked by delaying sample processing (Mertins et al., 2014) (Figure S7A). In the other dataset (Olsen et al., 2010), HeLa S3 cells were synchronized in different phases of the cell cycle, including mitosis—a context that can result in AMPK activation (Banko et al., 2011; Vazquez-Martin et al., 2009) (Figure S7B). Searching these datasets for AMPK phosphorylation sites (Figure 7A, middle panel) revealed that phosphorylation of ACC1 at S80 increased during both ischemia (Figure 7B) and mitosis (Figure 7C), consistent with the notion that AMPK is likely active under these conditions. Not all previously known AMPK sites were dynamically regulated during these processes (Figures S7C and S7D), which suggests that AMPK activity may not be optimal and/or is directed toward other substrates under these conditions. Several of the AMPK phosphorylation sites we identified in our screen, including a number of high-confidence sites, also increased during ischemia (Figures 7B and S7C) or mitosis (Figures 7C and S7D). Thus, this type of analysis may help generate hypotheses for the relevance of AMPK substrates in specific contexts.

As these quantitative phosphoproteomic datasets contain thousands of phosphopeptides, they could also be analyzed more globally to predict additional AMPK-like sites and their dynamics (Figure 7A, bottom panel). We first increased the robustness of the PWM algorithm by combining the phosphorylation sites identified in our screen with the well-validated AMPK sites, generating a matrix from 109 AMPK phosphorylation sites (Figure S7E, *List S6*). We then scored and ranked the motifs of sites in each phosphoproteomic dataset (Figures S7E and S7F, see *Experimental Procedures*). This analysis identified 630 AMPK-like phosphorylation sites in the ischemia dataset and 266 in the cell-cycle dataset (Figures 7D and 7E; Figure S7F;

A

Uniprot	Protein	Identified Phosphosite	Times Seen	Previously Identified?	Validated?	Function
O60716	CTNND1	S268	11			promotes stability of cadherin-catenin cell-cell adhesion complexes
Q9UHR4	BAIAP2L1	S329	10	■		promotes clustering of short actin bundles and cell migration
Q96RT1	ERBB2IP	S913 S915 T917	9			Her2 adaptor that inhibits cell migration and mitogenic signaling
<b>Q7Z628</b>	<b>NET1/NET1A</b>	<b>S100/S46</b>	<b>7</b>		<b>yes</b>	<b>RHOA GEF; NET1 regulates proliferation; NET1A regulates migration &amp; invasion</b>
<b>Q00587</b>	<b>CDC42EP1</b>	<b>S192</b>	<b>7</b>		<b>yes</b>	<b>TC10 and CDC42 effector protein; regulates persistent directional migration</b>
Q8IZQ1	WDFY3	S2278	6			autophagy adaptor protein that targets ubiquitinated protein aggregates for degradation
<b>Q95721</b>	<b>SNAP29</b>	<b>S163</b>	<b>6</b>		<b>yes</b>	<b>inhibits disassembly of SNARE complexes; regulates endocytic recycling of β1-integrin</b>
Q86T10	TBC1D1	S237	5	○		RAB GAP that prevents GLUT4 translocation to the cell surface
Q92974	ARHGEF2	S151	5			RHO GEF that controls RHOA activation at the leading edge during cell migration
Q9UQB8	BAIAP2	S366	5	○		essential for induction of membrane ruffling; promotes filopodia formation with CDC42
Q14980	NUMA1	S1853	5			localizes to spindle poles and promotes asymmetric cell division
<b>Q5TCZ1</b>	<b>SH3PXD2A</b>	<b>S1002</b>	<b>4</b>		<b>yes</b>	<b>adaptor protein required for podosome and invadopodia formation and function</b>
Q8N122	RPTOR	S721 S722	4	○		member of the mTORC1 complex; important for its activation
<b>Q9H019</b>	<b>MTFR1L</b>	<b>S103</b>	<b>4</b>		<b>yes</b>	<b>member of the MTFR1 family and could therefore be involved in mitochondrial fission</b>
Q9NNQ7	SLC35C2	S335	4			GDP-fucose transporter required for optimal Notch signaling
P20020	ATP2B1	S1177 S1178	4			Ca2+ transporter localized to plasma membrane
Q9H0B6	KLC2	S545	4	○		facilitates organelle transport
Q5SNT2	TMEM201	S454	4			nuclear envelope transmembrane protein; localizes to the mitotic spindle during mitosis
Q9NQX3	GPHN	S305	4	■		helps immobilize GABA(A)Rs through microtubule binding; may promote mTOR activity
Q99959	PKP2	S82	4			desmosomal component that promotes focal adhesion turnover and cell motility
Q13085	ACC1	S80	4	○		catalyzes long-chain fatty acid biogenesis
Q9P0V3	SH3BP4	S246	4			inhibits mTORC1 activation by preventing mTORC1 localization to the lysosome
<b>Q96PK6</b>	<b>RBM14</b>	<b>T629</b>	<b>4</b>		<b>yes</b>	<b>transcriptional coactivator; works with CREB-binding protein to activate transcription</b>
Q9NYL2	MLTK	S648	4			regulates actin stress fibers and cellular morphology; activates mitogenic signaling
<b>Q15036</b>	<b>SNX17</b>	<b>S437</b>	<b>4</b>		<b>yes</b>	<b>rescues β1-integrins and other transmembrane proteins from lysosomal degradation</b>
Q14683	TP53I11	S14	4			p53 target that promotes apoptosis
Q14974	PPP1R12A	S445	3	■		phosphatase regulatory subunit that regulates cytoskeletal dynamics
P0C7U0	ELFN1	S735	3			postsynaptic regulation of presynaptic neurotransmitter release
Q9Y6M7	SLC4A7	S242	3	■		sodium bicarbonate cotransporter
<b>Q14974</b>	<b>PPP1R12A</b>	<b>S910</b>	<b>3</b>	<b>■</b>		<b>phosphatase regulatory subunit that regulates cytoskeletal dynamics</b>
Q13439	GOLGA4	S89	3	■		trans-Golgi network vesicle transport
Q14639	ABLIM1	S450 S452	3			may regulate axonal guidance

- Known AMPK substrate
- Known AMPK substrate and phosphorylation site

B

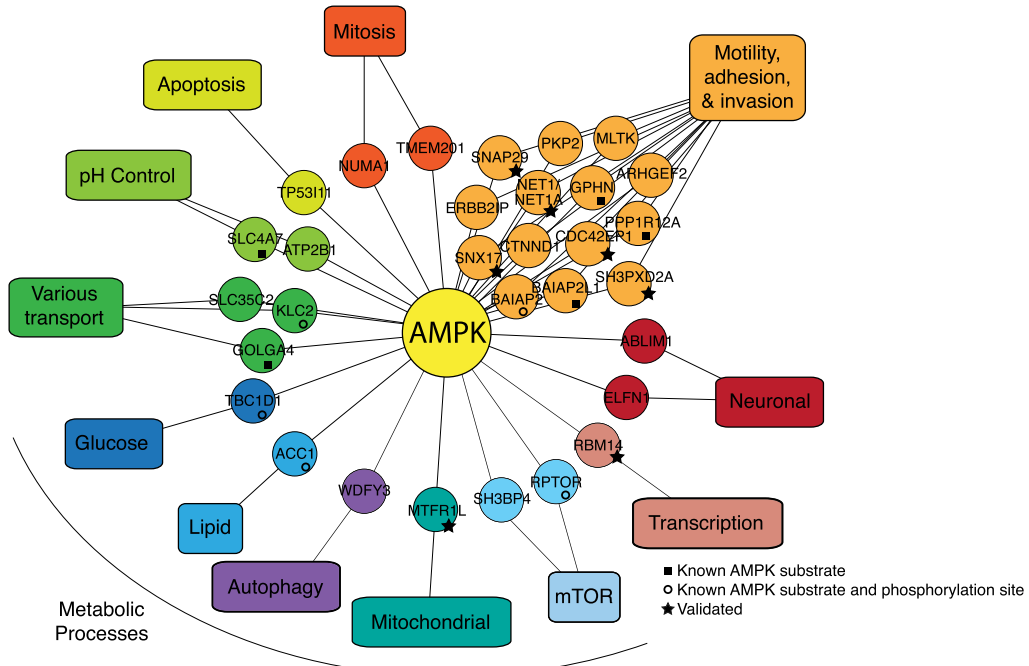


**Figure 4. Many High-Confidence AMPK Substrates Have Known Roles in Cell Motility, Adhesion, and Invasion**

(A) All Group A substrates and the most frequently identified phosphorylation site(s) on the phosphopeptide. “|,” ambiguity in the mass spectrometry placement of the phosphorylation site; “Times seen,” number of biological samples the phosphopeptide was identified in; “Previously identified” indicates whether the phosphorylation site (open circle) or the protein (but not phosphorylation site) (closed square) was a previously known AMPK substrate; “Validated” indicates

*(legend continued on next page)*

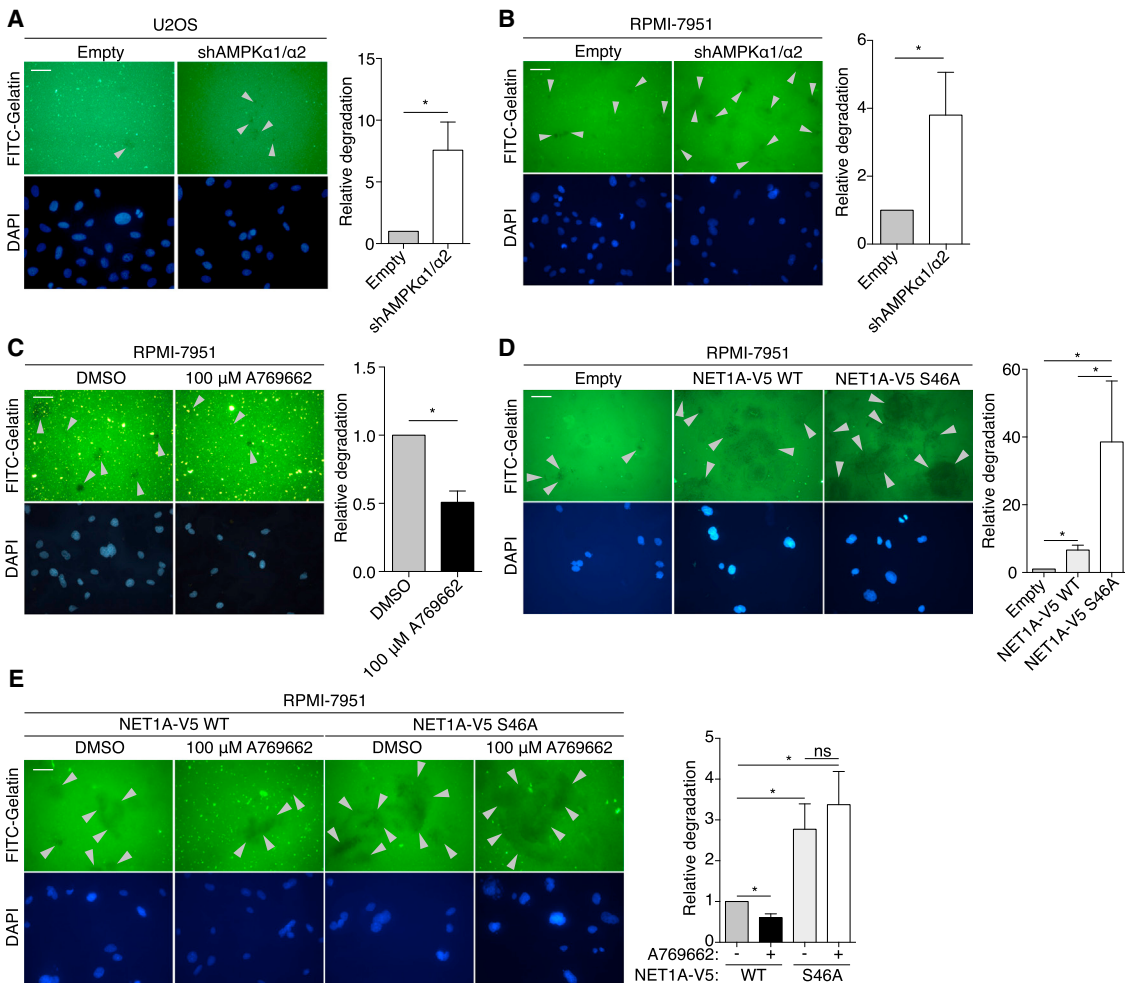


**Figure 5. AMPK Phosphorylation of NET1A Inhibits Extracellular Matrix Degradation**

(A) Knockdown of AMPK increases ECM degradation in U2OS cells. Cells stably expressing an shRNA against both AMPK $\alpha$ 1 and  $\alpha$ 2 or empty vector control (Empty) cells were cultured on fluorescein isothiocyanate (FITC)-conjugated gelatin-coated coverslips for 3 days. Fixed cells were stained for DAPI and analyzed. Grey arrowheads indicate points of gelatin degradation. Within each experiment, approximately 15–20 20 $\times$  fields per sample were quantified and averaged; displayed images are 40 $\times$ . Error bars represent mean  $\pm$  SEM of the averaged values from six independent experiments; the control samples in four of the experiments were the same used in four of the experiments in Figure S5G. \*p < 0.05 by two-tailed Wilcoxon matched-pairs signed-rank test; scale bar, 50  $\mu$ M.

(B) Knockdown of AMPK increases ECM degradation in RPMI-7951 cells. Cells stably expressing an shRNA against both AMPK $\alpha$ 1 and  $\alpha$ 2 or empty vector control cells were analyzed, and results are represented as in Figure 5A. Seven independent experiments were quantified.

(C) Activation of AMPK inhibits ECM degradation. RPMI-7951 cells were plated on FITC-conjugated gelatin-coated coverslips for 3–4 hr prior to administration of 100  $\mu$ M A769662 or DMSO vehicle control for 16 hr. Analysis and results are represented as in Figure 5A. Six independent experiments were quantified.

(D) Loss of the AMPK phosphorylation site on NET1A increases ECM degradation. RPMI-7951 cells expressing similar levels of doxycycline-inducible NET1A-V5 WT or S46A (Figures S5C and S5D) were plated on FITC-conjugated gelatin-coated coverslips and allowed to adhere overnight. 2  $\mu$ g/ml doxycycline was added, and cells were cultured for an additional 2 days. Analysis and results are as in Figure 5A. Six independent experiments were quantified.

(E) Activation of AMPK inhibits ECM degradation in the presence of WT, but not S46A, NET1A. RPMI-7951 cells expressing similar levels of doxycycline-inducible NET1A-V5 WT or S46A (Figures S5C and S5D) were plated on FITC-conjugated gelatin-coated coverslips for 3 hr prior to addition of 2  $\mu$ g/ml doxycycline and either 100  $\mu$ M A769662 or DMSO vehicle control for 20 hr. Media and drugs were replaced with fresh stocks after 10 hr. Analysis and results are represented as in Figure 5A. Six independent experiments were quantified; ns, not significant.

List S7). These AMPK-like sites could be AMPK substrates, although they could also be targets of other related kinases. During ischemia, phosphorylation increased on 150 of the 630

AMPK-like sites and decreased on 28 (Figure 7D, List S7). During mitosis, phosphorylation increased on 74 of the 266 AMPK-like sites and decreased on 13 (Figure 7E; List S7). Of the 131

whether the protein was validated as a substrate of AS-AMPK (Figures 3 and S3). Orange background, proteins with known roles in cell motility, adhesion, or invasion (see Figure S4B); note that two different sites were identified on PPP1R12A. Bold type, validated substrates.

(B) Many Group A substrates are proteins involved in cell motility, adhesion, and invasion. Twelve substrates involved in motility, adhesion, and invasion were classified by mining the literature (Figure S4B), while an additional two were identified using a curated list of GO terms (Figures S4A and S4B).

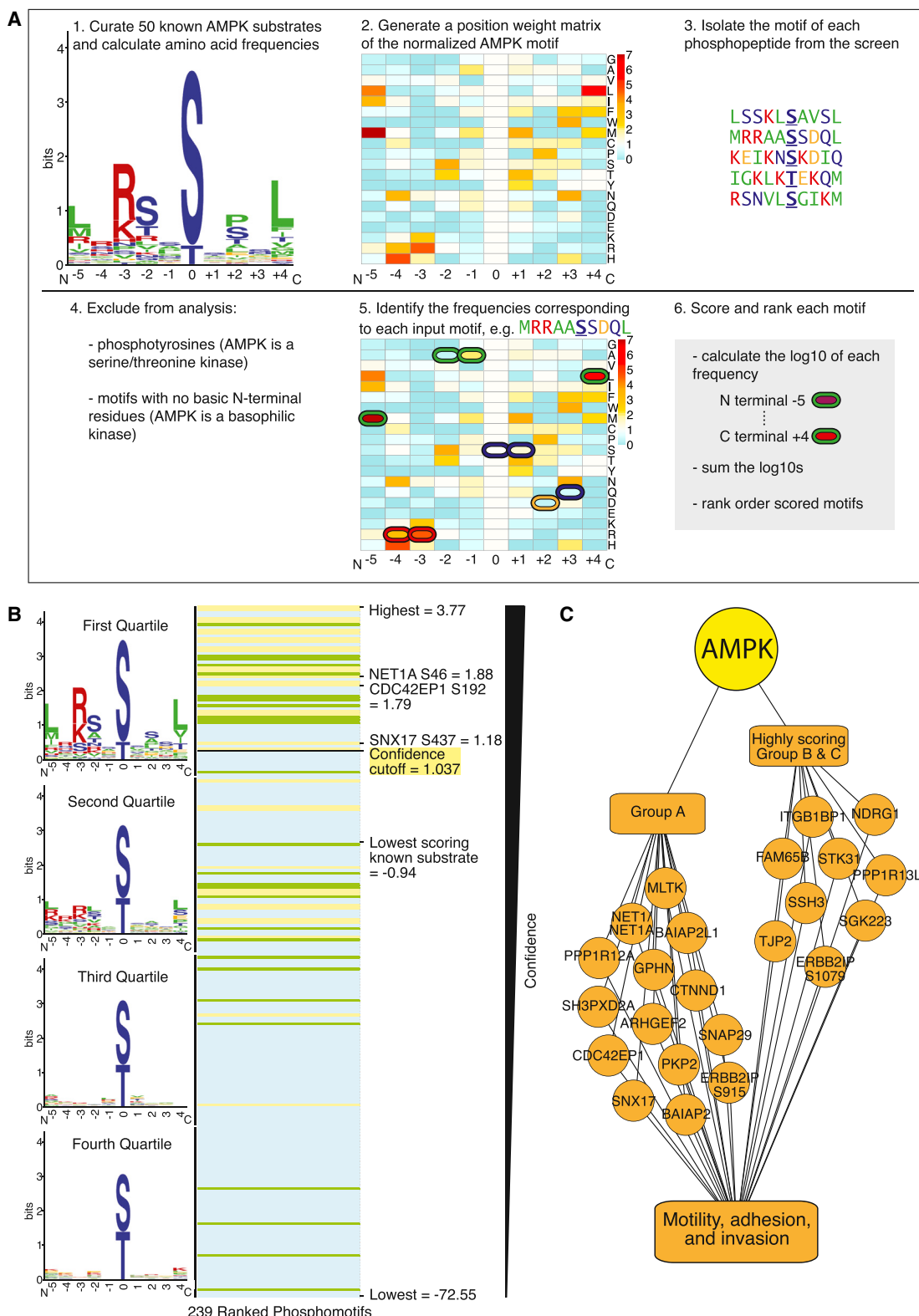


**Figure 6. Use of the AMPK Phosphorylation Motif to Rank Phosphorylation Sites Identified at Low Frequency in the Screen**

(A) Schematic of the pipeline used to score resemblance to the AMPK phosphorylation motif. The logo motif (1.) represents the phosphorylation motif of 50 known *in vivo* AMPK substrates. See Figure 2B for amino acid color coding. The heatmap (2. and 5.) represents the standardized frequencies of the 50 known AMPK substrates, with red indicating enrichment and blue indicating depletion in the AMPK motif compared with background (see Figure S6A).

(legend continued on next page)

AMPK-like sites that were present in both studies ([List S7](#)), 47 increased specifically in either ischemia (25) (e.g., CDC42EP4 S140) or mitosis (22) (e.g., SNX5 S152), while 9 increased in both (e.g., CCDC131 S352 and the Group A substrate TMEM201 S454) ([Figures 7F; List S7](#)). This predictive approach allows rapid identification of potential AMPK substrates and their regulation in different contexts, although this could also reflect experimental conditions and/or contributions of other kinases.

As high-quality phosphoproteomics datasets become available, analyzing AMPK site dynamics and predicting new substrates in context-specific scenarios will likely yield important hypotheses to test experimentally. To facilitate this, we have made both the AMPK motif matrix and our algorithm available to the community at [https://github.com/BrunetLabAMPK/AMPK\\_motif\\_analyzer](https://github.com/BrunetLabAMPK/AMPK_motif_analyzer) (see [Supplemental Experimental Procedures](#)). These tools complement existing resources that scan proteins for specific motifs, such as Scansite ([Obenauer et al., 2003](#)) and MEME (FIMO) ([Bailey et al., 2009; Grant et al., 2011](#)) ([Figure S7G](#)). The comprehensive AMPK motif matrix we generated ([List S6](#)) can also be uploaded to Scansite and MEME to query protein sequences for the presence of AMPK-like motifs ([Figure S7G](#) and [Supplemental Experimental Procedures](#)).

In summary, using a biochemical screen for direct AMPK substrate identification, we identified 57 previously unknown AMPK phosphorylation sites ([Figure 7G](#)), highlighting a role for this energy sensor in cell motility, adhesion, and invasion. We also developed an *in silico* approach to predict AMPK substrates and analyze their phosphorylation dynamics ([Figure 7G](#)), providing resources for future studies on AMPK.

## DISCUSSION

### Identification of Direct AMPK Substrates and Phosphorylation Sites

Our screen is the first large-scale identification of direct kinase substrates and phosphorylation sites in cells and identified 57 previously unknown AMPK phosphorylation sites. Seven substrates and three phosphorylation sites validated as direct targets of AS-AMPK. It is possible that the AS system, which involves digitonin permeabilization and overexpression of a mutated form of the alpha subunit of AMPK, alters the specificity of AMPK. However, our screen identified known substrates of AMPK (e.g., ACC1 S80 and RAPTOR S722), and two of the previously uncharacterized substrates (SNX17 and NET1A) were confirmed to be substrates of endogenous AMPK, suggesting that this screen identified bona fide AMPK targets.

While successful in identifying direct AMPK phosphorylation sites, the screening conditions were subject to background and low saturation. In addition, not all known AMPK substrates were found. Several factors may help explain this. For example, not all tryptic peptides are detectable by mass spectrometry, and the peptide capture approach results in the loss of cysteine-containing peptides from the sample, as they irreversibly bind to the iodoacetyl groups ([Blelloch et al., 2008](#)). Furthermore, some

endogenous kinases may also use the bulky ATP $\gamma$ S. Developing methods to decrease background phosphopeptides and increase retention of bona fide thiophosphopeptides will help make this method more widely applicable to other kinases.

### AMPK Phosphorylates Many Substrates Involved in Cell Motility, Adhesion, and Invasion

An important finding of this screen is the number of substrates involved in different aspects of cell motility, adhesion, and invasion. We found that AMPK inhibits ECM degradation, a key early step in cell invasion, in part through NET1A. NET1A was recently implicated in cell invasion ([Carr et al., 2013](#)), but its importance during ECM degradation and regulation by AMPK were completely unknown. NET1A does not appear to localize to invadopodia (B.E.S. and A.B., unpublished data), but it does localize to focal adhesions and binds focal adhesion kinase (FAK) ([Carr et al., 2013](#)). FAK helps regulate the balance between invadopodia and focal adhesions ([Chan et al., 2009](#)), so AMPK phosphorylation of NET1A could alter the ability of FAK to modulate this balance. Alternatively, phosphorylation of NET1A by AMPK could affect the function of specific invadopodia components. Importantly, AMPK may regulate additional targets to inhibit ECM degradation, including other previously unknown substrates, like the invadopodia component SH3PXD2A ([Seals et al., 2005](#)), or well-known ones such as ACC1. Indeed, ACC1 mediates AMPK-dependent inhibition of ECM degradation ([Scott et al., 2012](#)). As ECM degradation is an initial step in metastasis ([Eckert et al., 2011](#)), these results raise the possibility that AMPK could inhibit early stages of metastasis.

### In Silico Approach to Predict AMPK Phosphorylation Sites in Phosphoproteomics Datasets

Exploring AMPK substrates in different contexts is an important but difficult experimental task, and a well-defined AMPK motif can be used to more accurately predict substrates in other contexts. Previous approaches have successfully used an AMPK motif defined by *in vitro* peptide scanning ([Gwinn et al., 2008](#)) or by mutational analyses of AMPK substrates ([Marin et al., 2015; Towler and Hardie, 2007](#)). Here, we develop an *in silico* approach based on *in vivo* AMPK phosphorylation sites to predict likely AMPK sites in phosphoproteomics datasets, notably quantitative ones. As quantitative datasets already contain information about the dynamics of phosphorylation sites, data are immediately available regarding the regulation of an AMPK-like site in that context. Caveats of this approach are that phosphoproteomic datasets are often generated using different experimental procedures and do not capture all phosphorylated peptides. In addition, the experimental conditions used (e.g., pharmacological cell synchronization) may result in aberrant AMPK activity, and AMPK-like sites may be phosphorylated by other kinases. Nevertheless, comparison of the predicted AMPK phosphorylation sites between different phosphoproteomic datasets could generate hypotheses concerning context-specific phosphorylation.

(B) Ranked list of the scored motifs corresponding to the Group A (yellow lines), B (green lines), and C (blue lines) phosphorylation sites. The logo motif for each quartile of ranked motifs is shown. Scores of interest are noted.

(C) Nine highly scoring Group B and C phosphorylation sites are on proteins with known roles in cell motility, adhesion, and invasion. When combined with Group A, this totals 24 phosphorylation sites on 22 proteins involved in these processes (2 sites are on PPP1R12A and ERBB2IP).

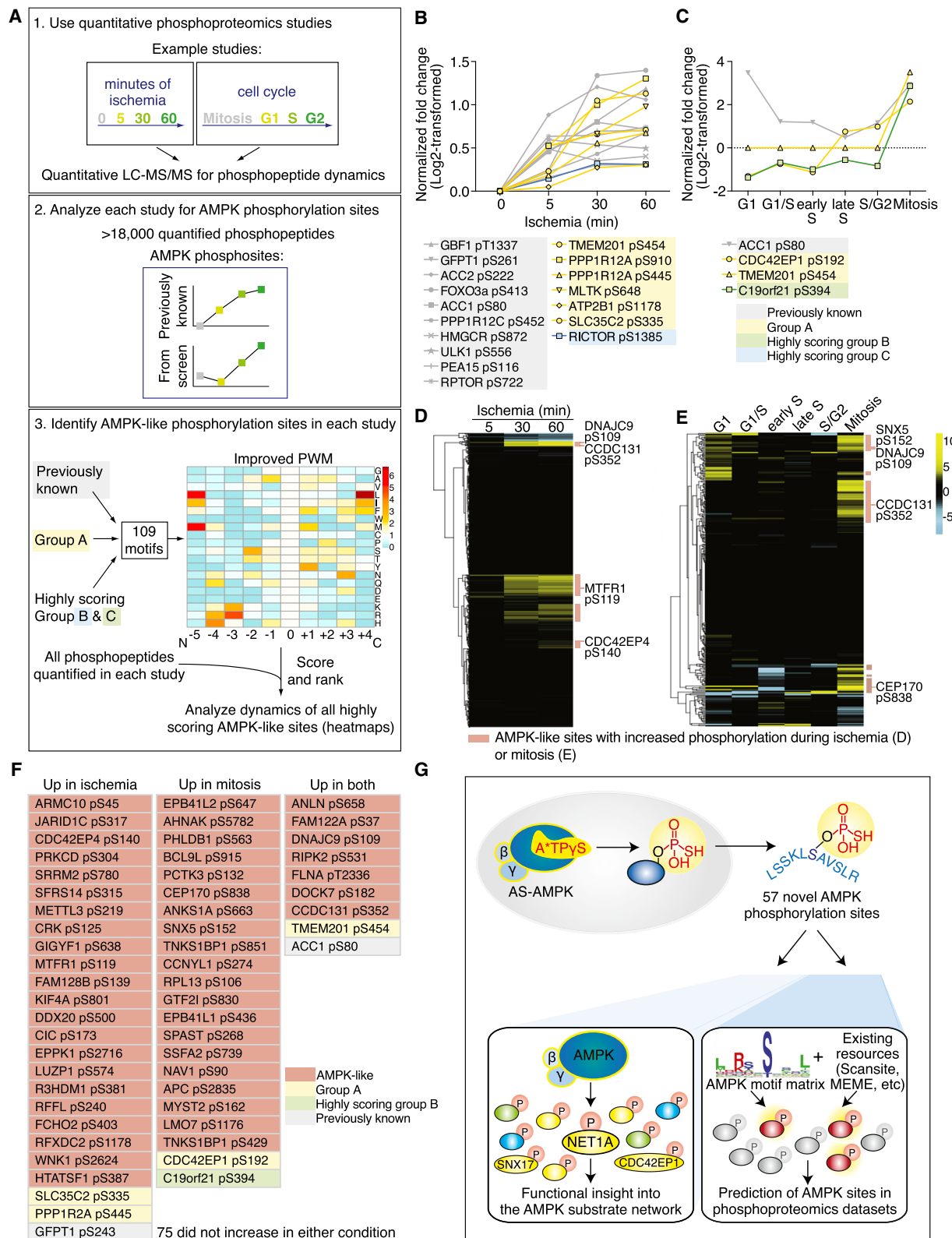


**Figure 7. In Silico Analysis of AMPK Network Dynamics and Prediction of AMPK Phosphorylation Sites**

(A) (1) General schematic of quantitative phosphoproteomic studies. (2) Datasets were queried for the presence of known AMPK phosphorylation sites and their dynamics during the biological processes analyzed. (3) A PWM constructed from 109 AMPK phosphorylation sites from both the literature and this study (List S6)

(legend continued on next page)

Our work provides the first large-scale identification of direct AMPK phosphorylation sites, extending the AMPK network and facilitating the generation of a platform to help predict additional AMPK targets. As promising therapeutic roles of AMPK continue to emerge for diseases like cancer (Kato et al., 2002; Liang and Mills, 2013; Xiang et al., 2004) and diabetes (Winder and Hardie, 1999), as well as for aging (Apfeld et al., 2004; Greer et al., 2007; Mair et al., 2011), the substrates we identified and the platform we created could help properly harness AMPK's full therapeutic potential.

## EXPERIMENTAL PROCEDURES

Full protocols and additional information are provided in the [Supplemental Experimental Procedures](#).

### Thiophosphorylation of AS-AMPK Substrates

In-cell thiophosphorylation of AS-AMPK substrates was performed as in Banko et al. (2011), but without addition of AMP to the thiophosphorylation labeling buffer (see [Supplemental Experimental Procedures](#)). Samples processed for western blot analysis were alkylated using *p*-nitrobenzyl mesylate. Samples generated for peptide capture were processed as outlined below.

### Peptide Capture of Thiophosphorylated Peptides and Identification via Liquid Chromatography-Tandem Mass Spectrometry

Peptide capture of thiophosphorylated peptides was performed according to Blelhow et al. (2008) and Hertz et al. (2010). Experiment-specific modifications to the full protocol detailed under [Supplemental Experimental Procedures](#) are in [List S1](#). LC-MS/MS and processing was performed as in Hengeveld et al. (2012).

### Analysis of Mass Spectrometry Data

Mass spectrometry peaklists were generated with an in-house (UCSF) software named PAVA and searched against the SwissProt *Homo sapiens* database (downloaded on March 21, 2012) using Protein Prospector (version 5.10.10). Phosphopeptides identified in the AS-AMPK samples were compared to those identified in control samples across all experiments (phosphopeptides identified in control samples; [List S2](#), second tab), and overlapping phosphopeptides were removed as background. The peptide, irrespective of phosphosite placement, was used for this filtering step, accounting for possible missed trypsinization events or other peptide overlap. See [Supplemental Experimental Procedures](#) for more details.

### Scoring Phosphorylation Motifs Based on Similarity to the AMPK Motif

To determine the similarity of phosphorylation motifs to the AMPK motif, a position-weight matrix (PWM) was constructed using the frequencies of amino

was generated to score and rank the motifs surrounding each quantified site in (1). The dynamics of sites with motifs scoring above the cutoff ([Figure S7F](#)) were analyzed.

(B) Seventeen AMPK phosphorylation sites present in the ischemia study (Mertins et al., 2014) increased significantly during ischemia (significance determined in Mertins et al., 2014). Sites in yellow are from Group A; blue, highly scoring Group C substrates; gray, previously known. Phosphorylation site location was standardized to isoform 1 in Uniprot. The 5, 30, and 60 min time points were standardized to the 0 min time point and log<sub>2</sub> transformed in Mertins et al. (2014). (C) Four AMPK phosphorylation sites present in the cell-cycle dataset (Olsen et al., 2010) increased at least 2-fold (following log<sub>2</sub> transformation) during mitosis. Sites with yellow lines are from Group A; green, highly scoring Group B substrates; gray, previously known. Site location was standardized to isoform 1 in Uniprot. All time points were standardized to an asynchronously cycling population, normalized to protein level, and log<sub>2</sub> transformed in Olsen et al., (2010).

(D) 630 AMPK-like phosphorylation sites were present in the ischemia dataset, and a subset are dynamically phosphorylated ([List S7](#)). Yellow, relative increase; blue, relative decrease compared to the 0 min time point. The time points were standardized as in [Figure 7B](#) and Mertins et al. (2014).

(E) 266 AMPK-like phosphorylation sites were present in the cell-cycle dataset, and a subset are dynamically phosphorylated ([List S7](#)). Yellow, relative increase; blue, relative decrease compared to an asynchronously cycling population. The relative changes were standardized as in [Figure 7C](#) and Olsen et al. (2010).

(F) Highly scoring AMPK-like sites quantified in both the ischemia and cell-cycle datasets and whose phosphorylation increased during ischemia and/or mitosis. A total of 131 quantified AMPK-like sites were present in both datasets ([List S7](#)). Phosphorylation sites are as reported in the ischemia study (based on protein GI accessions).

(G) Summary of the proteomic and in silico approaches used here to identify AMPK phosphorylation sites and understand the AMPK functional network. The datasets used in [Figure 7](#) are from Mertins et al. (2014), reprinted with permission from ASBMB, and Olsen et al. (2010), reprinted with permission from AAAS.

acids in the motifs surrounding 50 well-validated *in vivo* AMPK phosphorylation sites (see [Supplemental Experimental Procedures](#) and [List S4](#)) ([Figure 6](#)) or 109 AMPK phosphorylation sites that were previously validated or were discovered in our screen ([Figure 7](#)). Each amino acid frequency in the AMPK motif was standardized to a background frequency generated by averaging the amino acid occurrences in 10,000 randomly sampled datasets of matched number and phosphoS:T ratio from a compendium of human phosphorylation sites. Query motifs were scored by summing the log<sub>10</sub> of each location's amino acid standardized frequency from the N-terminal 5 to the C-terminal 4 position. Motifs lacking basic residues within 5 N-terminal amino acids or surrounding phosphotyrosines were discarded. If a phosphopeptide contained more than one possible phosphorylation site, the site with the highest scoring motif was used ([Figure 6](#)). Scored motifs were rank ordered. The standardized frequencies of the 50 well-validated AMPK sites are in the second tab of [List S4](#); those of the 109 AMPK sites are in [List S6](#) (matrix form) and on GitHub (tab-delimited list form). The code to score and rank input motifs is available on GitHub ([https://github.com/BrunetLabAMPK/AMPK\\_motif\\_analyzer](https://github.com/BrunetLabAMPK/AMPK_motif_analyzer)) (see [Supplemental Experimental Procedures](#)).

### Logo Motif Generation

To visualize phosphorylation motifs, logo motifs were generated using Berkeley's WebLogo generator (Crooks et al., 2004; Schneider and Stephens, 1990).

Antibody information, primer sequences and construct generation, cell culture methods, generation of stable cell lines, cell lysis and immunoprecipitation in non-AS-based assays, immunoprecipitation of AS-AMPK substrates, preparation of fluorescein isothiocyanate (FITC)-conjugated gelatin-coated coverslips, analysis of gelatin degradation, using the AMPK motif matrix and GitHub access, and general data plotting and statistical analyses are detailed in the [Supplemental Experimental Procedures](#).

## SUPPLEMENTAL INFORMATION

Supplemental Information includes Supplemental Experimental Procedures, seven figures, and seven lists and can be found with this article online at <http://dx.doi.org/10.1016/j.cmet.2015.09.009>.

## AUTHOR CONTRIBUTIONS

B.E.S. and A.B. designed the study. B.E.S. conducted all the experiments, unless otherwise indicated, and constructed the pipelines for data analysis. N.T.H. and R.S.L. contributed equally: they helped develop the peptide capture approach and conducted mass spectrometry experiments under the supervision of K.M.S. T.J.M. and R.J.S. provided intellectual contributions and mentorship to B.E.S. M.L.S. performed most of the extracellular matrix degradation assays and some western blots. P.E.H. designed and conducted assays to detect NET1A phosphorylation under the guidance of R.J.S. B.A.B. provided guidance in computational analyses. M.R.B. cloned several AMPK $\alpha$ 1 constructs. K.M.S. provided intellectual contributions for the analog-specific system. R.J.S. and K.M.S. had equal

contributions. B.E.S. and A.B. wrote the paper, and other authors commented on the manuscript.

#### ACKNOWLEDGMENTS

We thank Lauren Booth, Salah Mahmoudi, Itamar Harel, Elizabeth Pollina, Aaron Daugherty, Parag Mallick, Elizabeth Schroeder, Josh Elias, and Monte Winslow for helpful discussion and carefully reading the manuscript. We thank Param Priya Singh for establishing the GitHub repository and verifying the Perl codes, Aaron Daugherty and Katja Hebestreit for verifying R and Perl codes, and Carman Li and Tyler Jacks for the protocol on FITC-gelatin-coated coverslip preparation. This work was supported by grants CIRM RB4-06087 and NIH R01 AG031198 (A.B.), NSF GRFP (B.E.S.), the Robert M. and Anne T. Bass Stanford Graduate Fellowship (B.E.S.), NIH T32 CA09302 (B.E.S.), Howard Hughes Medical Institute (K.M.S.), and NIH R01 DK080425 and P01 CA120964 (R.J.S.). Mass spectrometry was provided by the Bio-Organic Biomedical Mass Spectrometry Resource at UCSF (A.L. Burlingame, Director), supported by the Biomedical Technology Research Centers program of the NIH National Institute of General Medical Sciences, NIH NIGMS 8P41GM103481 (the Thermo Scientific LTQ-Orbitrap Velos is specifically supported by P41GM103481 and Howard Hughes Medical Institute), and the Vincent Coates Foundation Mass Spectrometry Laboratory, Stanford University Mass Spectrometry, with specific thanks to Chris Adams and NIH S10RR027425 (National Center For Research Resources).

Received: January 9, 2015

Revised: July 28, 2015

Accepted: September 8, 2015

Published: October 8, 2015

#### REFERENCES

- Amato, S., Liu, X., Zheng, B., Cantley, L., Rakic, P., and Man, H.Y. (2011). AMP-activated protein kinase regulates neuronal polarization by interfering with PI 3-kinase localization. *Science* 332, 247–251.
- Andersson, U., Filipsson, K., Abbott, C.R., Woods, A., Smith, K., Bloom, S.R., Carling, D., and Small, C.J. (2004). AMP-activated protein kinase plays a role in the control of food intake. *J. Biol. Chem.* 279, 12005–12008.
- Apfeld, J., O'Connor, G., McDonagh, T., DiStefano, P.S., and Curtis, R. (2004). The AMP-activated protein kinase AAK-2 links energy levels and insulin-like signals to lifespan in *C. elegans*. *Genes Dev.* 18, 3004–3009.
- Bailey, T.L., Boden, M., Buske, F.A., Frith, M., Grant, C.E., Clementi, L., Ren, J., Li, W.W., and Noble, W.S. (2009). MEME SUITE: tools for motif discovery and searching. *Nucleic Acids Res.* 37, W202–W208.
- Banko, M.R., Allen, J.J., Schaffer, B.E., Wilker, E.W., Tsou, P., White, J.L., Villén, J., Wang, B., Kim, S.R., Sakamoto, K., et al. (2011). Chemical genetic screen for AMPK $\alpha$ 2 substrates uncovers a network of proteins involved in mitosis. *Mol. Cell* 44, 878–892.
- Bettencourt-Dias, M., Giet, R., Sinka, R., Mazumdar, A., Lock, W.G., Balloux, F., Zafiropoulos, P.J., Yamaguchi, S., Winter, S., Carthew, R.W., et al. (2004). Genome-wide survey of protein kinases required for cell cycle progression. *Nature* 432, 980–987.
- Blethrow, J.D., Glavy, J.S., Morgan, D.O., and Shokat, K.M. (2008). Covalent capture of kinase-specific phosphopeptides reveals Cdk1-cyclin B substrates. *Proc. Natl. Acad. Sci. USA* 105, 1442–1447.
- Bowden, E.T., Coopman, P.J., and Mueller, S.C. (2001). Invadopodia: unique methods for measurement of extracellular matrix degradation in vitro. *Methods Cell Biol.* 63, 613–627.
- Burkewitz, K., Zhang, Y., and Mair, W.B. (2014). AMPK at the nexus of energetics and aging. *Cell Metab.* 20, 10–25.
- Carr, H.S., Zuo, Y., Oh, W., and Frost, J.A. (2013). Regulation of focal adhesion kinase activation, breast cancer cell motility, and amoeboid invasion by the RhoA guanine nucleotide exchange factor Net1. *Mol. Cell. Biol.* 33, 2773–2786.
- Chan, K.T., Cortesio, C.L., and Huttenlocher, A. (2009). FAK alters invadopodia and focal adhesion composition and dynamics to regulate breast cancer invasion. *J. Cell Biol.* 185, 357–370.
- Chen, S., Murphy, J., Toth, R., Campbell, D.G., Morrice, N.A., and Mackintosh, C. (2008). Complementary regulation of TBC1D1 and AS160 by growth factors, insulin and AMPK activators. *Biochem. J.* 409, 449–459.
- Cool, B., Zinker, B., Chiou, W., Kifle, L., Cao, N., Perham, M., Dickinson, R., Adler, A., Gagne, G., Iyengar, R., et al. (2006). Identification and characterization of a small molecule AMPK activator that treats key components of type 2 diabetes and the metabolic syndrome. *Cell Metab.* 3, 403–416.
- Crooks, G.E., Hon, G., Chandonia, J.M., and Brenner, S.E. (2004). WebLogo: a sequence logo generator. *Genome Res.* 14, 1188–1190.
- Dale, S., Wilson, W.A., Edelman, A.M., and Hardie, D.G. (1995). Similar substrate recognition motifs for mammalian AMP-activated protein kinase, higher plant HMG-CoA reductase kinase-A, yeast SNF1, and mammalian calmodulin-dependent protein kinase I. *FEBS Lett.* 361, 191–195.
- Davies, S.P., Sim, A.T., and Hardie, D.G. (1990). Location and function of three sites phosphorylated on rat acetyl-CoA carboxylase by the AMP-activated protein kinase. *Eur. J. Biochem.* 187, 183–190.
- Ducharme, N.A., Hales, C.M., Lapierre, L.A., Ham, A.J., Oztan, A., Apodaca, G., and Goldenring, J.R. (2006). MARK2/EMK1/Par-1Balpha phosphorylation of Rab11-family interacting protein 2 is necessary for the timely establishment of polarity in Madin-Darby canine kidney cells. *Mol. Biol. Cell* 17, 3625–3637.
- Ducommun, S., Deak, M., Sumpton, D., Ford, R.J., Núñez Galindo, A., Kussmann, M., Viollet, B., Steinberg, G.R., Foretz, M., Dayon, L., et al. (2015). Motif affinity and mass spectrometry proteomic approach for the discovery of cellular AMPK targets: identification of mitochondrial fission factor as a new AMPK substrate. *Cell. Signal.* 27, 978–988.
- Eckert, M.A., Lwin, T.M., Chang, A.T., Kim, J., Danis, E., Ohno-Machado, L., and Yang, J. (2011). Twist1-induced invadopodia formation promotes tumor metastasis. *Cancer Cell* 19, 372–386.
- Egan, D.F., Shackelford, D.B., Mihaylova, M.M., Gelino, S., Kohnz, R.A., Mair, W., Vasquez, D.S., Joshi, A., Gwinn, D.M., Taylor, R., et al. (2011). Phosphorylation of ULK1 (HATG1) by AMP-activated protein kinase connects energy sensing to mitophagy. *Science* 331, 456–461.
- Goodwin, J.M., Svensson, R.U., Lou, H.J., Winslow, M.M., Turk, B.E., and Shaw, R.J. (2014). An AMPK-independent signaling pathway downstream of the LKB1 tumor suppressor controls Snail1 and metastatic potential. *Mol. Cell* 55, 436–450.
- Grant, C.E., Bailey, T.L., and Noble, W.S. (2011). FIMO: scanning for occurrences of a given motif. *Bioinformatics* 27, 1017–1018.
- Greer, E.L., Dowlatshahi, D., Banko, M.R., Villen, J., Hoang, K., Blanchard, D., Gygi, S.P., and Brunet, A. (2007). An AMPK-FOXO pathway mediates longevity induced by a novel method of dietary restriction in *C. elegans*. *Curr. Biol.* 17, 1646–1656.
- Gwinn, D.M., Shackelford, D.B., Egan, D.F., Mihaylova, M.M., Mery, A., Vasquez, D.S., Turk, B.E., and Shaw, R.J. (2008). AMPK phosphorylation of raptor mediates a metabolic checkpoint. *Mol. Cell* 30, 214–226.
- Hardie, D.G., and Ashford, M.L. (2014). AMPK: regulating energy balance at the cellular and whole body levels. *Physiology (Bethesda)* 29, 99–107.
- Hardie, D.G., and Carling, D. (1997). The AMP-activated protein kinase—fuel gauge of the mammalian cell? *Eur. J. Biochem.* 246, 259–273.
- Hawley, S.A., Fullerton, M.D., Ross, F.A., Schertzer, J.D., Chevtzoff, C., Walker, K.J., Peggie, M.W., Zibrova, D., Green, K.A., Mustard, K.J., et al. (2012). The ancient drug salicylate directly activates AMP-activated protein kinase. *Science* 336, 918–922.
- Hengeveld, R.C., Hertz, N.T., Vromans, M.J., Zhang, C., Burlingame, A.L., Shokat, K.M., and Lens, S.M. (2012). Development of a chemical genetic approach for human aurora B kinase identifies novel substrates of the chromosomal passenger complex. *Mol. Cell. Proteomics* 11, 47–59.
- Hertz, N.T., Wang, B.T., Allen, J.J., Zhang, C., Dar, A.C., Burlingame, A.L., and Shokat, K.M. (2010). Chemical genetic approach for kinase-substrate mapping by covalent capture of thiophosphopeptides and analysis by mass spectrometry. *Curr. Protoc. Chem. Biol.* 2, 15–36.
- Johnson, C., Tinti, M., Wood, N.T., Campbell, D.G., Toth, R., Dubois, F., Geraghty, K.M., Wong, B.H., Brown, L.J., Tyler, J., et al. (2011). Visualization

- and biochemical analyses of the emerging mammalian 14-3-3-phosphoproteome. *Mol. Cell. Proteomics* 10, 005751.
- Kato, K., Ogura, T., Kishimoto, A., Minegishi, Y., Nakajima, N., Miyazaki, M., and Esumi, H. (2002). Critical roles of AMP-activated protein kinase in constitutive tolerance of cancer cells to nutrient deprivation and tumor formation. *Oncogene* 21, 6082–6090.
- Kudo, N., Barr, A.J., Barr, R.L., Desai, S., and Lopaschuk, G.D. (1995). High rates of fatty acid oxidation during reperfusion of ischemic hearts are associated with a decrease in malonyl-CoA levels due to an increase in 5'-AMP-activated protein kinase inhibition of acetyl-CoA carboxylase. *J. Biol. Chem.* 270, 17513–17520.
- Kurth-Kraczek, E.J., Hirshman, M.F., Goodyear, L.J., and Winder, W.W. (1999). 5' AMP-activated protein kinase activation causes GLUT4 translocation in skeletal muscle. *Diabetes* 48, 1667–1671.
- Lee, J.H., Koh, H., Kim, M., Kim, Y., Lee, S.Y., Karess, R.E., Lee, S.H., Shong, M., Kim, J.M., Kim, J., and Chung, J. (2007). Energy-dependent regulation of cell structure by AMP-activated protein kinase. *Nature* 447, 1017–1020.
- Liang, J., and Mills, G.B. (2013). AMPK: a contextual oncogene or tumor suppressor? *Cancer Res.* 73, 2929–2935.
- Liu, D., Shi, M., Duan, C., Chen, H., Hu, Y., Yang, Z., Duan, H., and Guo, N. (2013). Downregulation of Erbin in Her2-overexpressing breast cancer cells promotes cell migration and induces trastuzumab resistance. *Mol. Immunol.* 56, 104–112.
- Mair, W., Morantte, I., Rodrigues, A.P., Manning, G., Montminy, M., Shaw, R.J., and Dillin, A. (2011). Lifespan extension induced by AMPK and calcineurin is mediated by CRTC-1 and CREB. *Nature* 470, 404–408.
- Marin, T.L., Gongol, B., Martin, M., King, S.J., Smith, L., Johnson, D.A., Subramaniam, S., Chien, S., and Shyy, J.Y. (2015). Identification of AMP-activated protein kinase targets by a consensus sequence search of the proteome. *BMC Syst. Biol.* 9, 13.
- Mertins, P., Yang, F., Liu, T., Mani, D.R., Petyuk, V.A., Gillette, M.A., Clouser, K.R., Qiao, J.W., Gritsenko, M.A., Moore, R.J., et al. (2014). Ischemia in tumors induces early and sustained phosphorylation changes in stress kinase pathways but does not affect global protein levels. *Mol. Cell. Proteomics* 13, 1690–1704.
- Nakano, A., Kato, H., Watanabe, T., Min, K.D., Yamazaki, S., Asano, Y., Seguchi, O., Higo, S., Shintani, Y., Asanuma, H., et al. (2010). AMPK controls the speed of microtubule polymerization and directional cell migration through CLIP-170 phosphorylation. *Nat. Cell Biol.* 12, 583–590.
- Obenauer, J.C., Cantley, L.C., and Yaffe, M.B. (2003). Scansite 2.0: Proteome-wide prediction of cell signaling interactions using short sequence motifs. *Nucleic Acids Res.* 31, 3635–3641.
- Olsen, J.V., Vermeulen, M., Santamaria, A., Kumar, C., Miller, M.L., Jensen, L.J., Gnad, F., Cox, J., Jensen, T.S., Nigg, E.A., et al. (2010). Quantitative phosphoproteomics reveals widespread full phosphorylation site occupancy during mitosis. *Sci. Signal.* 3, ra3.
- Russell, R.R., 3rd, Li, J., Coven, D.L., Pypaert, M., Zechner, C., Palmeri, M., Giordano, F.J., Mu, J., Birnbaum, M.J., and Young, L.H. (2004). AMP-activated protein kinase mediates ischemic glucose uptake and prevents postischemic cardiac dysfunction, apoptosis, and injury. *J. Clin. Invest.* 114, 495–503.
- Schneider, T.D., and Stephens, R.M. (1990). Sequence logos: a new way to display consensus sequences. *Nucleic Acids Res.* 18, 6097–6100.
- Scott, J.W., Norman, D.G., Hawley, S.A., Kontogiannis, L., and Hardie, D.G. (2002). Protein kinase substrate recognition studied using the recombinant catalytic domain of AMP-activated protein kinase and a model substrate. *J. Mol. Biol.* 317, 309–323.
- Scott, K.E., Wheeler, F.B., Davis, A.L., Thomas, M.J., Ntambi, J.M., Seals, D.F., and Kridel, S.J. (2012). Metabolic regulation of invadopodia and invasion by acetyl-CoA carboxylase 1 and de novo lipogenesis. *PLoS ONE* 7, e29761.
- Seals, D.F., Azucena, E.F., Jr., Pass, I., Tesfay, L., Gordon, R., Woodrow, M., Resau, J.H., and Courtneidge, S.A. (2005). The adaptor protein Tks5/Fish is required for podosome formation and function, and for the protease-driven invasion of cancer cells. *Cancer Cell* 7, 155–165.
- Shah, K., Liu, Y., Deirmengian, C., and Shokat, K.M. (1997). Engineering unnatural nucleotide specificity for Rous sarcoma virus tyrosine kinase to uniquely label its direct substrates. *Proc. Natl. Acad. Sci. USA* 94, 3565–3570.
- Sim, A.T., and Hardie, D.G. (1988). The low activity of acetyl-CoA carboxylase in basal and glucagon-stimulated hepatocytes is due to phosphorylation by the AMP-activated protein kinase and not cyclic AMP-dependent protein kinase. *FEBS Lett.* 233, 294–298.
- Simonsen, A., Birkeland, H.C., Gillooly, D.J., Mizushima, N., Kuma, A., Yoshimori, T., Slagsvold, T., Brech, A., and Stenmark, H. (2004). Alfy, a novel FYVE-domain-containing protein associated with protein granules and autophagic membranes. *J. Cell Sci.* 117, 4239–4251.
- Towler, M.C., and Hardie, D.G. (2007). AMP-activated protein kinase in metabolic control and insulin signaling. *Circ. Res.* 100, 328–341.
- Vazquez-Martin, A., Oliveras-Ferraro, C., and Menendez, J.A. (2009). The active form of the metabolic sensor: AMP-activated protein kinase (AMPK) directly binds the mitotic apparatus and travels from centrosomes to the spindle midzone during mitosis and cytokinesis. *Cell Cycle* 8, 2385–2398.
- Wang, Z., Wilson, W.A., Fujino, M.A., and Roach, P.J. (2001). Antagonistic controls of autophagy and glycogen accumulation by Snf1p, the yeast homolog of AMP-activated protein kinase, and the cyclin-dependent kinase Pho85p. *Mol. Cell. Biol.* 21, 5742–5752.
- Winder, W.W., and Hardie, D.G. (1999). AMP-activated protein kinase, a metabolic master switch: possible roles in type 2 diabetes. *Am. J. Physiol.* 277, E1–E10.
- Xiang, X., Saha, A.K., Wen, R., Ruderman, N.B., and Luo, Z. (2004). AMP-activated protein kinase activators can inhibit the growth of prostate cancer cells by multiple mechanisms. *Biochem. Biophys. Res. Commun.* 321, 161–167.
- Yuan, J., Ossendorf, C., Szatkowski, J.P., Bronk, J.T., Maran, A., Yaszemski, M., Bolander, M.E., Sarkar, G., and Fuchs, B. (2009). Osteoblastic and osteolytic human osteosarcomas can be studied with a new xenograft mouse model producing spontaneous metastases. *Cancer Invest.* 27, 435–442.
- Zadra, G., Photopoulos, C., Tyekucheva, S., Heidari, P., Weng, Q.P., Fedele, G., Liu, H., Scaglia, N., Priolo, C., Sicinska, E., et al. (2014). A novel direct activator of AMPK inhibits prostate cancer growth by blocking lipogenesis. *EMBO Mol. Med.* 6, 519–538.
- Zhang, H., Zha, X., Tan, Y., Hornbeck, P.V., Mastrangelo, A.J., Alessi, D.R., Polakiewicz, R.D., and Comb, M.J. (2002). Phosphoprotein analysis using antibodies broadly reactive against phosphorylated motifs. *J. Biol. Chem.* 277, 39379–39387.
- Zhang, L., Li, J., Young, L.H., and Caplan, M.J. (2006). AMP-activated protein kinase regulates the assembly of epithelial tight junctions. *Proc. Natl. Acad. Sci. USA* 103, 17272–17277.
- Zheng, B., and Cantley, L.C. (2007). Regulation of epithelial tight junction assembly and disassembly by AMP-activated protein kinase. *Proc. Natl. Acad. Sci. USA* 104, 819–822.
- Zhou, G., Myers, R., Li, Y., Chen, Y., Shen, X., Fenyk-Melody, J., Wu, M., Ventre, J., Doeberer, T., Fujii, N., et al. (2001). Role of AMP-activated protein kinase in mechanism of metformin action. *J. Clin. Invest.* 108, 1167–1174.

**Cell Metabolism, Volume 22**

**Supplemental Information**

**Identification of AMPK Phosphorylation Sites Reveals a Network of Proteins Involved in Cell Invasion and Facilitates Large-Scale Substrate Prediction**

Bethany E. Schaffer, Rebecca S. Levin, Nicholas T. Hertz, Travis J. Maures, Michael L. Schoof, Pablo E. Hollstein, Bérénice A. Benayoun, Max R. Banko, Reuben J. Shaw, Kevan M. Shokat, and Anne Brunet

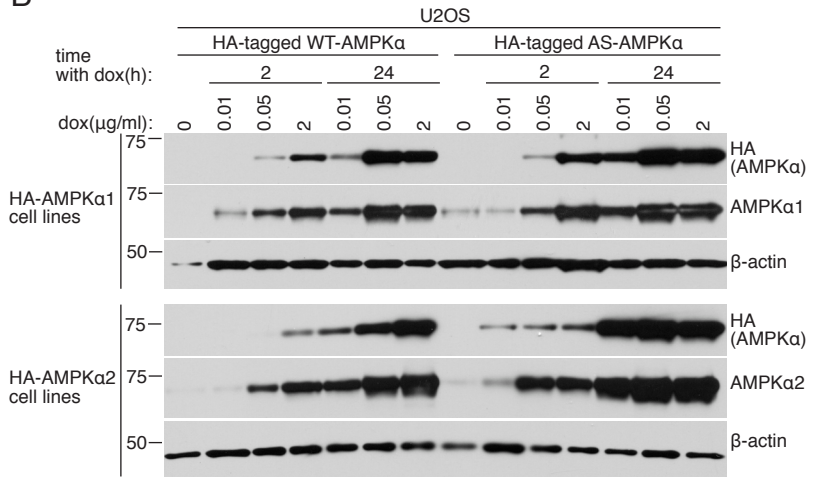
Figure S1, related to Figure 1

A

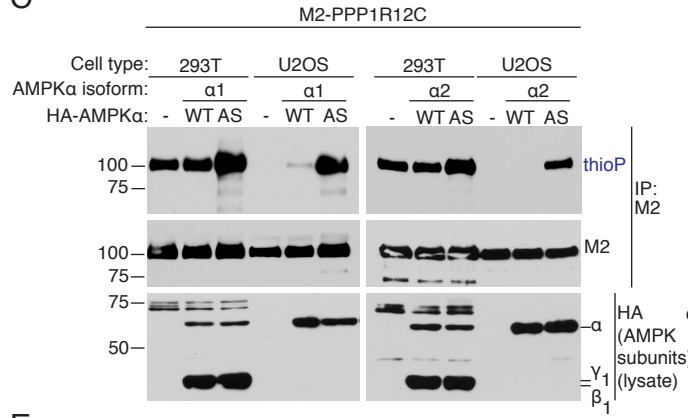
AMPK $\alpha$ 1 residue:	96
H.s. AMPK $\alpha$ 1	S D I F M V
H.s. AMPK $\alpha$ 2	T D F F M V
H.s. CDK2	N K L Y L V
M.m. Jnk1	Q D V Y I V
M.m. Pka ca	S N L Y M V
S.c. CDC28	H K L Y L V
S.c. CLA4	E E L W V I

Modified from Banko et al, 2011

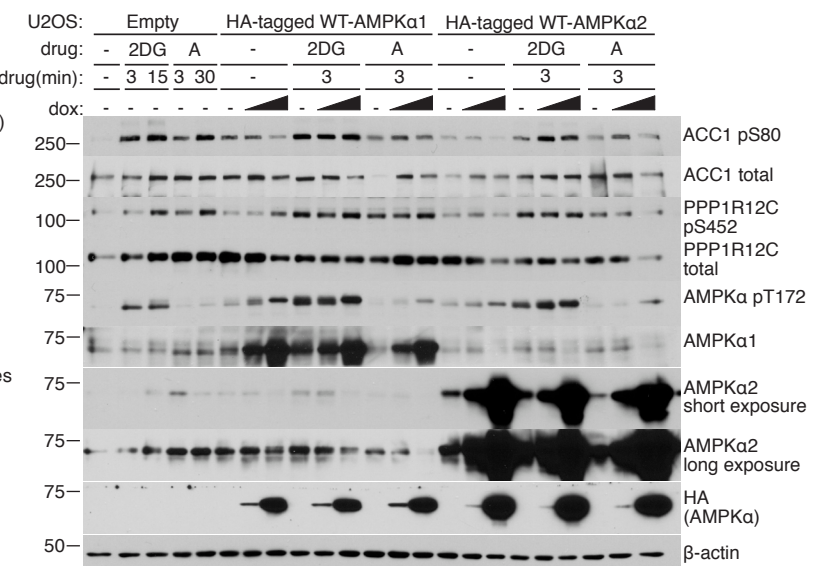
B



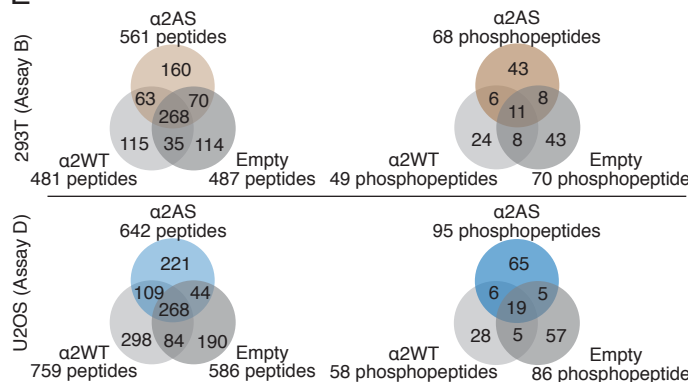
C



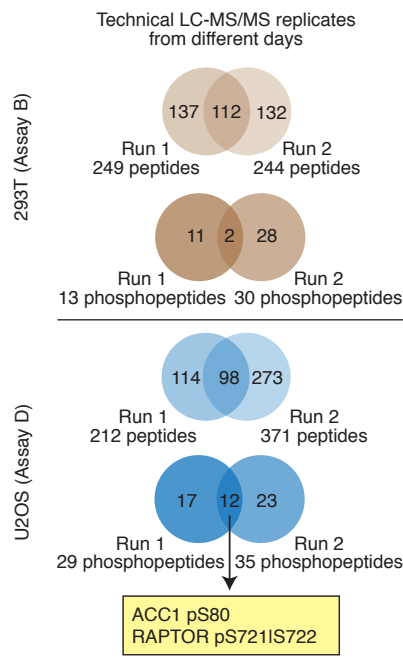
D



E



F



G

Summary of phosphopeptide identification by LC-MS/MS in different biological experiments

Cell type	AMPK activator	Assay ID	dox( $\mu$ g/ml; incubation time)	AS-AMPK isoform	Total phosphopeptides identified				AS-specific phosphopeptides
					AS	Empty	$\alpha$ 1WT	$\alpha$ 2WT	
293T	(-)serum + 2DG	A	n/a	$\alpha$ 2	170	159	NA	147	73 59
		B	n/a	$\alpha$ 2	101	101	NA	70	50 43
	2DG	C	2 $\mu$ g/ml; overnight	$\alpha$ 1 $\alpha$ 2	164 119	17	81	84	105 74 86 65
		D	2 $\mu$ g/ml; overnight	$\alpha$ 1 $\alpha$ 2	115 138	98	74	77	65 43 89 60
		E	2 $\mu$ g/ml; overnight	$\alpha$ 1 $\alpha$ 2	37 43	28	19	30	23 22 28 22
		F	2 $\mu$ g/ml; overnight	$\alpha$ 1 $\alpha$ 2	69 78	80	72	81	24 23 32 30
		G	0.01 $\mu$ g/ml; 4 hrs (no dox As $\alpha$ 2)	$\alpha$ 1 $\alpha$ 2	49 73	67	60	68	14 14 27 26
		H	2 $\mu$ g/ml; overnight	$\alpha$ 1 $\alpha$ 2	59 43	42	63	39	18 17 14 13
U2OS	A769662	I	2 $\mu$ g/ml; overnight	$\alpha$ 1 $\alpha$ 2	19 109	40	5	12	4 3 74 59
		J	2 $\mu$ g/ml; overnight	$\alpha$ 1 $\alpha$ 2	17 24	17	45	43	11 11 15 15
		K	2 $\mu$ g/ml; overnight	$\alpha$ 1 $\alpha$ 2	57 71	57	57	58	26 24 37 32
		L	2 $\mu$ g/ml; overnight	$\alpha$ 1 $\alpha$ 2	42 53	52	45	42	16 16 23 22
		Total # unique phosphopeptides:				691	822		478

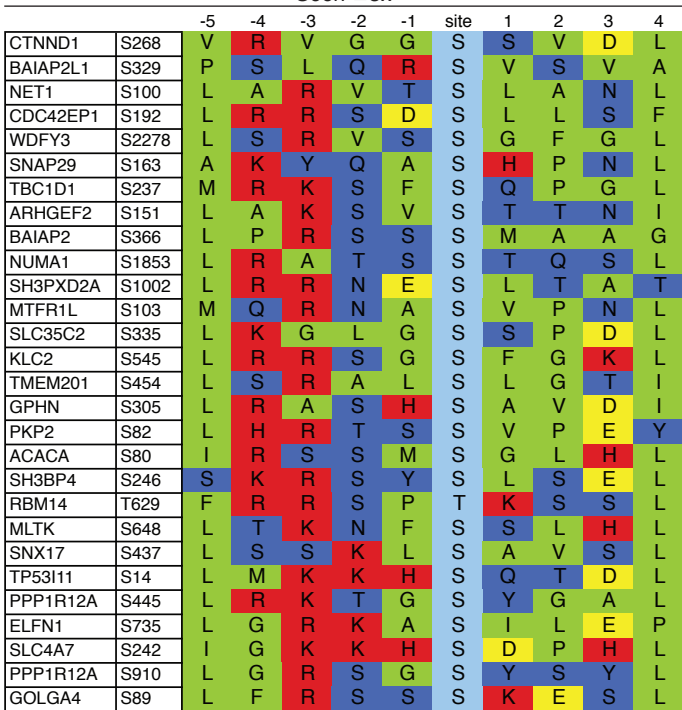
Figure S2, related to Figure 2

A

Protein	Peptide ID #1	Peptide ID #2	Peptide ID #3	Peptide ID #4	Peptide ID #5	Assigned Phosphosite
SLC35C2	S335	S335IS336	S335IS336	S335	S335	S335
TMEM201	S454	S454	S454	S454	-	S454
ABLIM1	S450IS452	S450IS452	S450IT451IS452	S450IS452	S450IT451IS452	?
AHNAK	S572	S570IS572	-	-	-	S572
NAGLU	S581IY583IS585	-	-	-	-	?
DCHS1	S3055	-	-	-	-	S3055

B

Seen ≥3x



C

Seen 2x

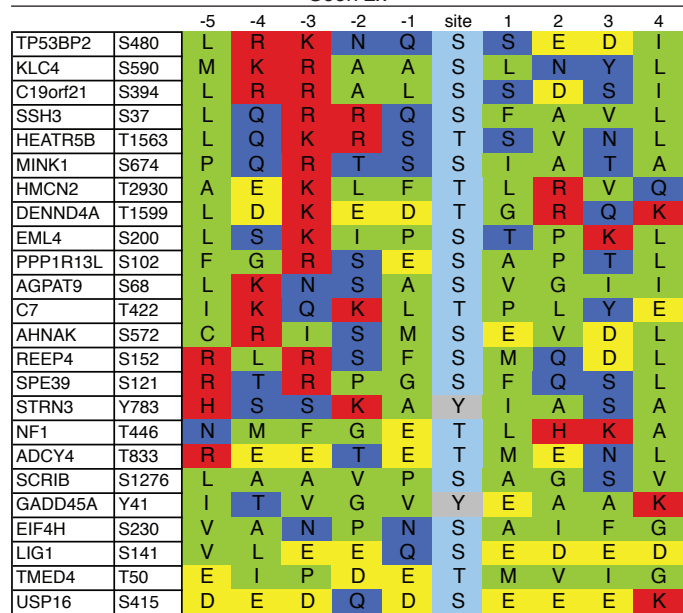


Figure S3, related to Figure 3

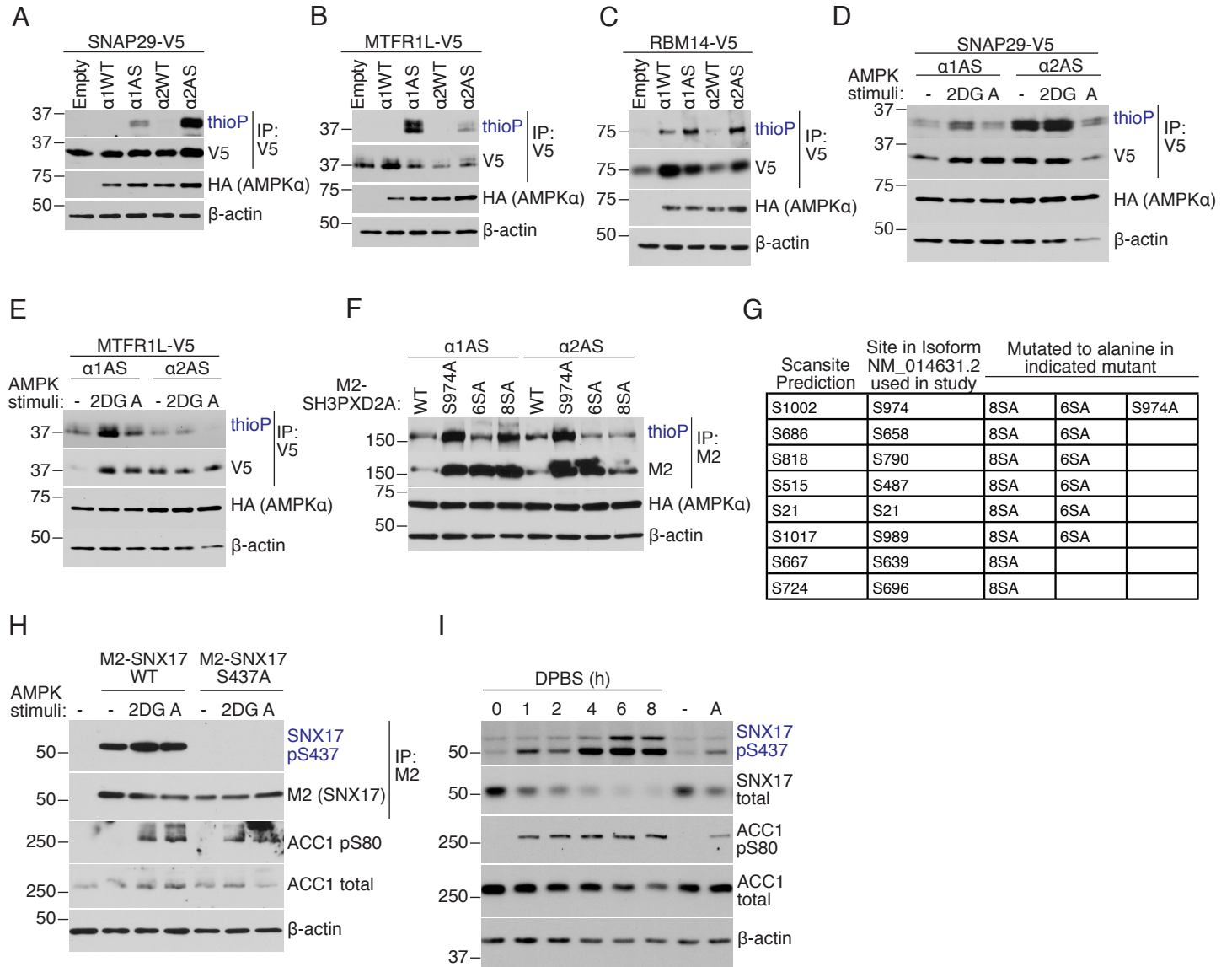


Figure S4, related to Figure 4

A

GO Number	GO Term
GO:0048870	cell motility
GO:0007155	cell adhesion
GO:0030863	cortical cytoskeleton
GO:0014731	spectrin-associated cytoskeleton
GO:0046847	filopodium assembly
GO:0030027	lamellipodium
GO:0071437	invadopodium
GO:0030057	desmosome
GO:0032319	regulation of Rho GTPase activity
GO:0032862	activation of Rho GTPase activity
GO:0005100	Rho GTPase activator activity
GO:0050839	cell adhesion molecule binding
GO:0005925	focal adhesion
GO:0005912	adherens junction
GO:0005201	extracellular matrix structural constituent
GO:0005923	tight junction
GO:2000251	positive regulation of actin cytoskeleton reorganization
GO:0030833	regulation of actin filament polymerization
GO:0030054	cell junction
GO:0001725	stress fiber
GO:0035023	regulation of Rho protein signal transduction
GO:0031274	positive regulation of pseudopodium assembly
GO:0007266	Rho protein signal transduction

B

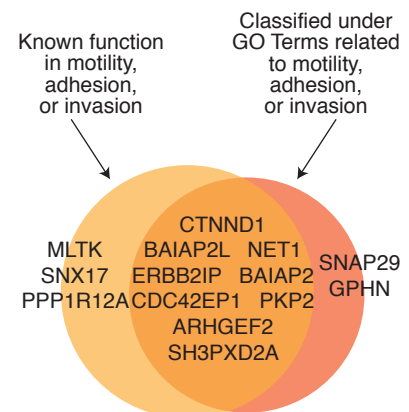


Figure S5, related to Figure 5

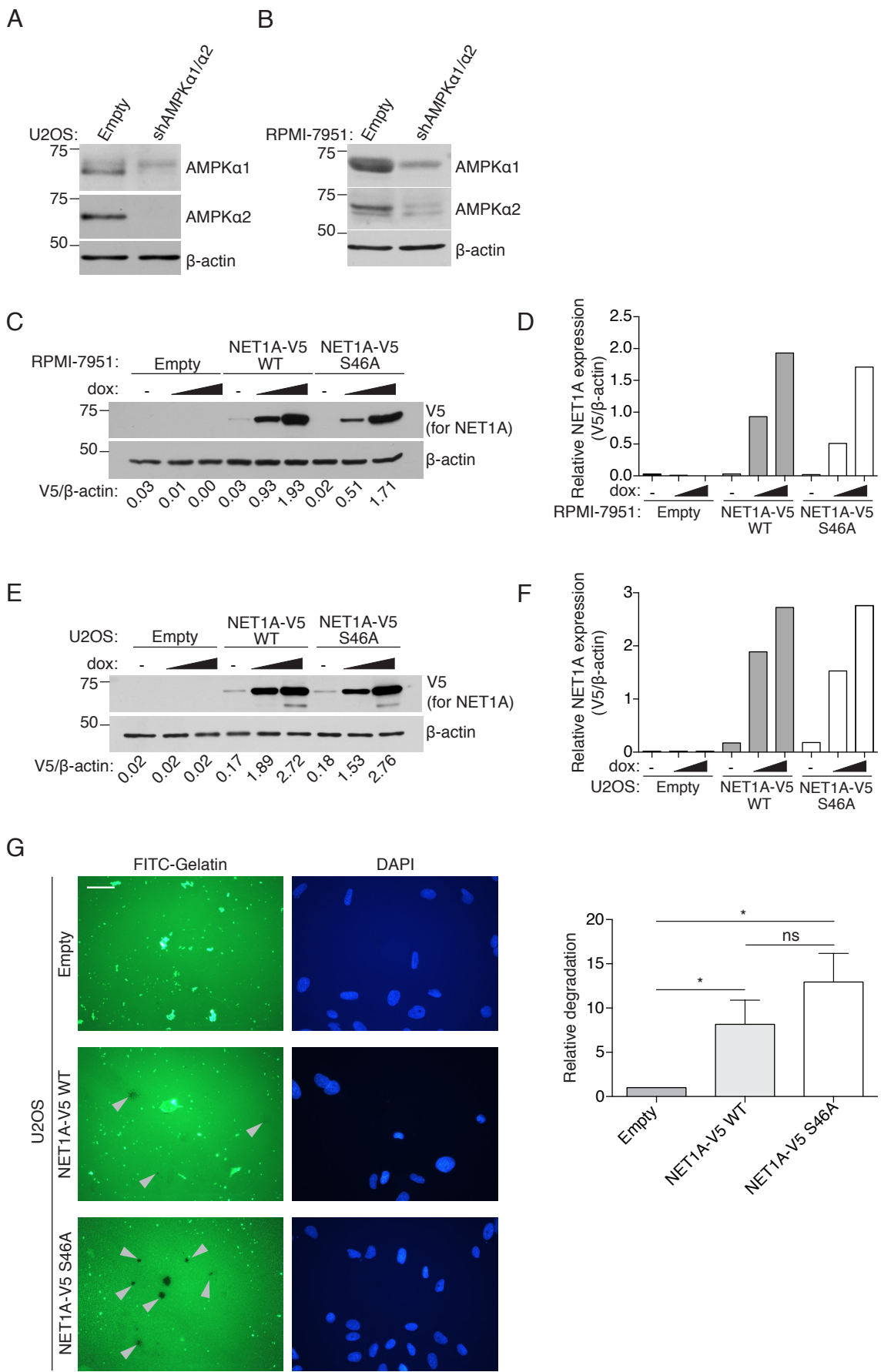
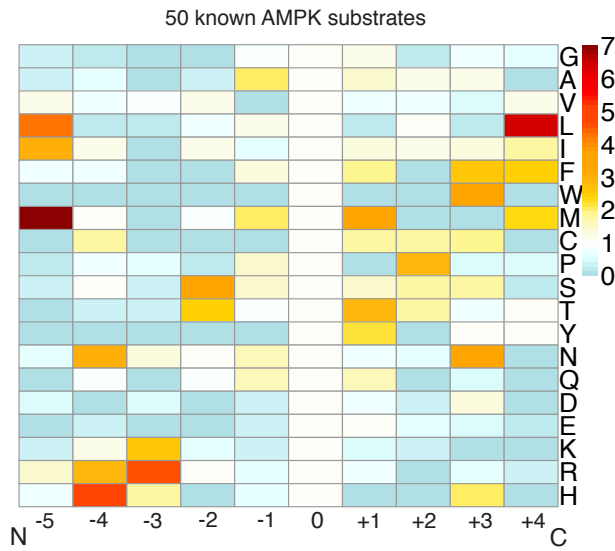


Figure S6, related to Figure 6

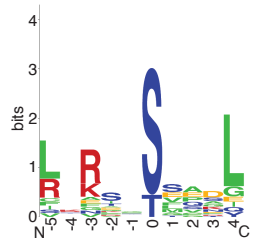
A



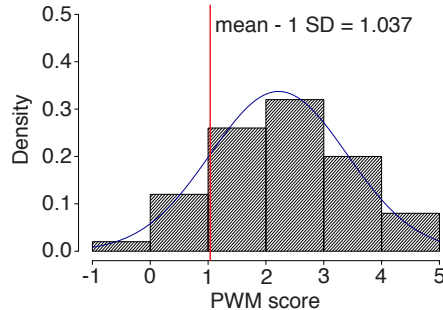
B

Ranking Quartile	Group based on # times seen		
	A	B	C
First	19	12	29
Second	11	7	42
Third	2	4	54
Fourth	0	4	55

C



D



E

Uniprot	Protein	Phosphosite	Times Seen	Previously Identified?	PWM Score	Function
Q9P2D3	HEATR5B	T1563	2		2.646	unknown
Q8TE77	SSH3	S37	2		2.304	Slingshot family of phosphatases; dephosphorylates cofilin promoting directional migration; bound by 14-3-3
Q92597	NDRG1	S330	2		2.178	critical for proper Schwann cell function; inhibits EMT and metastasis
Q13625	TP53BP2	S480	2	■	2.175	enhances p53 transactivation and promotes p53-mediated apoptosis
Q9UDY2	TJP2	S978	2		1.953	tight junction component and likely tumor suppressor; loss is embryonic lethal
Q7Z460	CLASP1	S600	2		1.680	kinetochore component that regulates microtubule dynamics; helps stabilize interphase microtubules
Q96RT1	ERBB2IP	S1079	2		1.654	HER2 adaptor that inhibits cell migration and mitogenic signaling
Q8IVT2	C19orf21	S394	2		1.485	promotes spindle pole positioning and orientation during mitosis
Q8WUF5	PPP1R13L	S102	2		1.406	oncogene; inhibits NF-kappaB and p53; over-expression promotes cell migration
Q53EU6	AGPAT9	S68	2		1.371	acyltransferase involved in triacylglycerol production
Q9NSK0	KLC4	S590	2		1.363	kinesin light chain; by similarity, functions in organelle transport along microtubules
O14713	ITGB1BP1	T38	1		3.074	binds the cytoplasmic tail of beta1-integrins, inhibiting cell adhesion
Q6GYQ0	RALGAPA1	S797	1		2.994	member of the RalGAP complex; inhibits the GTPases RALA and RALB; bound by 14-3-3
Q9Y4F9	FAM65B	S21	1		2.640	promotes myoblast differentiation; binds to and inhibits RHOA, inhibiting migration
Q8WXH2	JPH3	S230	1		2.570	forms junctional membrane complexes that connect to intracellular Ca2+ stores
Q8TEV9	SMCR8	S489	1		2.455	coimmunoprecipitates with the autophagy regulatory subunit RB1CC1; may function as a GEF
Q86YV5	SGK223	S694	1		2.307	RND2 effector; SRC substrate and pseudotyrosine kinase; promotes cell invasion and RHOA activity
Q01814	ATP2B2	T1139	1		2.177	Ca2+ ATPase plasma membrane pump
O94915	FRYL	S1978	1		1.876	human homologue of Drosophila fury gene, which maintains integrity of polarized cell extensions
Q13586	STIM1	S521	1		1.769	promotes store operated calcium entry, sensing calcium depletion and promoting calcium influx
Q8TAD1	SPANXE	S47	1		1.729	member of the SPANX cancer/testis-associated gene group
P30260	CDC27	S379	1	○	1.699	anaphase promoting complex component important for mitotic progression
Q8WZ42	TTN	S19879	1		1.562	in muscle, connects filaments within the sarcomere
Q8N9W8	FAM71D	S6	1		1.452	may promote proliferation; present as fusion product with MPP5 in some cancers
Q6R327	RICTOR	S1385	1		1.346	member of the mTORC2 complex; involved in cytoskeletal regulation; activates AKT
Q32P44	EML3	S176	1		1.311	localizes to spindle microtubules during mitosis and promotes proper metaphase chromosome alignment
Q9BXU1	STK31	S594	1		1.306	cell cycle regulated serine/threonine kinase; inhibits differentiation; promotes tumorigenesis and migration
Q6P597	KLC3	S466	1		1.226	kinesin light chain protein; associates with microtubules and may function in organelle transport
Q92614	MYO18A	T228	1		1.224	promotes Golgi budding by connecting it to the cytoskeleton; binds PAK2 and promotes motility
Q7L804	RAB11FIP2	S227	1		1.224	RAB11 effector involved in vesicle recycling and transport
P56645	PER3	S1006	1		1.117	member of the PERIOD gene family; may not be essential for proper circadian rhythm

■ Known AMPK substrate

○ Known AMPK substrate and phosphorylation site

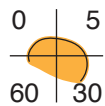
Figure S7, related to Figure 7

A

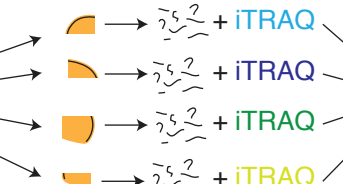
Mertins et al, 2014 (PMID: 24719451)



Harvest luminal breast cancer xenograft



Split tumor into four pieces to induce ischemia for the indicated number of minutes



LC-MS/MS

Digest proteins and label with iTRAQ tags for relative quantification

Combine samples and analyze by LC-MS/MS

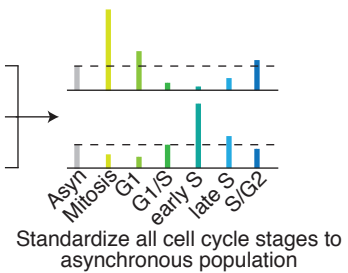
B

Olsen et al, 2010 (PMID: 20068231)

isotopes:	K0, R0	K4, R6	K8, R10
M phase			
Nocodazole: 30 min release	Asynchronous	early S Thymidine: 2.5 h release	
G1		late S Thymidine: 5.5 h release	
Nocodazole: 3 h release	Asynchronous		
G1/S		S/G2	
Thymidine: 0 h release	Asynchronous	Thymidine: 7.5 h release	

Synchronize light, medium, and heavy labeled HeLa S3 cells as indicated.  
Combine two synchronized phases with an asynchronous control.

Measure relative abundance of phosphopeptides with LC-MS/MS



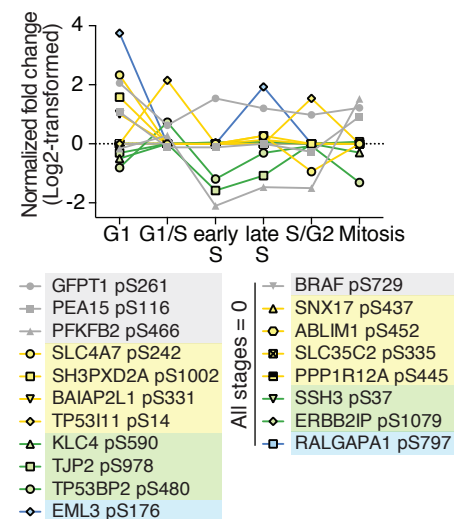
Standardize all cell cycle stages to asynchronous population

C

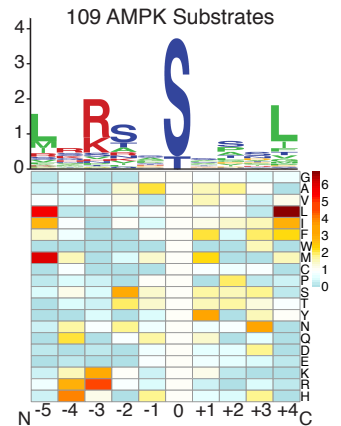
Protein	Ischemia (min)		
	5	30	60
HDAC5 pS259	-0.014	0.096	0.109
PIKFYVE pS307	-0.074	0.026	-0.129
PFKFB2 pS466	-0.006	0.024	0.042
BRAF pS729	-0.010	0.162	0.177
PAK2 pS20	-0.201	-0.109	-0.255
ULK1 pS467	-0.033	0.163	0.237
TBC1D1 pS237	0.124	0.052	0.053
BAIAP2 pS366	0.014	0.135	0.074
KLC2 pS545	0.621	0.856	0.935
CTNNND1 pS268	-0.217	-0.118	-0.138
ERBB2IP pS915	0.370	0.159	0.239
CDC42EP1 pS192	-0.131	-0.195	-0.005
SNAP29 pS163	-0.238	-0.248	0.004
WDFY3 pS2278	0.228	-0.040	-0.114
GPHN pS305	0.102	0.320	0.392
MTFR1L pS103	0.106	0.282	0.208
PKP2 pS82	0.028	-0.008	0.149
SH3BP4 pS246	-0.063	0.159	0.107
SH3PXD2A pS1002	0.093	0.122	0.178
SNX17 pS437	0.027	0.209	0.053
TP53I11 pS14	0.234	-0.293	-0.382

Protein	5	30	60
ABLIM1 pS452	0.077	0.395	0.299
SLC4A7 pS242	0.083	-0.169	-0.018
C19orf21 pS394	0.062	0.130	0.292
CLASP1 pS600	0.190	0.093	0.122
ERBB2IP pS1079	0.189	0.358	0.476
HEATR5B pT1563	0.101	0.244	0.420
KLC4 pS590	0.140	0.295	0.321
NDRG1 pS330	0.028	0.103	0.165
PPP1R13L pS102	0.280	-0.020	0.042
SSH3 pS37	0.050	-0.113	-0.291
TJP2 pS978	-0.176	-0.219	-0.181
TP53BP2 pS480	-0.002	-0.099	0.009
EML3 pS176	0.354	0.221	0.343
FAM65B pS21	0.064	0.234	0.122
FRYL pS1978	-0.345	-0.546	-0.761
MYO18A pT228	-0.017	-0.155	-0.015
RAB11FIP2 pS227	0.060	0.052	0.012
RALGAPA1 pS797	0.051	0.036	0.020
SGK223 pS694	0.042	-0.133	-0.100
SMCR8 pS489	0.131	0.156	0.110
STIM1 pS521	0.424	0.662	0.524

D



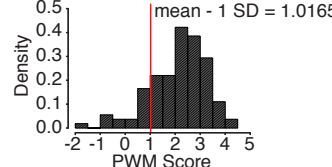
E



G

Tool	AMPK motif provided?	Type of input	All information from user-defined input file retained?	Interface	Ideal use	URL
Scansite	Yes (based on in vitro peptide library)	Single proteins or a predefined proteome database	n/a	Web-accessible	Searching a protein of interest or protein database for likely AMPK phosphorylation sites	<a href="http://scansite.mit.edu">http://scansite.mit.edu</a>
FIMO (MEME Suite)	No (users provide their own motif)	Single proteins, predefined proteome database, or user-defined .fasta file of protein sequences	No	Web-accessible	Searching a protein database or .fasta file for the presence of a user-defined motif	<a href="http://meme-suite.org/tools/fimo">http://meme-suite.org/tools/fimo</a>
AMPK motif PWM (this study)	Yes (based on validated in vivo AMPK substrates)	User-defined tab delimited text file of phosphorylation motifs (motifs only from N terminal 5 to C terminal 4)	Yes	Command line	Searching phosphoproteomics data for AMPK-like sites	<a href="https://github.com/BruNetLabAMPK/AMPK_motif_analyzer">https://github.com/BruNetLabAMPK/AMPK_motif_analyzer</a>

F



## Supplemental Figure Legends

### Figure S1. Characterization of the cellular systems generated to screen for AS-AMPK substrates and thiophosphorylation sites, and summary of the resulting datasets. Associated with Figure 1.

(A) The gatekeeper residue of analog specific (AS) AMPK $\alpha$ 1 (M96) is located in a similar sequence to that of AS-AMPK $\alpha$ 2 and other kinases previously used in the analog specific approach. This figure was modified with permission from (Banko et al., 2011).

*H.s., Homo sapiens; M.m., Mus musculus; S.c., Saccharomyces cerevisiae.*

(B) U2OS cell lines over-express N terminal HA-tagged wild type (WT) AMPK $\alpha$ 1, AS-AMPK $\alpha$ 1, WT-AMPK $\alpha$ 2, and AS-AMPK $\alpha$ 2 in a doxycycline (dox) dependent manner. Empty vector control cell lines are not shown. Cells were incubated with the indicated dose of doxycycline for the indicated time. Whole cell lysates were analyzed by western blot for the indicated antibodies.

(C) AS-AMPK $\alpha$ 1 and  $\alpha$ 2 thiophosphorylate the known AMPK substrate PPP1R12C in U2OS cell lines (Figure S1B) without over-expression of the supporting  $\beta$  and  $\gamma$  subunits. 293T cells transiently expressing HA-tagged AMPK $\alpha$ 2,  $\beta$ 1, and  $\gamma$ 1 were previously used to study AS-AMPK $\alpha$ 2 (Banko et al., 2011) and serve here as a comparison and positive control. AMPK was activated with 2 hours of serum starvation and 5 minutes of 100 mM 2-deoxy-D-glucose. Transiently expressed M2-PPP1R12C was immunoprecipitated with an antibody against M2 and analyzed by western blot for the presence of thiophosphorylation. The AMPK $\alpha$ 1 and  $\alpha$ 2 panels are from separate experiments and not directly comparable.

(D) Over-expression of HA-tagged WT-AMPK $\alpha$ 1 or  $\alpha$ 2 in U2OS cell lines does not

substantially alter AMPK activity towards the endogenous substrates ACC1 or PPP1R12C. U2OS cell lines (Figure S1B) were incubated with no doxycycline (“-”) and with two increasing doses of doxycycline: 0.05 µg/ml for 2 hours and 2 µg/ml overnight (represented by the small and large portions of the triangle, respectively). AMPK was activated with 50 mM 2-deoxy-D-glucose (2DG) or 300 µM A769662 (A) for the indicated times, and AMPK activity towards the known AMPK substrates ACC1 pS80 and PPP1R12C pS452 is shown. Whole cell lysates were analyzed by western blot with the indicated antibodies. “dox,” doxycycline.

(E) The peptide capture approach results in a high level of background peptide and phosphopeptide identifications. Comparisons of the overlapping and sample-specific peptides and phosphopeptides identified in AS-AMPK $\alpha$ 2 ( $\alpha$ 2AS), WT-AMPK $\alpha$ 2 ( $\alpha$ 2WT), and Empty vector controls (Empty) from assays B (293T cells, all AMPK subunits over-expressed, see Figure S1G) and D (U2OS cell lines, WT and AS-AMPK $\alpha$ 1 and  $\alpha$ 2 over-expressed with 2 µg/ml doxycycline overnight, see Figure S1G) are shown. The numbers shown are the number of unique (not total) peptides and phosphopeptides identified. The number of phosphopeptides identified here as specific to AS-AMPK $\alpha$ 2 in Assay D (n=65) is higher than the number in the last column of Figure S1G (n=60) because the latter also includes filtering against WT-AMPK $\alpha$ 1 background and accounts for events such as missed trypsinization.

(F) Technical MS replicates of the same AS-AMPK samples show low overlap of peptide and phosphopeptide identifications between liquid chromatography-tandem mass spectrometry (LC-MS/MS) analyses. However, known AMPK substrates and phosphorylation sites were identified. Comparisons of the overlapping and replicate-

specific peptides and phosphopeptides identified in 2 AS-AMPK $\alpha$ 2 technical replicates from assays B (293T cells, all AMPK subunits over-expressed, see Figure S1G) and D (U2OS cell lines, WT and AS-AMPK $\alpha$ 1 and  $\alpha$ 2 over-expressed with 2  $\mu$ g/ml doxycycline overnight, see Figure S1G) are shown. “|”, ambiguity in the mass-spectrometry placement of the phosphopeptide. The numbers displayed represent the number of unique (not total) peptides and phosphopeptides identified before accounting for missed trypsinization or other peptide overlap.

(G) Table of the number of phosphopeptide identifications within each biological sample. “Total”, total number of phosphopeptide identifications across technical replicates for the indicated AS-AMPK $\alpha$  isoform (AS-AMPK $\alpha$ 1 or  $\alpha$ 2); “Unique”, total number of unique phosphopeptide identifications across technical replicates for the indicated AS-AMPK $\alpha$  isoform (accounts for missed trypsinization and other peptide overlap, see Supplemental Experimental Procedures). The total number of unique phosphopeptides displayed in the bottom row accounts for missed trypsinization events and includes phosphopeptides that were unique to the AS-AMPK condition within a biological experiment but were later excluded as background due to their presence in the background samples from other biological experiments. The AS-AMPK $\alpha$ 2 lines were not incubated with doxycycline in Assay G because the exogenous AMPK promoter in these cells was sufficiently leaky to equal exogenous AS- or WT-AMPK $\alpha$  expression with the very low dose of doxycycline applied to the other cell lines. “(-)serum +2DG”, AMPK was activated by 2 hours of serum-starvation with 5 minutes of 100 mM 2-deoxy-D-glucose (2DG); “2DG”, 15 minutes of 50 mM 2DG; “A769662”, 30 minutes of 300  $\mu$ M A769662; “n/a”, not applicable; “Empty”, Empty vector control; “ $\alpha$ 1WT”, WT-AMPK $\alpha$ 1; “ $\alpha$ 2WT”, WT-

AMPK $\alpha$ 2.

**Figure S2. Analysis of phosphorylation sites on AS-AMPK specific phosphopeptides.**

**Associated with Figure 2.**

(A) Example phosphorylation site assignment per phosphopeptide based on the most commonly identified phosphorylation site across all experiments. A single phosphorylation site indicates a unique MS-identified site on the phosphopeptide. “|”, ambiguity by the mass spectrometer regarding correct phosphorylation site placement. “-”, space-holder for phosphopeptides that were identified fewer than 5 times. “?”, no single phosphorylation site was identified most frequently on the phosphopeptide due to ambiguous mass spectrometer phosphorylation site placement or multiple phosphorylation sites on the same phosphopeptide.

(B,C) Group A (B) and Group B (C) phosphorylation motifs surrounding the most frequently occurring phosphorylation site on a phosphopeptide. These phosphorylation sites comprise the logo motifs in Figures 2B and 2C. Green, hydrophobic residues; red, basic residues; yellow, acidic residues; blue, neutral polar amino acids; grey, phosphotyrosines.

**Figure S3. Validation of the substrates and phosphorylation sites in Group A as**

**direct AMPK targets. Associated with Figure 3.**

(A-C) AS-AMPK thiophosphorylates SNAP29-V5, MTFR1L-V5, and RBM14-V5. The indicated tagged proteins were over-expressed in empty vector or AMPK $\alpha$ -expressing (WT or AS-AMPK $\alpha$ 1 or  $\alpha$ 2) U2OS cell lines, immunoprecipitated with an antibody

against V5, and analyzed by western blot for the presence of thiophosphorylation. AMPK was activated in all conditions with 15 minutes of 50 mM 2-deoxy-D-glucose. Note: RBM14 was the only validated substrate to show thiophosphorylation in some control conditions, although this was not as strong as AS-AMPK-induced thiophosphorylation. This indicates that kinases other than AS-AMPK may use the bulky ATP $\gamma$ S to thiophosphorylate RBM14. “Empty”, Empty vector; “ $\alpha$ 1WT”, WT-AMPK $\alpha$ 1; “ $\alpha$ 1AS”, AS-AMPK $\alpha$ 1, “ $\alpha$ 2WT”, WT-AMPK $\alpha$ 2, “ $\alpha$ 2AS”, AS-AMPK $\alpha$ 2. Each panel is representative of at least two independent experiments.

(D) SNAP29 is more strongly thiophosphorylated by AS-AMPK $\alpha$ 2 than by AS-AMPK $\alpha$ 1. SNAP29-V5 was over-expressed in U2OS AS-AMPK $\alpha$ 1 and  $\alpha$ 2 cell lines, immunoprecipitated with an antibody against V5, and analyzed by western blot with an antibody against thiophosphate. “-”, no pharmacological activation of AMPK (note that the nutrient deplete thiophosphorylation buffer also activates AMPK); 2DG, 2-deoxy-D-glucose (15 minutes, 50 mM); A, A769662 (30 minutes, 300  $\mu$ M).

(E) MTFR1L is more strongly thiophosphorylated by AS-AMPK $\alpha$ 1 than by AS-AMPK $\alpha$ 2. MTFR1L-V5 was over-expressed in U2OS AS-AMPK $\alpha$ 1 and  $\alpha$ 2 cell lines, immunoprecipitated with an antibody against V5, and analyzed by western blot with an antibody against thiophosphate. “-”, no pharmacological activation of AMPK (note that the nutrient deplete thiophosphorylation buffer also activates AMPK); 2DG, 2-deoxy-D-glucose (15 minutes, 50 mM); A, A769662 (30 minutes, 300  $\mu$ M). Representative of two independent experiments.

(F) AS-AMPK thiophosphorylation of SH3PXD2A is not substantially altered by mutation of up to eight potential AMPK phosphorylation sites (Figure S3G). WT M2-

SH3PXD2A and the indicated serine to alanine mutants (see Figure S3G) were over-expressed in U2OS AS-AMPK $\alpha$ 1 and  $\alpha$ 2 cell lines, immunoprecipitated with an antibody against M2, and analyzed by western blot for the presence of thiophosphorylation. AMPK was activated in all conditions with 15 minutes of 50 mM 2-deoxy-D-glucose. S974 was identified as an AMPK phosphorylation site in this screen; Scansite (Obenauer et al., 2003) was used to predict the 7 additional potential AMPK phosphorylation sites.

(G) Table of the serine to alanine mutations in SH3PXD2A for each indicated clone. S974 was identified in the screen, and Scansite was used to predict the 7 additional potential AMPK phosphorylation sites (Obenauer et al., 2003).

(H) A phosphoantibody against SNX17 pS437 recognizes WT, but not phosphomutant (S437A) SNX17. WT and S437A M2-SNX17 were over-expressed in U2OS cells, immunoprecipitated with an antibody against M2, and analyzed by western blot with the indicated antibodies. “-“, no AMPK activation; 2DG, 2-deoxy-D-glucose (15 minutes, 50 mM); A, A769662 (30 minutes, 300  $\mu$ M). Representative of two independent experiments.

(I) Complete nutrient deprivation decreases SNX17 protein levels. U2OS cells were incubated in Dulbecco’s PBS (DPBS) containing 0.9 mM CaCl<sub>2</sub> and 0.49 mM MgCl<sub>2</sub> for the indicated amount of time. Cell lysates were analyzed by western blot with the indicated antibodies. “-“, no AMPK activation (DMSO vehicle control); A, A769662 (60 minutes, 300  $\mu$ M). Representative of 2 independent experiments.

**Figure S4. Many Group A AMPK substrates are classified under GO Terms encompassing cellular motility, adhesion, and invasion. Associated with Figure 4.**

(A) GO Terms encompassing different aspects of cellular motility, adhesion, and invasion.

(B) Fourteen Group A substrates have known roles in cell motility, adhesion, and invasion. Twelve were classified under these processes by literature mining (see Supplemental List 3), and 11 were identified using a curated list of GO Terms, comprising 9 that overlap with our literature mining and an additional 2 (SNAP29 and GPHN) (see Figure S4A). The overlap of the circles indicates substrates that were classified under these processes by both methods of classification.

**Figure S5. AMPK phosphorylation of NET1A inhibits extracellular matrix degradation. Associated with Figure 5.**

(A) U2OS cell lines stably express either an shRNA against AMPK $\alpha$ 1 and  $\alpha$ 2 or an empty vector control (Empty) and were originally published in (Banko et al., 2011). Cell lysates were analyzed by western blot with the indicated antibodies.

(B) RPMI-7951 cell lines stably express either an shRNA against AMPK $\alpha$ 1 and  $\alpha$ 2 or an empty vector control. Cell lysates were analyzed by western blot with the indicated antibodies.

(C) RPMI-7951 cell lines express NET1A-V5 wild type (WT) or NET1A-V5 S46A in a doxycycline (dox)-inducible manner. Cells were incubated with no doxycycline (“-“) and with two increasing doses of doxycycline: 0.05  $\mu$ g/ml for 2 hours and 2  $\mu$ g/ml for 24 hours (represented by the small and large portions of the triangle, respectively). Cell lysates were analyzed by western blot for the indicated antibodies. Quantification of the V5 band, standardized to  $\beta$ -actin, is shown beneath each sample.

- (D) Graph of the standardized V5 quantification shown in Figure S5C.
- (E) U2OS cell lines express NET1A-V5 WT or NET1A-V5 S46A in a doxycycline (dox)-inducible manner. Cells were incubated with no doxycycline (“-“) and with two increasing doses of doxycycline: 0.05 µg/ml for 2 hours and 2 µg/ml for 24 hours (represented by the small and large portions of the triangle, respectively). Cell lysates were analyzed by western blot for the indicated antibodies. Quantification of the V5 band, standardized to β-actin, is shown beneath each sample.
- (F) Graph of the standardized V5 quantification shown in S5E.
- (G) Over-expression of NET1A in U2OS cells increases extracellular matrix degradation. U2OS cells expressing similar levels of doxycycline-inducible NET1A-V5 WT or NET1A-V5 S46A (Figures S5E and S5F) were plated on FITC-conjugated gelatin coated coverslips and allowed to adhere overnight. 2 µg/ml doxycycline was added the following morning, and cells were cultured for an additional 2 days, fixed, stained for DAPI, and analyzed. Grey arrowheads indicate points of gelatin degradation. Within each experiment, approximately 15-20 20x fields per sample were quantified and averaged; displayed images are 40x. Error bars represent mean +/- SEM of the averaged values from 7 independent experiments; the control samples in 4 of the experiments were the same used in 4 of the experiments in Figure 5A. \*, p < 0.05 by two-tailed Wilcoxon matched-pairs signed ranked test; ns, not significant; scale bar = 50 µM.

**Figure S6. Ranking of infrequently identified AS-AMPK specific phosphorylation sites based on the AMPK phosphorylation motif. Associated with Figure 6.**

- (A) Heat map representing the frequencies of amino acid occurrences in the motifs

surrounding 50 known AMPK phosphorylation sites standardized to a background frequency (see Experimental Procedures and Supplemental Experimental Procedures). Briefly, the background frequencies were generated by averaging the amino acid occurrences in 10,000 randomly sampled datasets of matched number and phosphoS:T ratio from a compendium of human phosphorylation sites. Red indicates an enrichment for a given amino acid in the AMPK phosphorylation motif relative to background. Blue indicates a depletion for a given amino acid in the AMPK phosphorylation motif relative to background. The phosphorylation site itself is white because the background matches the AMPK motif in phosphoS:T frequency. This is a larger version of the heat map in the schematic in Figure 6A.

- (B) Overlap of Group A, B, and C phosphorylation motifs based on their ranking quartile.
- (C) A subset of poorly scoring phosphorylation motifs matches the known AMPK phosphorylation motif. If a phosphorylation motif contained an amino acid at any location that was never seen in the known AMPK phosphomotif, it received a scoring penalty regardless of how well the other sites matched the motif. The logo motif represents phosphorylation sites ranked from 97-116 in the first tab of Supplemental List 5.
- (D) Position weight matrix (PWM) score distribution of the 50 known AMPK phosphorylation sites. 50 known AMPK substrates were used to generate the PWM (Figures 6A and S6A) and then ranked in the same PWM. The score distribution is compatible with a normal distribution ( $p = 0.5451$ , Shapiro-Wilk normality test). The mean of the score distribution (2.219) minus one standard deviation (1.183) is 1.037 and is used as the cutoff for the ranked phosphorylation sites (“Confidence cutoff” in Figure

6B).

(E) Table of all Group B and C substrates that passed the cutoff criteria, with the associated scored phosphorylation site, identification information, PWM score, and known protein function. “Times seen” indicates the total number of biological mass spectrometry samples the phosphopeptide was identified in. “Previously identified”, indicates whether the substrate and phosphorylation site were previously identified as AMPK targets (open circles) or whether the substrate but not the phosphorylation site was known (closed squares). The green background indicates Group B phosphopeptides; the blue background indicates Group C phosphopeptides.

**Figure S7. In silico analysis of AMPK phosphorylation sites. Associated with Figure 7.**

(A) Schematic of the quantitative phosphoproteomics ischemia study (Mertins et al., 2014). Briefly, tumor xenographs were harvested and cut into four sections. Each section was processed after the indicated number of minutes. Proteins were digested, and peptides were labeled with iTRAQ tags to allow relative quantification in LC-MS/MS (Mertins et al., 2014).

(B) Schematic of the quantitative phosphoproteomics cell cycle study (Olsen et al., 2010). Briefly, cells were grown in combinations of heavy and light isotopes, synchronized in the indicated stages of the cell cycle, and processed for relative quantification via LC-MS/MS. The rows in the first panel represent cell cycle stages that were combined for LC-MS/MS analysis (Olsen et al., 2010).

(C) AMPK phosphorylation sites in the ischemia dataset (Mertins et al., 2014) that did not significantly increase during the ischemic time-course (significant changes determined in (Mertins et al., 2014)). Phosphorylation site location was standardized to isoform 1 in Uniprot. Sites in grey were known prior to this study; yellow, Group A; green and blue, highly scoring substrates from Groups B and C, respectively. The 5, 30, and 60 minute time-points were standardized to the 0 minute time-point and log<sub>2</sub>-transformed (Mertins et al., 2014).

(D) AMPK phosphorylation sites in the cell cycle dataset (Olsen et al., 2010) that did not increase during mitosis (i.e. sites that did not change 2-fold or more following log<sub>2</sub> transformation in (Olsen et al., 2010)). Phosphorylation site location was standardized to isoform 1 in Uniprot. Sites in grey were known prior to this study; yellow, Group A; green and blue, highly scoring substrates from Groups B and C, respectively. All timepoints were standardized to an asynchronously cycling population, normalized to protein level, and log<sub>2</sub>-transformed in (Olsen et al., 2010).

(E) Phosphorylation motif of 109 AMPK phosphorylation sites comprised of phosphorylation sites from the literature, all Group A sites, and the rescued Group B and C sites (Supplemental List 6). Top: Logo motif of the 109 AMPK phosphorylation sites. Bottom: Heat map representing the frequencies of amino acid occurrences in the surrounding motif of the 109 AMPK phosphorylation sites divided by a background frequency. The background frequency was generated by averaging the amino acid occurrences in 10,000 randomly sampled datasets of matched number and phosphoS:T ratio from a compendium of human phosphorylation sites.

(F) Position weight matrix (PWM) score distribution of the 109 AMPK phosphorylation sites represented in Figure S7E. 109 AMPK substrates were used to generate the PWM used in Figures 7 and S7 and ranked in that PWM. The mean of the score distribution (2.1251) minus one standard deviation (1.1085) is 1.0165 and is used as the cutoff score applied to define AMPK-like phosphorylation sites (Figures 7A, 7D, 7E, and 7F; Supplemental List 7). The red line represents the acceptance cutoff. Phosphorylation motifs from the publically available datasets scoring above the cutoff are considered highly similar to the AMPK motif.

(G) Table comparing the AMPK motif PWM and scoring algorithm (this study) with other resources commonly used for identifying specific phosphorylation motifs: Scansite (Obenauer et al., 2003) and FIMO (a MEME Suite Motif Scanning algorithm) (Grant et al., 2011). “n/a”, not applicable.

The datasets used in Figure S7 are from “Mertins, P., Yang, F., Liu, T., Mani, D.R., Petyuk, V.A., Gillette, M.A., Clauser, K.R., Qiao, J.W., Gritsenko, M.A., Moore, R.J., *et al.* (2014). Ischemia in tumors induces early and sustained phosphorylation changes in stress kinase pathways but does not affect global protein levels. *Mol Cell Proteomics* *13*, 1690-1704,” reprinted with permission from ASBMB and “Olsen, J.V., Vermeulen, M., Santamaria, A., Kumar, C., Miller, M.L., Jensen, L.J., Gnad, F., Cox, J., Jensen, T.S., Nigg, E.A., *et al.* (2010). Quantitative phosphoproteomics reveals widespread full phosphorylation site occupancy during mitosis. *Sci Signal* *3*, ra3,” reprinted with permission from AAAS.

## **Index of Supplemental Lists**

**Supplemental List 1.xlsx** Modifications to the peptide capture protocol in Extended Experimental Procedures for each biological experiment conducted. Associated with Figure 1.

**Supplemental List 2.xlsx** First tab: List of all phosphopeptides, with associated protein IDs, unique to the AS-AMPK $\alpha$ 1 and  $\alpha$ 2 conditions within a given biological experiment. The list is ordered based on each phosphopeptide's lack of occurrence in control samples and the number of AS-AMPK biological samples it was identified in. Second tab: List of all phosphopeptides, with associated protein IDs, identified in control empty vector, WT-AMPK $\alpha$ 1, and WT-AMPK $\alpha$ 2 samples. Associated with Figure 2.

**Supplemental List 3.xlsx** List of functions and corresponding PMID references of Group A proteins. Similar to Figure 4A, but includes the PMID references. Associated with Figure 4.

**Supplemental List 4.xlsx** First tab: List of 50 previously identified AMPK phosphorylation sites and the associated PMIDs where the site was characterized as an AMPK phosphorylation site. Second tab: Table of the standardized amino acid frequencies in the motifs surrounding 50 AMPK phosphorylation sites. Third tab: list of 41 published AMPK phosphorylation sites that did not pass the criteria to be included in the PWM algorithm. Associated with Figure 6.

**Supplemental List 5.xlsx** First tab: Position weight matrix (PWM) ranked list of phosphorylation sites identified in the screen. For Group A phosphopeptides that had ambiguous phosphorylation site placement, if the most frequently identified site reported in Figure 4A or Figure S2B is different from the site that received the highest score in the PWM, this is noted next to the scored site in column H. This occurred for 3 Group A phosphopeptides. Second tab: List of functions and corresponding PMID references of Group B and C proteins whose phosphorylation sites scored highly in the PWM. Similar to Figure S6E, but includes the PMID references. Third and fourth tabs: Discarded phosphorylation sites (see Figure 6A). Associated with Figure 6.

**Supplemental List 6.xlsx** First tab: table of the standardized amino acid frequencies in the motifs surrounding 109 AMPK phosphorylation sites. Second tab: list of phosphorylation sites used to construct the PWM frequencies in the first tab. This includes the 50 previously known AMPK phosphorylation sites, all Group A sites, and the Group B and C sites that scored above the cutoff in Figure 6. Associated with Figure 7.

**Supplemental List 7.xlsx** First tab: 630 AMPK-like phosphorylation sites from the ischemia study (Mertins et al., 2014) that scored highly in the PWM. Protein IDs and phosphorylation site locations are reported as in the original study. Second tab: 266 AMPK-like phosphorylation sites from the cell cycle study (Olsen et al., 2010) that scored highly in the PWM. Protein IDs and phosphorylation site locations are reported as

in the original study. Third tab: 131 highly scoring phosphorylation sites present in both the ischemia and cell cycle studies, classified as being up in both mitosis and ischemia, up in mitosis, up in ischemia, or no increase in either ischemia or mitosis. Protein IDs and phosphorylation site locations are reported as in the ischemia study (Mertins et al., 2014). Associated with Figure 7.

## **Supplemental Experimental Procedures**

### **Antibodies**

Cell Signaling Technology custom developed the pS437 SNX17 antibody for this study. The antibody will be commercially available as product number 17559. The V5 antibodies were obtained from Millipore (AB3792), Sigma (V8012), or Invitrogen (R960-25). The M2 antibodies (F3165 and F7425) were obtained from Sigma. Custom antibodies against pS452 PPP1R12C and total PPP1R12C were described previously (Banko et al., 2011). Total antibodies against AMPK $\alpha$ 1 were obtained from Cell Signaling Technology (2795S) or Bethyl Laboratories, Inc (A300-507A). The total antibody against AMPK $\alpha$ 2 (A300-508A) was obtained from Bethyl Laboratories, Inc. The antibodies to pT172 AMPK $\alpha$  (2535S), phosphoS/T AMPK substrate motif (5759), total ACC (3676S), and pS79 ACC (3661S) were obtained from Cell Signaling Technology. The total antibody to SNX17 (10275-1-AP) was obtained from Proteintech. The antibody against thiophosphate ester (2686-1) was obtained from Epitomics. The HA 12CA5 antibody (11583816001) was obtained from Roche. The antibody against  $\beta$ -actin (NB600-501) was obtained from Novus Biologicals.

### **Constructs**

The constructs encoding pECE HA-tagged wild type (WT) AMPK $\alpha$ 2, pECE HA-tagged analog specific (AS) AMPK $\alpha$ 2, pECE HA-tagged WT AMPK $\beta$ 1, pECE HA-tagged WT AMPK $\gamma$ 1, pECE M2-PPP1R12C, PSR Empty Vector, and PSR shAMPK $\alpha$ 1/ $\alpha$ 2 have been previously described (Banko et al., 2011).

The constructs encoding HA-AMPK $\alpha$ 1 (BC037303), M2-TKS5 (NM\_014631.2) and M2-SNX17 (BC014620) were generated by cloning the respective cDNAs into the pECE mammalian expression vector, in frame with the HA or M2 (Flag) tags. The constructs encoding NET1A-V5 (BC010285), CDC42EP1-V5 (BC009356), SNAP29-V5 (BC009715), FAM54B-V5 (BC017175), and RBM14-V5 (BC000488) were generated by inserting the cDNA into the pcDNA 3.2/V5-DEST construct using the Gateway recombination cloning system (Life Technologies). The TKS5 human cDNA was purchased as pReceiver M13 hTKS5-flag from GeneCopoeia. All other human cDNAs were obtained from the Orfeome library of cDNA (Open Biosystems).

The HA-tagged AMPK $\alpha$ 1 M96G mutant (AS-AMPK $\alpha$ 1), NET1A-V5 S46A mutant, CDC42EP1-V5 S192A mutant, M2-SNX17 S437A mutant, M2-TKS5 S21A, S487A, S639A, S658A, S696A, S790A, S974A, and S989A mutants were generated by site-directed mutagenesis (Agilent Technologies, 200519-5 and 210515-5). Sequencing was used over the entire cDNA to verify the presence of the desired mutation and the absence of other mutations. All mutated residues are numerically referenced to include the leading methionine. Lentiviral constructs expressing HA-tagged WT-AMPK $\alpha$ 1, HA-tagged AS-AMPK $\alpha$ 1, HA-tagged WT-AMPK $\alpha$ 2, HA-tagged AS-AMPK $\alpha$ 2, NET1A-V5 WT, and NET1A-V5 S46A in a doxycycline inducible manner were generated by cloning the respective cDNAs into the lentiviral vector FUW TetO (FUW TetO construct generation: (Brambrink et al., 2008)).

### **Primers used for cloning and site-directed mutagenesis**

Primers for cloning into pECE:

HA-AMPK $\alpha$ 1 forward:

ATAGAATTCGCGACAGCCGAGAAGCAGAACACGAC

HA-AMPK $\alpha$ 1 reverse:

ATATCTAGATTATTGTGCAAGAATTAAATTAGATTGC

M2-SNX17 EcoR1 forward:

ATAGAATTCGCACTTTCCATTCCGAAACCGAGTC

M2-SNX17 Xba1 reverse:

ATATCTAGATTACAGATCCTCATCTCCAATGCCCTC

M2-TKS5 Mfe1 forward:

ATACAATTGGCTGCCTACTGCGTGCAGGAT

M2-TKS5 Xba1 reverse:

ATATCTAGATTAGTTCTTTCTCAAGGTAGTTGGAAGGC

Primers for cloning into FUW-TetO:

HA-AMPK $\alpha$ 1 and  $\alpha$ 2 BstB1 forward:

ATATTCGAAACCATGTATGATGTTCCCTGATTATGCTAGC

HA-AMPK $\alpha$ 1 Pac1 reverse:

ATATTAATTAAATTATTGTGCAAGAATTAAATTAGATTGC

HA-AMPK $\alpha$ 2 Pac1 reverse:

ATATTAATTAAATTACGGGCTAAAGTAGTAATCAGACTGGC

NET1A-V5 Pac1 forward:

ATATTAATTAAACCATGGTGGCACATGATGAGACTGGAG

NET1-V5 Nhe1 reverse:

ATAGCTAGCTAACCGGTACGCGTAGAATCGAGAC

Primers for site-directed mutagenesis:

HA-AMPK $\alpha$ 1 M96G forward:

CCATCTGATATTCATGGTGGGGAAATATGTCTCAGGAGGAGAG

HA-AMPK $\alpha$ 1 M96G reverse:

CTCTCCTCCTGAGACATATTCCCCCACCATGAAAATATCAGATGG

NET1A-V5 S46A forward:

CTGGCTCGTGTACGGCCTGGCAAATTAAATC

NET1A-V5 S46A reverse:

GATTAAATTGCCAAGGCCGTGACACGAGGCCAG

CDC42EP1-V5 S192A forward:

CTTCGCCGCTCTGACGCTCTTGTCCCTCCGC

CDC42EP1-V5 S192A reverse:

GCGGAAGGACAAGAGAGCGTCAGAGCGGCGAAG

M2-SNX17 S437A forward:

CAAACCTCTCAAGTAAGCTGGCTGCCGTGAGCTTGCGGG

M2-SNX17 S437A reverse:

CCCGCAAGCTCACGGCAGCCAGCTTACTTGAGAGTTG

M2-TKS5 S974A forward:

CTGCGGAGGAATGAGGCACTCACGGCCACTGATG

M2-TKS5 S974A reverse:

CATCAGTGGCCGTGAGTGCCTCATTCCCTCCGCAG

M2-TKS5 S658A forward:

GAAATGGGGAAGAACCAACGCCCTCAGCCTCCTTCC

M2-TKS5 S790A forward:

GTGAGGGGTCTAGGAGAGCCTCATCCGACCTCATCAC

M2-TKS5 S487A forward:

CCTGAGCCGCCGCACAGCCACCGCTGACCCGGCCCAAG

M2-TKS5 S21A forward:

GAGAAGCGGAGGAACCCGCCAAGCACTACGTATAC

M2-TKS5 S639A forward:

CTCCCCAAGTCATCAGCACTCCTAAAGCTCAAG

M2-TKS5 S696A forward:

GAAGCCCCGCTCTGCTGCGGACGCAGGCATCCGC

M2-TKS5 S989A forward:

GTCCGACGGAACTCCGCCTTAGCACTGCTCGC

## Cell culture

HEK293T (293T) human epithelial kidney, U2OS human osteosarcoma, and RPMI-7951 human melanoma cell lines were cultured at 37°C in 5% CO<sub>2</sub> and 95% humidity in DMEM, McCoy's 5a Medium, and EMEM, respectively, supplemented with 10% fetal bovine serum (Gibco) and 1% Penicillin/Streptomycin/Glutamine (Invitrogen). To induce nutrient starvation (Figure S3I), U2OS cells were incubated in Dulbecco's PBS containing 0.9 mM CaCl<sub>2</sub> and 0.49 mM MgCl<sub>2</sub> (Gibco 14040).

## **Generation of stable cell lines**

Cells stably expressing proteins in a doxycycline-inducible manner were generated as follows: 293T cells were seeded at  $3.5 \times 10^6$  cells per 10 cm plate and transfected with 10 µg of the FUW TetO construct of interest, or with a FUW rtta expression construct, together with 5 µg of the PMDL, 2.5 µg of the RSV, and 2.5 µg of the VsVg helper plasmids using a calcium phosphate procedure (FUW TetO system and supporting helper plasmids were created in (Brambrink et al., 2008)). The medium was changed 8-15 hours after transfection. The following day, U2OS or RPMI-7951 cells were plated at  $1 \times 10^6$  cells/10 cm plate and allowed to attach overnight before being infected 3 times over 36 hours with 0.45 µm-filtered viral supernatant in the presence of 1.7 µg/ml polybrene (Sigma). Viral supernatants from FUW TetO gene and FUW rtta plates were pooled just prior to each infection. Following the third infection, cells were maintained in 200 µg/ml Zeocin (Invitrogen). To create U2OS cell lines containing both FUW TetO NET1A-V5 WT and pSicoR (PSR) shAMPKα1/α2, FUW TetO NET1A-V5 WT was infected into the U2OS PSR shAMPKα1/α2 cell lines created in (Banko et al., 2011), and maintained in 200 µg/ml Zeocin (Invitrogen, R25001) and 5 µg/ml Puromycin (InvivoGen, ant-pr-1).

RPMI-7951 cells stably expressing an shRNA against shAMPKα1/α2 or an empty vector control were generated as follows. 293T cells were seeded at  $3.5 \times 10^6$  cells per 10 cm plate and transfected with 10 µg pSicoR (PSR) shAMPKα1/α2 or empty vector control DNA, together with 5 µg of the VsVg and 5 µg of the Δ8.2 helper plasmids (PSR system: (Ventura et al., 2004)). The medium was changed 8-15 hours after transfection. The following day, RPMI-7951 cells were plated at  $1 \times 10^6$  cells/10 cm plate and allowed

to attach overnight before being infected three times over 36 hours with 0.45 µm-filtered viral supernatant (either PSR empty vector or shAMPK $\alpha$ 1/ $\alpha$ 2) in the presence of 1.7 µg/ml polybrene (Sigma). Following the third infection, cells were maintained in 5 µg/ml Puromycin (InvivoGen, ant-pr-1).

### **Cell lysis and immunoprecipitation in non-AS-AMPK assays**

A SDS-based lysis buffer was used to analyze whole cell lysates in assays with no immunoprecipitation (2% SDS, 50 mM Tris pH 6.8, 50 mM NaF, 40 mM  $\beta$ -glycerophosphate, 2 mM Na<sub>3</sub>VO<sub>4</sub>, 1 mM PMSF, 1% aprotinin stock (Sigma)).

To analyze endogenous AMPK phosphorylation of over-expressed and immunoprecipitated M2-SNX17 WT versus S437A, 8 x 10<sup>5</sup> U2OS cells were plated per 6 cm plate on Day 1. On Day 2, 2.76 µg pECE M2-SNX17 WT or S437A was transiently transfected into cells using polyethylenimine (Polysciences, 24765-2). Cells were fed with fresh media 5-6 hours following transfection. On Day 4, AMPK was activated as indicated, and plates were washed twice with PBS prior to lysis for ten minutes in 0.5% Triton-X, 0.5% sodium deoxycholate, 50 mM Tris HCl pH 8, 150 mM NaCl, 80 mM  $\beta$ -glycerophosphate, 50 mM NaF, 1 mM Na<sub>3</sub>VO<sub>4</sub>, 1 mM EDTA, 1% aprotinin stock (Sigma), and 1 mM PMSF. Samples were collected and spun on a table-top centrifuge for ten minutes, 4°C, at maximum speed. A small portion of the lysate was saved for western analysis, and the remaining was incubated with agarose beads preconjugated to anti-M2 (Sigma, F2426) for 2 hours, rotating at 4°C. Samples were then washed three times in 20 mM Tris HCl pH 8, 125 mM NaCl, 5 mM MgCl<sub>2</sub>, and 0.5% Triton-X. Sample was eluted

by boiling in Elution Buffer (333 mM Tris pH 6.8, 33% glycerol, and 0.072 g/ml SDS). Following elution, the supernatant was mixed with  $\beta$ -mercaptoethanol (15-17% of final sample volume) and bromophenol blue. Samples were boiled an additional time at 100°C for 2 minutes, resolved by SDS-PAGE, and immunoblotted with the indicated antibodies.

To analyze endogenous AMPK phosphorylation of over-expressed and immunoprecipitated NET1A-V5, NET1A-V5 WT or S46A was over-expressed from a doxycycline-inducible promoter in U2OS cell lines (see “Generation of stable cell lines” above). The effect of AMPK knockdown on NET1A phosphorylation was analyzed through stable, shRNA-mediated knock-down of AMPK $\alpha$ 1 and  $\alpha$ 2 in the context of doxycycline-inducible NET1A-V5 (see “Generation of stable cell lines” above). Cells expressing NET1A-V5 were maintained in McCoy’s 5a with 10% fetal bovine serum and 1% Penicillin/Streptomycin/Glutamine (PSQ) and 200  $\mu$ g/ml zeocin. Cells with additional knockdown of AMPK $\alpha$ 1 and  $\alpha$ 2 were cultured with 5  $\mu$ g/ml puromycin. On day 1 of the assay, 1 million cells of the indicated cell type were plated in a 15 cm dish with McCoy’s 5a containing 10% fetal bovine serum and 1% PSQ. On the evening of day 2, each plate was washed twice in 10 ml of PBS and fed with McCoy’s 5a containing 1% PSQ and no serum. The absence of serum was important to decrease basal NET1A phosphorylation. On the morning of day 3, doxycycline was added to each plate for two hours prior to cell lysis. A low concentration of doxycycline was used to promote a low level of NET1A-V5 over-expression. Doxycycline concentrations ranging from 0.015 to 0.12  $\mu$ g/ml were used, with different concentrations per cell line to achieve relatively equal amounts of NET1A-V5 over-expression among the different cell lines. In Figure

3K, U2OS cell lines were incubated with the following doxycycline concentrations for two hours: NET1A-V5 WT, 0.02 µg/ml doxycycline; NET1A-V5 WT with shAMPK $\alpha$ 1/ $\alpha$ 2, 0.08 µg/ml doxycycline; NET1A-V5 S46A 0.06 µg/ml doxycycline. Thirty minutes prior to cell lysis, 300 µM A769662 or the equivalent volume of DMSO vehicle was added to each plate. Immediately prior to lysis, each plate was washed 3x on ice with cold PBS. Each 15 cm plate was lysed in 1 ml lysis buffer (50 mM Tris pH 8, 150 mM NaCl, 1% NP-40, 0.1% SDS, 10 mM EDTA, 10 mM HEPES [pH 7.3], 50 mM KOAc, 2.5 mM NaOAc, 1 mM MgOAc<sub>2</sub>, 0.5 mM EGTA, 5 mM MgCl<sub>2</sub>, 0.25 mM DTT, 15 µg/ml digitonin, phosphatase inhibitor cocktail 3 (Sigma), EDTA-free complete protease inhibitors (~1 tablet per 10 ml buffer, Roche), PhosSTOP tablets (~1 tablet per 10 ml buffer, Roche)). Cells were incubated in the lysis buffer for 30 minutes at 4°C with gentle shaking and collected with a cell scraper. Lysates were centrifuged at maximum speed on a table-top centrifuge for 7 minutes at 4°C to remove insoluble debris, and 100 µl of each lysate was saved for whole cell lysate immunoblot analysis. NET1A-V5 was precipitated for 2-3 hours with V5-conjugated agarose beads (Sigma), washed three times in wash buffer (50 mM TrisHCl pH 7.5, 100 mM NaCl, 5 mM EDTA, and 0.4% Triton-X, 50 mM NaF, 40 mM β-glycerophosphate, 2 mM Na<sub>3</sub>VO<sub>4</sub>, 1 mM PMSF, 0.023 mg/ml aprotinin, and ~1 PhosSTOP tablet (Roche) per 10 ml of buffer). Samples were eluted by incubating in 40 µl Elution Buffer (see above paragraph) for 5 minutes at 100°C, with gentle shaking of tubes every 1-2 minutes. Following elution, samples were centrifuged briefly, and the eluted sample was mixed with 8 µl β-mercaptoethanol with bromophenol blue. Proteins were resolved by SDS-PAGE and probed with the indicated antibodies.

### **Thiophosphorylation of AS-AMPK substrates**

In vivo thiophosphorylation of AMPK substrates was conducted as previously described (Banko et al., 2011). Briefly, following AMPK activation, cells were washed 2x in PBS, and incubated at room temperature in labeling buffer (150 µl per well of a 6 well plate; 700 µl per 15 cm plate) for 20-40 minutes while shaking gently (Labeling Buffer: 20 mM HEPES [pH 7.3], 100 mM KOAc, 5 mM NaOAc, 2 mM MgOAc<sub>2</sub>, 1 mM EGTA, 10 mM MgCl<sub>2</sub>, 0.5 mM DTT, 5 mM creatine phosphate (Calbiochem), 57 µg/ml creatine kinase (Calbiochem), 30 µg/ml digitonin, 5 mM GTP, 0.1 mM ATP, 0.1 mM N<sup>6</sup>-(phenethyl) ATPγS (Axxora, BLG-P026-05), phosphatase inhibitor cocktails 2 and 3 (Sigma), and EDTA-free complete protease inhibitors (Roche)). The labeling buffer contains digitonin to permeabilize the cells, allowing N<sup>6</sup>-(phenethyl) ATPγS entry.

For immunoprecipitation and western blot analysis, thiophosphorylated substrates were alkylated following the thiophosphorylation reaction as previously described (Banko et al., 2011). Briefly, 2X RIPA (100 mM Tris pH 8, 300 mM NaCl, 2% NP-40, 0.2% SDS, and 20 mM EDTA) with 2.5 mM *p*-nitrobenzyl mesylate (PNBM) (Epitomics) was added to the labeling buffer and cells were incubated for an additional 1-2 hours at room temperature. Cell lysates were either resolved on a SDS-PAGE gel or candidate substrates were immunoprecipitated using agarose beads coupled to either M2 or V5 antibodies prior to western blot analysis. For the full protocol on analysis of candidate substrates, see section “Immunoprecipitation of candidate AS-AMPK substrates” below.

### **Immunoprecipitation of candidate AS-AMPK substrates**

Cells were plated in 6 well plates (293T:  $4 \times 10^5$  cells/well; U2OS:  $3.5 \times 10^5$  cells/well) and transfected with 1.25 µg tagged substrate DNA (293T only: with 1.25 µg each pECE HA-AMPK subunit). 293T cells were transfected using calcium phosphate; U2OS cells were transfected using polyethylenimine (Polysciences, 24765-2). 2 µg/ml doxycycline was added to U2OS FUW TetO HA-AMPK lines to induce expression of AMPK $\alpha$ 1 or  $\alpha$ 2 the day prior to thiophosphorylation of AMPK substrates. AMPK was activated with the indicated stimuli, and the thiophosphorylation and alkylation reactions were carried out as outlined above (see “Thiophosphorylation of AS-AMPK substrates”). Following alkylation, lysates were collected and centrifuged. A small amount of lysate was saved for western analysis, and the rest was incubated with anti-M2 or anti-V5 antibody conjugated agarose beads (M2, Sigma, F2426; V5, Sigma, A7345) that had been pre-washed 3 times in 50 mM Tris HCl pH 7.5, 100 mM NaCl, 5 mM EDTA, and 0.4% Triton-X. Lysates were incubated with the beads for 2 hours at 4°C while rotating then washed 3x in 50 mM TrisHCl pH 7.5, 100 mM NaCl, 5 mM EDTA, and 0.4% Triton-X, 50 mM NaF, 40 mM  $\beta$ -glycerophosphate, 2 mM Na<sub>3</sub>VO<sub>4</sub>, 1 mM PMSF, and 0.023 mg/ml aprotinin. Depending on the specific tagged protein, samples were eluted either by peptide competition or by boiling the samples in Elution Buffer (see “Cell lysis and immunoprecipitation in non-AS-AMPK assays”). Following elution using the Elution Buffer, samples were mixed with  $\beta$ -mercaptoethanol (15-17% of final sample volume) and bromophenol blue. Proteins were resolved by SDS-PAGE and probed with the indicated antibodies.

### **Peptide capture of thiophosphorylated peptides**

Peptide capture of thiophosphorylated peptides has been described previously in detail (Blethrow et al., 2008; Hertz et al., 2010) and is outlined below. Optimization was done over the course of the assays, so modifications from the protocol described below are noted in Supplemental List 1 for each assay. The lysis buffers used are detailed in section “Peptide capture lysis buffers” below.  $7.5 \times 10^6$  293T or  $3.3 \times 10^6$  U2OS cells were plated per 15 cm plate, and 1-4 plates were used per condition, as listed in Supplemental List 1. For U2OS cells only, 2 µg/ml doxycycline was added the following day to induce expression of AMPK alpha overnight, while 293T cells were transfected with 12 µg of each pECE HA-AMPK subunit ( $\alpha 2$ ,  $\beta 1$ ,  $\gamma 1$ ). On the fourth day after 293T plating and the third day after U2OS cell plating, AMPK was activated as indicated, cells were washed twice with PBS, and 700 µl labeling buffer (see “Thiophosphorylation of AS-AMPK substrates”) was added to each plate for 20-40 minutes. Directly following in-cell thiophosphorylation of AMPK substrates, samples were lysed with one of the buffers detailed in Supplemental List 1 (also in “Peptide capture lysis buffers” below) and/or sonicated (1-2x 30 seconds at 18 watts; see Supplemental List 1). Samples were denatured with 60% urea and 10 mM Tris(2-carboxyethyl)phosphine hydrochloride for 1 hour at 55°C. The samples were diluted with 2x volume 50 mM ammonium bicarbonate in ddH<sub>2</sub>O. Tris(2-carboxyethyl)phosphine hydrochloride concentration was readjusted to 10 mM. Trypsin (Promega, V5113) was added at a minimum 1:20 ratio µg trypsin: µg lysate, and the pH was adjusted to 8 using 5% sodium hydroxide. Samples were incubated rotating overnight at 37°C. An additional 20 µg trypsin was added an hour prior to quenching enzymatic activity by adjusting to pH 3 with trifluoroacetic acid (TFA). Samples were centrifuged at maximum speed on a table-top centrifuge for 10

minutes. Sep Paks (Waters Sep-Pak Classic C18 Cartridges, WAT051910) were used for sample clean-up and were prepared by passing ~10 ml 100% acetonitrile (ACN) over the columns 3 times, followed by 1x 10 ml 70% ACN 0.1% TFA, and 1x 10 ml 0.1% TFA. Samples were gravity filtered over Sep Paks, and the flow through was passed over the column an additional three times. Sep Paks were washed with 25 ml of 0.1% TFA, and the peptides were eluted with 1 ml 70% ACN 0.1% TFA followed by 200  $\mu$ l 70% ACN 0.1% TFA. Residual eluate was forced out of the Sep Pak using a 3 ml syringe. Samples were concentrated to roughly 40  $\mu$ l over ~4 hours on a Speedvac. Following concentration, 1x sample volume of 200 mM Hepes pH 7.3 in ddH<sub>2</sub>O and 2x sample volume 100% ACN were added to samples. The pH was adjusted to 7 using 5% NaOH. 100  $\mu$ l of Sulfolink Coupling Resin (Thermo Scientific, 20401) per sample was washed once in 200 mM Hepes. 5  $\mu$ l of 5  $\mu$ g/ml bovine serum albumin was added to the Sulfolink Coupling Resin prior to sample addition. Samples were rotated overnight with the Sulfolink Coupling Resin at room temperature in the dark. Fritted columns were equilibrated with 500  $\mu$ l 50% ACN, then 500  $\mu$ l ddH<sub>2</sub>O. Samples were loaded onto fritted columns and washed one time each with 1 ml ddH<sub>2</sub>O, 1 ml 5 M sodium chloride, 1 ml 50% ACN, and 1 ml 5% formic acid, all pushed through to 1 bed level above the resin layer. The samples were incubated with 1 ml of 10 mM dithiothreitol (DTT) for 10 minutes, and the remaining DTT was gently driven out. Samples were eluted with 100  $\mu$ l of 1 mg/ml Oxone (Sigma, 228036). Following flow-through, an additional 200  $\mu$ l 1 mg/ml Oxone was added to the samples for 20-30 minutes and gently driven out, followed by an additional 50  $\mu$ l Oxone that was forcefully pushed over the sample with a pipet. Samples were desalting using Zip Tips (Millipore ZTC18S096). Tips were

equilibrated with 3x 70% ACN 0.1% TFA washes followed by 3x 0.1% TFA washes. Samples were passed over the column 14 times and eluted with 3x 20 µl volumes of 70% ACN 0.1% TFA. Samples were stored at -20°C and analyzed with LC-MS/MS (see “Identification of phosphopeptides by mass spectrometry” below).

### **Peptide capture lysis buffers**

The following lysis buffers were used in the peptide capture assays (see “Peptide capture of thiophosphorylated peptides” above and Supplemental List 1): Lysis Buffer 1: 10 mM MgCl<sub>2</sub>, 100 mM NaCl, 20 mM Tris pH 7.5, 0.5 mM DTT, protease inhibitor cocktail (Roche) 1:100, 1% Triton-X, 1% cholic acid, and 0.2% digitonin. Lysis Buffer 2: 20 mM Tris HCl pH 8.0, 150 mM NaCl, 1% Nonidet P-40, 10% glycerol, 1 mM Na<sub>3</sub>VO<sub>4</sub>, 20 mM β-glycerophosphate, complete protease inhibitor cocktail tablet (1 tablet dissolved in 1 ml H<sub>2</sub>O then 265.6 µl added per 5 ml lysis buffer) (Roche 11 836 170 001), phosphatase inhibitor cocktails (Sigma P0044 and P5726) each at 2% final volume. Lysis Buffer 3: same as lysis buffer 2 with 20 mM EDTA. Lysis buffer 4: 50 mM Tris HCl pH 7.5-8, 100 mM NaCl, 5 mM EDTA, 50 mM NaF, 40 mM β-glycerophosphate, 0.4% Triton-X, 2 mM Na<sub>3</sub>VO<sub>4</sub>, 1 µM Microcystin LR, 1 mM PMSF, 0.05-0.1 TIU/ml Aprotinin (Sigma A6279 at 100x).

### **Identification of phosphopeptides by mass spectrometry**

Liquid chromatography-tandem mass spectrometry (LC-MS/MS) analysis and processing was performed essentially as described in (Hengeveld et al., 2012). Briefly, all desalted peptides (see “Peptide capture of thiophosphorylated peptides”) were resuspended into 10

$\mu$ l of 0.1% Formic Acid. Peptides were loaded on to a nanoACQUITY (Waters) UPLC instrument for reversed-phase chromatography with a C18 column (BEH130, 1.7- $\mu$ m bead size, 100  $\mu$ m  $\times$  100 mm) in front of an LTQ Orbitrap Velos. The LC was operated at a 600 nL/min flow rate and peptides were separated over an 80 minute gradient from 2-50% Buffer B (Buffer A: water and 0.1% formic acid, Buffer B: acetonitrile and 0.1% formic acid). Survey scans were recorded over a 350 – 1800 m/z range and MS/MS fragmentation was performed using Higher-energy collisional dissociation on the top 8 peaks. Peaklists were generated with an in-house (UCSF) software named PAVA and searched against the SwissProt Homo Sapiens database (downloaded on March 21, 2012) using Protein Prospector (version 5.10.10). Data was searched with a 20 ppm tolerance for parent and fragment ions, allowing for standard variable modifications and S/T/Y phosphorylation.

### **Online access to mass spectrometry datasets**

The processed Protein Prospector mass spectrometry datasets (peaklists matched to peptides) are available, with filename descriptions, at

[https://github.com/BrunetLabAMPK/AMPK\\_MS\\_Datasets](https://github.com/BrunetLabAMPK/AMPK_MS_Datasets). In addition, most processed and raw mass spectrometry files are available for download from the ProteomeXchange PRIDE database at <ftp://ftp.pride.ebi.ac.uk/pride/data/archive/2015/10/PXD003019>, with project information located at <http://www.ebi.ac.uk/pride/archive/projects/PXD003019>.

### **Analysis of mass spectrometry data**

To determine which phosphopeptides were unique to the AS-AMPK conditions, several filtering steps were taken. Initially, the phosphopeptides from all mass spectrometry analyses were selected, and all non-phosphorylated peptides were discarded. Within each biological experiment, the AS-AMPK $\alpha$ 1 and AS-AMPK $\alpha$ 2 phosphopeptides were compared to all background phosphopeptides (empty vector, AMPK $\alpha$ 1 WT, and AMPK $\alpha$ 2 WT), and any phosphopeptides identified in the AS-AMPK datasets that were also found in the background were discarded. The unmodified forms of the phosphopeptides were used in the comparison to control for ambiguous phosphorylation site assignment by the mass spectrometer and prevent background peptides from passing the filter. For example, the same phosphorylation event could be detected as S99 or as an ambiguous S99|T100 placement.

All phosphopeptides from the 22 AS-AMPK $\alpha$ 1 and  $\alpha$ 2 datasets were combined into one dataset, retaining experimental information and phosphorylation site information. This list was compared against all phosphopeptides identified across all background datasets, again using the unmodified peptide and additionally accounting for possible missed trypsinization events (e.g. VVSSIEQKTEGAEKK, VVSSIEQKTEGAEK, and VVSSIEQK would be considered the same peptide when removing background). In addition, if a peptide matched part of another peptide, it was removed as background (e.g. EKETEK would match VMEKETEKR), and for both AS-AMPK and background peptides over 6 amino acids in length, the full peptide was compared in this manner, as was the peptide with the leading and trailing amino acids removed. This stringent filter was applied because of the high level of background

phosphopeptides and aimed to remove phosphopeptides that closely resembled background. Any peptide found to overlap was discarded as background, even if found more frequently in the AS-specific datasets.

All AS-AMPK specific phosphopeptides can be found in the first tab of Supplemental List 2. In addition, this list contains phosphopeptides that were unique to AS-AMPK samples within a given biological experiment but were identified in background control samples in independent biological experiments (Supplemental List 2, bottom of list in gray). All phosphopeptides identified in background control samples are in the second tab of Supplemental List 2. In both the AS-AMPK specific and background control lists in Supplemental List 2, if multiple peptides were found over the same region due to missed trypsinization or other peptide overlap (e.g. VVSSIEQKTEGAEK and VVSSIEQK), only one is reported in the “Peptide sequence identified in MS” column.

### **Identification of the most frequently occurring phosphorylation site on a phosphopeptide**

In Figures 2 and S2, logo motifs (Figures 2B, 2C, and 2D) and individual motifs (Figures S2B and S2C) are displayed for phosphorylation sites that were identified on AS-AMPK specific phosphopeptides. For these figures, the most frequently identified phosphorylation site on each phosphopeptide is used to generate the motif. Only one phosphorylation site was identified on some phosphopeptides, so that single phosphorylation site was used. However, many phosphopeptides contained more than one phosphorylation site. This occurred for two reasons: 1) the mass spectrometer could not accurately determine which residue a phosphorylation site was located on (e.g.

“ambiguous” placement) or 2) the phosphopeptide contained multiple, independent phosphorylation sites. For all these phosphopeptides, the most frequently identified phosphorylation site was determined by summing the total occurrence of each possible phosphorylation site. For example, if the mass spectrometer identified both S40 and S45 as phosphorylated during the first identification of a hypothetical phosphopeptide, but on the second identification, S40 was not detected as phosphorylated, but S45 was, then S45 was chosen as the phosphorylation site. This same protocol applied to phosphopeptides with ambiguous phosphorylation site placement or combinations of ambiguous placement and multiple independent phosphorylation events. If no single phosphorylation site was identified more than the others, that phosphopeptide was not used in Figures 2B, 2C, 2D, S2B, or S2C, as selection of one phosphorylation site over the other would be arbitrary. As a result of this, 4 phosphopeptides were excluded from Figures 2B and S2B, 18 were excluded from Figures 2C and S2C, and 168 from Figure 2D). The more times a phosphopeptide was identified, the more likely it was to have a phosphorylation site that occurred most often, as additional phosphopeptide identifications could help serve as “tie breakers” for phosphopeptides with multiple or ambiguous phosphorylation sites.

Figure 4A also reports the most frequently occurring phosphorylation site, and reports the “tied” sites for phosphopeptides that did not have a most frequently occurring site. The position weight matrix algorithm (Figures 6 and 7) was constructed to select phosphorylation sites in an unbiased manner. Note that for all but 3 Group A sites (BAIAP2L1 S329 and S331, ARHGEF2 S151 and T153, and NUMA1 S1853 and

S1852), the most frequently identified site also matched the site with the highest score in the position weight matrix.

### **Preparation of FITC-gelatin coated coverslips**

This protocol was a kind gift from Carman Li in Tyler Jack's Laboratory. Fifteen mM glass coverslips were autoclaved, transferred to 12 well plates, and incubated at 55°C in 1 M HCl overnight. The coverslips were washed 10 times in H<sub>2</sub>O, treated with 50 µg/ml poly-D-lysine for twenty minutes at room temperature, and washed once with PBS prior to addition of FITC-labeled gelatin (Invitrogen, G13187, resuspended as 0.2% gelatin in PBS with 2% sucrose). Coverslips were incubated with 0.2% FITC-labeled gelatin for 10 minutes in the dark. Subsequent steps were performed with a minimum of light exposure. The FITC-labeled gelatin was removed, and coverslips were dried at an angle for 60 minutes. The coverslips were transferred to ice, and 0.5% fresh glutaraldehyde in cold PBS was added for 15 minutes, after which the coverslips were transferred to room temperature to incubate in the glutaraldehyde for an additional 30 minutes. Coverslips were washed 6 times in PBS, 1 mg/ml sodium borohydride was added for nine minutes (dissolved in PBS and used while still bubbling), and washed a final 3 times in PBS. The coverslips were stored at 4°C in PBS containing 1% penicillin/streptomycin/glutamine for up to a week.

### **Gelatin degradation assays**

To analyze extracellular matrix degradation in both U2OS and RPMI-7951 cells under PSR empty vector and shAMPKα1/α2 conditions, cells were plated (Day 1) on FITC-

labeled gelatin coated coverslips in 12 well plates (see section “Preparation of FITC-gelatin coated coverslips” for preparation), two wells per cell type. 20,000 U2OS cells or 40,000 RPMI-7951 cells were plated per well. Cells were fed with fresh media on each of the following two days. On Day 4, cells were fixed in 4% formaldehyde, washed four times in PBS, permeabilized in 0.1% Triton-X in PBS for four minutes, washed three times in PBS, and mounted in Vectashield with Dapi (Vector Labs, H-1500). Samples were blinded, and, on average, approximately 10 fields were imaged per well (2 wells per sample). The cell number and percent area degraded were quantified for each field using ImageJ64 software. Fields that could not be accurately quantified were discarded while the samples were still blinded (~15-20 fields per sample were quantifiable). Within each experiment, the quantified values from the 15-20 fields were averaged, and the averaged values from each experiment were used to generate the graph (error bars represent the mean +/- SEM). A two-tailed Wilcoxon matched-pairs signed ranked test was performed on the averaged values from each experiment. Of the 6 experiments conducted in U2OS cell lines, in 4 of the assays, the control wells were the same controls used in the U2OS NET1A WT versus S46A experiments outlined below.

To analyze the effect of AMPK activation on extracellular matrix degradation, 40,000 RPMI-7951 cells were plated on FITC-labeled gelatin coated coverslips in 12 well plates, with two wells per condition. Three to four hours after plating, cells were fed with fresh media containing either 100 µM A769662 (LC Labs or ChemiTek) or the equivalent volume of DMSO. Sixteen hours after drug addition, cells were fixed, imaged, and analyzed as above.

To analyze the role of NET1A and the AMPK phosphorylation site S46 on extracellular matrix degradation, 20,000 U2OS or 40,000 RPMI-7951 FUW TetO Empty Vector, NET1A-V5 wild type (WT), and NET1A-V5 S46A cells were plated on FITC-labeled gelatin coated coverslips in 12 well plates in the evening of Day 1, with two wells per condition. The following morning, the cells were fed with 2 µg/ml doxycycline in fresh media. This was repeated the following evening. On Day 4, the cells were fixed, imaged, and analyzed as above. Of the 7 experiments conducted in U2OS cell lines, in 4 of the assays, the control wells were the same controls used in the U2OS shAMPK experiments outlined above.

To analyze the role of AMPK activation on NET1A WT versus the S46A phosphomutant, 40,000 RPMI-7951 FUW TetO NET1A WT and S46A cells were plated on FITC-labeled gelatin coated coverslips in 12 well plates, with two wells per condition. Three hours after plating, cells were fed with fresh media containing 2 µg/ml doxycycline and either 100 µM A769662 or the equivalent volume of DMSO. Ten hours later, media was removed and fresh media with 2 µg/ml doxycycline and either 100 µM A769662 or the equivalent volume of DMSO was added. Following an additional ten hours, cells were fixed, imaged, and analyzed as above.

### **General data plotting and statistical analyses**

Matrix analysis for data plotting and statistical computing were conducted using the R software (<http://CRAN.R-project.org/>), version 2.15.0. The two-tailed Wilcoxon

matched-pairs signed ranked tests performed in Figures 5 and S5 were conducted using Prism 6 software.

### **Image J quantification of western blots**

ImageJ64 software was used to quantify the intensity of V5 and β-actin bands in Figures S5C and S5E. Grayscale images were inverted and the intensity of each band was measured. Each intensity measurement was standardized to a blank control area of equal size. The standardized V5 measurements were then divided by the corresponding standardized β-actin measurement, and this number is reported beneath each sample and graphed in Figures S5D and S5F.

### **Curation of known in vivo AMPK substrates**

In order to analyze the in vivo AMPK motif, we curated a list of known AMPK phosphorylation sites containing the sites on the initial two AMPK substrates, ACC1 and HMGCR, and an additional 48 known in vivo AMPK phosphorylation sites (Supplemental List 4) that met the following criteria: 1) validation of a direct interaction of AMPK with the phosphorylation site in vitro through either 32P incorporation in a site-specific manner, mass spectrometry analysis, or phosphospecific antibodies on the wild type versus the phosphomutant; 2) confirmation that the site-specific phosphorylation event occurs in whole cells/tissues via either a phosphospecific antibody, band shift, or mass spectrometry, all with phosphosite resolution, under either A) conditions that specifically activate AMPK such as a constitutively active versus a dominant negative form of AMPK or use of the specific AMPK activators A769662 or

AICAR or B) conditions of more general AMPK activation (metformin, phenformin, glucose deprivation, etc) combined with AMPK inhibition (si/shRNA, dominant negative AMPK, or, less ideally, Compound C). Alternate to these conditions, data indicating the site is directly phosphorylated by AMPK in cells meets the criteria (e.g. AS-AMPK thiophosphorylation at the specific site). In any condition, if the substrate in question was over-expressed, the full-length protein had to be used. There were 41 published AMPK phosphorylation sites that did not meet these criteria (Supplemental List 4, third tab). Most of these are almost certainly bona fide AMPK substrates, but we only used those that met the criteria defined above.

**Scoring phosphorylation sites identified at low frequency in the AS-AMPK screen based on similarity to the *in vivo* AMPK phosphorylation motif**

To analyze the similarity of individual motifs surrounding phosphorylation sites identified in the screen to the AMPK phosphorylation motif, we constructed a position weight matrix (PWM). A list of 50 known *in vivo* AMPK substrates was compiled (see “Curation of known *in vivo* AMPK substrates”) and the frequency of each amino acid occurrence at each position was calculated from the N terminal 5 position to the C terminal 4 position. To control for events common to phosphorylation sites in general, we standardized these amino acid frequencies to a background frequency derived from repositories at PhosphositePlus, [www.phosphosite.org](http://www.phosphosite.org), (Hornbeck et al., 2012): Phosphorylation\_site\_dataset.gz, PhosphositePlus’s downloadable phosphoproteome, was downloaded on August 8, 2014 at 13:50:59 EDT, with the corresponding proteome file, Phosphosite\_deq.txt.gz. This list contained approximately 155,000 human phosphoserine and threonine residues, and the 50 known AMPK phosphorylation sites

were removed. Ten thousand randomly sampled matched (in list length and S:T ratio to the list of 50 known AMPK substrates) background datasets were generated from this phosphoproteome, and the average frequency for each amino acid occurrence across all 10,000 background datasets was calculated. For each frequency in the AMPK and background motifs,  $10 \times 10^{-16}$  was added to avoid occurrences of zero. The frequency of each amino acid in the AMPK motif was then divided by the average background frequency. To score each phosphopeptide identified in the screen, the  $\log_{10}$  of the divided frequencies was summed for each residue surrounding the phosphorylation site from the N terminal 5 to the C terminal 4 positions. If a phosphopeptide contained more than one possible phosphorylation site, a score for each phosphorylation site was generated, and the highest scoring site was reported, unless a particular phosphoresidue comprised 70% or more of all mass spectrometry phosphorylation site identifications for that phosphopeptide. In that case, the site occurring 70% or more of the time was used. Additionally, only phosphoserines and threonines and those sites containing a basic residue within five N terminal residues of the phosphorylated site were further considered, as AMPK is a basophilic serine/threonine kinase. The phosphorylation motifs were then rank ordered based on their score in the PWM. The original list of 50 known AMPK substrates was scored using the same PWM. Putative AMPK phosphorylation sites scoring above the mean minus one standard deviation of the scores of the 50 known AMPK substrates were considered to be highly similar to the AMPK motif.

### **Identification of known AMPK phosphorylation sites in quantitative phosphoproteomics datasets**

To identify whether AMPK substrates were present in publicly available quantitative phosphoproteomics studies generated during ischemia (Mertins et al., 2014) and the cell cycle (Olsen et al., 2010), we searched these datasets for the presence of 50 previously known AMPK substrates (see “Curation of known in vivo AMPK substrates”) and those substrates identified in our screen (all Group A, and those in Group B and C that matched the AMPK phosphorylation motif). We searched for the exact protein sequence from the N terminal 5 to the C terminal 4 positions, as each study used different protein identifiers. Olsen et al, 2010 provided the relevant motif sequence. To obtain the phosphorylation motifs for the sites identified in Mertins et al, 2014, the provided GenInfo Identifier (GI) accession numbers were used to access the full-length protein from NCBI, and the provided phosphorylation site number was used to isolate the motif sequence. In each dataset, we only queried quantified phosphopeptides where one high confidence phosphorylation site was present, as determined by the original authors. The overlap of each dataset with known AMPK substrates was manually verified. In some instances, the datasets used a different isoform of a protein and therefore reported different phosphorylation site numbers. In these cases, we double checked the accuracy of the overlap and reported the AMPK phosphorylation site location in Figures 7B, 7C, S7C, and S7D as reported in isoform 1 in Uniprot. Of note, for the 3 Group A phosphopeptides with different sites scored in the PWM than found most frequently (see “Identification of the most frequently occurring phosphorylation site on a phosphopeptide”), the site scored by the PWM was used in this analysis.

### **Identification of AMPK-like phosphorylation sites in quantitative phosphoproteomics datasets**

To determine which phosphorylation sites in the publicly available quantitative phosphoproteomics datasets generated during ischemia (Mertins et al., 2014) and the cell cycle (Olsen et al., 2010) matched the AMPK phosphorylation motif, we created a more robust PWM by incorporating the novel substrates identified in the screen into the PWM, totaling 109 inputs: 50 previously known *in vivo* AMPK phosphorylation sites- see “Curation of known *in vivo* AMPK substrates”, all Group A phosphorylation sites, and highly scoring Group B and C phosphorylation sites (Figure 6). More inputs help buffer the algorithm from incorrectly penalizing amino acids at certain locations because they were not present in any of the motifs used to build the algorithms due to low numbers instead of for biological reasons. We standardized the amino acid frequencies in the motifs surrounding these 109 AMPK phosphorylation sites to background frequencies and calculated a score for the phosphorylation sites identified in the two publicly available datasets (Mertins et al., 2014; Olsen et al., 2010) as in “Scoring phosphorylation sites identified at low frequency in the AS-AMPK screen based on similarity to the *in vivo* AMPK phosphorylation motif.” Only the phosphopeptides with a single high confidence phosphorylation site (e.g. “Class 1” in the mitosis dataset and no additional post-translational modification) and that were quantified across all conditions were used in this analysis. As the ischemia dataset was generated from xenographs, only sites matching to “*Homo sapiens*” or “*Homo sapiens|Mus musculus*” were analyzed, not those corresponding to “*Sus scrofa*,” “*Mus musculus*,” or “*Mus musculus|Homo sapiens*.”

To determine which sites to consider highly similar to the AMPK motif (i.e. AMPK-like), a cutoff score was determined. The 109 AMPK phosphorylation sites were

ranked in the PWM (the same PWM they were used to construct). The mean and the standard deviation of the 109 resulting scores were calculated. The mean minus one standard deviation was used as the cutoff score. All phosphorylation sites from the two publicly available datasets that scored above the cutoff were considered to have AMPK-like motifs. These AMPK-like sites were also required to be phosphoS/T (not phosphoY) and to have a basic residue in the N terminal portion of the motif, as AMPK is a basophilic serine/threonine kinase. Of note, in the ischemia dataset, pS1356 from myosin-IXb isoform 1 scored above the cutoff and was considered an “AMPK-like” site. However, two different phosphopeptides were quantified for this same site due to a missed trypsinization (RTSFsTSDVSK and TSFsTSDVSK). The corresponding quantifications for each phosphopeptide were different (one increased and one decreased in relative abundance during ischemia), so this site was discarded from the reported output in Figure 7 and Supplemental List 7. In the ischemia dataset, sites that changed significantly were determined in (Mertins et al., 2014). In the cell cycle dataset, sites were considered dynamically regulated if they changed at least 2-fold following log<sub>2</sub>-transformation, as this was used as the cutoff for some analyses in (Olsen et al., 2010).

To compare AMPK-like sites identified in both datasets, the protein sequences from the N terminal 5 to C terminal 4 positions were compared, as each study uses different protein identifiers. Sequences that matched 100% were considered the same phosphorylation site. In some instances, different isoforms are used as the main protein identifier, resulting in differential numbering of the same phosphorylation site. Therefore,

when relevant, figure legends indicate what dataset was used to report the phosphorylation site location.

### **Accessing the GitHub repository**

Access to the AMPK motif algorithm can be obtained through GitHub:

[https://github.com/BrunetLabAMPK/AMPK\\_motif\\_analyzer](https://github.com/BrunetLabAMPK/AMPK_motif_analyzer)

Several files are present:

- 1) ReadMe file: README.md (contains instructions on file format specifications and how to run the code)
- 2) AMPK motif algorithm: Rank\_AMPK\_Motifs.pl
- 3) AMPK motif standardized frequencies required to run the algorithm:  
AMPK\_motif\_109\_standardized\_log10.txt
- 4) Example input file: Example\_input.txt
- 5) Example output file that the algorithm generates: Example\_input\_scored.txt

The files are run by downloading and accessing locally in terminal (command line code is under README.md).

### **Uploading the AMPK motif matrix to MEME or Scansite**

The AMPK motif matrices in Supplemental Lists 6 (109 AMPK phosphorylation sites) or 4 (50 AMPK phosphorylation sites) can also be uploaded to motif analysis sites such as Scansite (Obenauer et al., 2003) or FIMO (Grant et al., 2011) (part of the MEME Suite

(Bailey et al., 2009)). The users will need to format the matrix to the sites' exact specifications, which are available on each platforms' website:

Scansite: <http://scansite.mit.edu/tutorial/faq.html>

FIMO: <http://meme-suite.org/doc/meme-format.html>

Briefly, in matrices uploaded to the MEME suite, the sum of scores for each site (e.g. N terminal 5 position) must equal 1, so each amino acid score in a given position in the AMPK motif matrix would be standardized by the sum total of all scores for that position. At the phosphorylation site, serine and threonine would each receive a score of 0.5. Similar to the AMPK motif PWM presented here, Scansite's format heavily penalizes any score below a 1, with a maximal score of 21. The AMPK motif PWM is on a smaller scale than 21, so the AMPK motif scores could be left as is, or scores in the AMPK motif matrix greater than 1 could be scaled accordingly. At the phosphorylation site, serine and threonine would each receive a score of 21; other residues receive a score of 0. Of note, each platform handles empty amino acid spaces (e.g. the site is near the termini of the protein) differently.

### **Heat map and Logo Motif generation**

The R package ‘pheatmap’ version 0.7.4 was used to generate all heat maps (<http://CRAN.R-project.org/package=pheatmap>, authored by Raivo Kolde) with R software version 2.15.0. Berkeley's Weblogo (Crooks et al., 2004; Schneider and Stephens, 1990) was used for motif visualization. Unless indicated, all motif heat maps

are representations of the sample frequency standardized to a background frequency, while Weblogo motifs are not standardized to a background frequency.

## Supplemental References

- Bailey, T.L., Boden, M., Buske, F.A., Frith, M., Grant, C.E., Clementi, L., Ren, J., Li, W.W., and Noble, W.S. (2009). MEME SUITE: tools for motif discovery and searching. *Nucleic Acids Res* 37, W202-208.
- Banko, M.R., Allen, J.J., Schaffer, B.E., Wilker, E.W., Tsou, P., White, J.L., Villen, J., Wang, B., Kim, S.R., Sakamoto, K., *et al.* (2011). Chemical genetic screen for AMPKalpha2 substrates uncovers a network of proteins involved in mitosis. *Mol Cell* 44, 878-892.
- Blethrow, J.D., Glavy, J.S., Morgan, D.O., and Shokat, K.M. (2008). Covalent capture of kinase-specific phosphopeptides reveals Cdk1-cyclin B substrates. *Proc Natl Acad Sci U S A* 105, 1442-1447.
- Brambrink, T., Foreman, R., Welstead, G.G., Lengner, C.J., Wernig, M., Suh, H., and Jaenisch, R. (2008). Sequential expression of pluripotency markers during direct reprogramming of mouse somatic cells. *Cell Stem Cell* 2, 151-159.
- Crooks, G.E., Hon, G., Chandonia, J.M., and Brenner, S.E. (2004). WebLogo: a sequence logo generator. *Genome Res* 14, 1188-1190.
- Grant, C.E., Bailey, T.L., and Noble, W.S. (2011). FIMO: scanning for occurrences of a given motif. *Bioinformatics* 27, 1017-1018.
- Hengeveld, R.C., Hertz, N.T., Vromans, M.J., Zhang, C., Burlingame, A.L., Shokat, K.M., and Lens, S.M. (2012). Development of a chemical genetic approach for human aurora B kinase identifies novel substrates of the chromosomal passenger complex. *Mol Cell Proteomics* 11, 47-59.
- Hertz, N.T., Wang, B.T., Allen, J.J., Zhang, C., Dar, A.C., Burlingame, A.L., and Shokat, K.M. (2010). Chemical genetic approach for kinase-substrate mapping by covalent capture of thiophosphopeptides and analysis by mass spectrometry. *Curr Protoc Chem Biol* 2, 15-36.
- Hornbeck, P.V., Kornhauser, J.M., Tkachev, S., Zhang, B., Skrzypek, E., Murray, B., Latham, V., and Sullivan, M. (2012). PhosphoSitePlus: a comprehensive resource for investigating the structure and function of experimentally determined post-translational modifications in man and mouse. *Nucleic Acids Res* 40, D261-270.
- Mertins, P., Yang, F., Liu, T., Mani, D.R., Petyuk, V.A., Gillette, M.A., Clauser, K.R., Qiao, J.W., Gritsenko, M.A., Moore, R.J., *et al.* (2014). Ischemia in tumors induces early and sustained phosphorylation changes in stress kinase pathways but does not affect global protein levels. *Mol Cell Proteomics* 13, 1690-1704.
- Obenauer, J.C., Cantley, L.C., and Yaffe, M.B. (2003). Scansite 2.0: Proteome-wide prediction of cell signaling interactions using short sequence motifs. *Nucleic Acids Res* 31, 3635-3641.

Olsen, J.V., Vermeulen, M., Santamaria, A., Kumar, C., Miller, M.L., Jensen, L.J., Gnad, F., Cox, J., Jensen, T.S., Nigg, E.A., *et al.* (2010). Quantitative phosphoproteomics reveals widespread full phosphorylation site occupancy during mitosis. *Sci Signal* *3*, ra3.

Schneider, T.D., and Stephens, R.M. (1990). Sequence logos: a new way to display consensus sequences. *Nucleic Acids Res* *18*, 6097-6100.

Ventura, A., Meissner, A., Dillon, C.P., McManus, M., Sharp, P.A., Van Parijs, L., Jaenisch, R., and Jacks, T. (2004). Cre-lox-regulated conditional RNA interference from transgenes. *Proc Natl Acad Sci U S A* *101*, 10380-10385.